Faculty of Engineering
Department of Civil Engineering

On the motion of vertical and oblique sand jets in stagnant immiscible liquids

by

Masoud Manzouri

A thesis
submitted to the Faculty of Graduate Studies
in partial fulfillment of the requirements for the degree of
Master of Science in Environmental Engineering

Thunder Bay, Ontario, Canada, 2019

This thesis is dedicated to my parents

for their love, endless support

and encouragement.

Abstract

Sand jets and particle clouds in water and viscous fluids have been a frequent subject of intense research and are pertinent to many environmental, industrial, and engineering processes. Mixing and dispersion of sand jets and particle clouds in water have been studied to design and optimize wastewater dredging disposal and marine bed capping. Motion of dispersed particles in viscous fluids is of great interest in design and operation of oil-sand tailing ponds and modeling magma flows. The motion of vertical and oblique sand jets passing through an immiscible layer is controlled by the properties of background fluids, the physical characteristics of sand particles, and the initial release conditions. Predicting the fate of the instantaneously released sediments in stratified oil-water system requires knowledge of how various physical factors contribute to the formation process of sediment clouds.

Laboratory experiments were conducted to study the behaviour of particle clouds passing through two immiscible fluids (i.e., oil and water), formed by instantaneous release of dry sand particles from different angles and various heights above the oil layer, and to understand the effects of controlling parameters on the formation of particle clusters. Different air release heights h, release angle θ, nozzle diameters d_o, and sand masses m were tested. Nozzle size and mass of sand particles were grouped to form a non-dimensional parameter as L/d_o where L is the length of pipe filled up with sand particles. Wide ranges of aspect ratios ($1 \leq L/d_o \leq 19.6$ for vertical and $1.5 \leq L/d_o \leq 24.5$ for oblique sand jets) were considered. Air release height was normalized to form non-dimensional air release height as η.

Effects of the characteristics of sand jets in air such as mass flow rate, sand impact velocity, and jet diameter on the evolution of oily sand jets were investigated. It was found that the diameter of sand jet in air linearly correlated with the nozzle diameter. Evolution of oily sand jets with time

was investigated using image processing and boundary visualization techniques. Different shapes of the frontal head and various evolution patterns were observed based on the initial parameters. The frontal width and velocity of oily sand were measured for different evolution times. Dimensional analysis was performed, and empirical correlations were introduced to predict the frontal width and velocity of particle clouds passing through immiscible layer. The average shear stress in the immiscible layer and in the early stages of evolution was calculated from the measurements: the normalised shear stress between sand particles and the immiscible layer was found to linearly increase with the impact momentum. The average drag coefficient of sand jet front was calculated and results were compared with the classical drag models. The average drag coefficient of oily sand jets was found to be smaller than the drag coefficient of individual sand particles in a steady-state condition.

Keywords: sand jets, particle clouds, oily sand jets, oblique jets, immiscible interface, plumes, two-phase flows, drag reduction

Acknowledgements

I would never have been able to finish my masters' work without the guidance of my committee members, the backing from a few organizations, the help from friends, and support from my family.

Foremost, I would like to express my sincere gratitude to my supervisor Dr. Amir H. Azimi for his continuous support, patience, motivation, enthusiasm, and immense knowledge. His guidance helped me throughout my research and during the writing of this thesis. I could not have imagined having a better supervisor for my M.Sc. study. I would like to thank Dr. Baoqiang Liao and Dr. Jian Deng who agreed to be my committee members and gave me valuable suggestions and advice.

I am grateful to NSERC Discovery Grant, Lakehead University International Office, and Lakehead University Student Union for providing the funding and facilities to execute my research.

I would like to thank my dear friends Ali Azizishirazi, Sara Pazirai, John and May Naimian, Fahimeh Mirshekari, and Saman Naderi for their generous and continuous support.

I especially thank my dearest family; my mother who has provided me with her unconditional love, my father who strove to prepare the best for his family and my siblings Leila, Laleh, and Ali who always supported me with their kindness and good wishes. My family has provided unconditional love and care and I would not have made it this far without them.

Contents

List of Figures

List of Tables

1 Introduction

1.1 General Information

Jet and plumes are turbulent flows, which are created by continuous sources of momentum and buoyancy, respectively. The study of these kinds of flows has application in many practical problems. The wide-range application of turbulent flows in industries has resulted in comprehensive research and studies. If both momentum and buoyancy are present at the source, momentum would be the leading effect in the region near the source. Buoyancy becomes important only when the momentum generated by the buoyancy force has exceeded the primary momentum at the source (Lee and Chu, 2003). Single-phase flows result from the discharge of a fluid with an initial momentum; however, when a second phase (e.g. solid or gas) is added to the flow, it is termed a two-phase flow. The characteristics of the two-phase flow are remarkably affected by the interaction between the two phases of the jet (Sheen et al., 1994) as well as the second phase concentration and particle size (Azimi et al., 2011). Solid-liquid and gas-liquid flows are two samples of two-phase flows. Wastewater discharge, dredging, marine bed capping (Bush et al., 2003; Azimi et al., 2011), and island building operations (Hall et al., 2010) are examples of solid-liquid flows.

Oil-sand is a mixture of sand, clay, and water that are saturated with a dense viscous form of petroleum called bitumen. Oil-sand mines are found in several countries including Canada, United States, Russia, and Venezuela. In Canada, the principal crude oil reserve is located in the province of Alberta. Oil-sand mines consume large volumes of water (i.e., 1 m^3 for 1 barrel of oil); therefore, it is important to reclaim consumed water.

Chapter 1 Introduction

Managing the volume of tailing in oil-sand tailing ponds was found to be one of the biggest environmental challenges in the oil industry. One of the effective methods of reclaiming tailing ponds is to discharge new slurries into the pond to accelerate the settling process of fine particles since very small particles are not heavy enough to settle on the bottom of the pond and will be suspended in the water media for many decades to form a solid surface. In this method, the volume of fine tailings will be reduced. Therefore, it is important to be able to identify the mixture of compounds and to understand the dynamics of sediments in those ponds. Studying the behaviour of sand particles passing through an immiscible layer of liquids and entering the ambient can be a suitable method to better understand the mixing and spreading process of sediments in tailing ponds.

1.2 Applications in Environmental and Natural Phenomena

Sand jets and particle clouds have many applications in civil and environmental engineering such as artificial island construction, marine bed capping, dredging, and discharge of industrial and urban wastewater. In artificial island construction, sand is continuously discharged from barges into marine environments to develop an island foundation. In most cases, sediments are discharged through a pipe with an angle respect to vertical axis. Marine sediment capping is a technique which can be used to cover waste sediment disposal. The cover layer remains in place to prevent the spread of waste material in aquatic environments.

Chapter 1 Introduction

Figure 1.1 Palm Islands construction in Dubai
https://www.aboutcivil.org/palm-island-dubai-megastructure.html

Dredging is the act of removing silt and other material from the bottom of lakes, rivers and other water bodies. It is a routine necessity in waterways around the world because sedimentation gradually fills channels. Dredging is also used as a way to replenish sand on some public beaches, where sand has been lost because of coastal erosion.

Figure 1.2 Dredging
http://www.theindependentbd.com/arcprint/details/134426/2018-01-26

Figure 1.3 Discharge of industrial waste material
https://helpsavenature.com/industrial-water-pollution

Particle dispersion is part of many natural phenomena such as magma flows and sediment-laden flows in lakes and oceans. Magma is a high-temperature fluid or semi-fluid with a mixture of molten and semi-molten rocks, volatiles and solids and could be modeled by a gravity-driven two-phase flow with a considerable density difference as enters into water bodies in an acceptable manner. Since it is difficult to study the behavior of magma flows owing to natural restrictions (e. g., high temperature and vaporized water in the vicinity of magma flows), cluster of particles could be modeled by encapsulated sand particles passing through an oil layer.

Oil-sand tailing ponds have noted as a recent practical example of the flow of sand jets and thermals through an immiscible interface. The processed oil-sand which contains a high concentration of fine sediments is discharged into tailing ponds to deposit sand particles and reclaim the processed water.

Figure 1.4 Magma flow
http://www.moehotglass.com/project/lava-burst-sculpture/

Figure 1.5 Oil-sand flows into tailing ponds
http://priceofoil.org/2014/02/24/tar-sands-tailing-ponds-leaking/

1.3 Objectives of the Present Study

When an amount of mass is injected into viscous fluids, a sand jet is formed which penetrates to a certain length and then breaks up into many particles. Suspended particles play a major role in the ecology and pollution of environmental systems such as oceans and atmosphere.

Chapter 1 Introduction

Understanding the dynamics and the interaction between sand particles and its ambient is important for efficient designing and for optimizing engineering systems.

The main objective of the present study is to investigate the motion of particles passing through an immiscible layer while the initial momentum is controlled by the air release height and release angle. This research aims to examine the effects of initial momentum and damping effects of the viscous immiscible layer on the motion of oily sand jets by investigating the variations of the jets' characteristics (penetration length, width, and frontal velocity) with the controlling parameters. The secondary objective of this study is to understand the motion of particles through and after the immiscible oil layer by evaluating dynamic parameters (shear stress between sand particles and the oil layer, shear stress surrounding the oily sand jets, and the average drag coefficient) in the early stages of evolution.

2 Literature Review

Dynamics of particle clouds and dispersion of solid particles in water and viscous fluids are pertinent factors in many environmental and industrial processes, and as such, they are frequent subjects of intense research. Mixing and dispersion of sand jets and particle clouds in water have been studied to design and optimize wastewater dredging disposal and marine bed capping (Rajaratnam and Mazurek, 2006; Azimi et al., 2014). Motion of dispersed particles in viscous fluids is of great interest in design and operation of oil-sand tailing ponds and to study the evolution of Earth and other terrestrial planets (Deguen et al., 2011, 2014). One particular feature of interest in the motion of particle cloud in viscous ambient fluid is magma flows wherein molten particles flow as clusters (Giraut et al., 2014; Mohammadidinani et al., 2017; Azimi, 2019). Magma is a high-temperature mixture of molten and semi-molten rocks, volatiles, and solids that can be modeled by a gravity-driven, two-phase flow with a considerable density difference as it enters into the ambient water. Natural restrictions make it difficult to study the behaviour of magma flows (i.e., high temperature and water vaporization in the vicinity of magma flows), but clusters of particles can be modeled by encapsulating sand particles with a thin layer of oil. In particular, oil sand tailing ponds have been noted as a recent practical example of the flow of sand jets and particle clouds through an immiscible interface (Miller et al., 2009; Mohammadidinani et al., 2017).

2.1 Uniform and Stratified miscible Ambient

Several studies have focused on the impingement of particles in uniform ambient and stratified miscible interface (Baines, 1975; Ching et al., 1993; Cotel and Breidenthal, 1997; Cotel et al., 1997; Larson and Jonsson, 1994; Noh et al., 1992; Shy, 1995; Noh, 2000; Bush et al., 2003).

Noh et al. (1992) investigated the dynamics of particles in particle clouds descending in uniform and stratified interfaces. It was observed that sedimentation is hardly affected by stratification when a particle cloud descends as a swarm of individually settling particles, but it is considerably influenced during the thermal regime where particle-particle interactions play an important role on motion and spread. Noh's experiments also showed a considerable increase in width and decrease in the frontal velocity of particle clouds passing through the stratified interface.

The evolution of particle clouds falling in homogeneous and stratified environments using the conservation of mass and momentum were modeled by Bush et al. (2003). They used normalized buoyancy $F_B/x^2u_\infty^2$ as the controlling parameter to classify two-phase particle clouds into thermal and swarm regimes where $F_B=(\pi d_o^2/4)L_o c_o g(\rho_p-\rho_w)/\rho_w$ is the buoyancy force, L_o is the equivalent length of sand column, c_o is the initial sand concentration (i.e., c_o=0.6), g is the acceleration due to gravity, and ρ_p is the density of sand particles, respectively. They found that particle clouds settle as a thermal if $F_B/x^2u_\infty^2$ becomes greater than 0.1. For $F_B/x^2u_\infty^2<0.1$, particles descended as swarm with a settling velocity close to u_∞. It was also found that particle deposition in a stratified fluid depends on the thickness of the top layer, fall out height and the intrusion height of the thermal. For a homogeneous ambient, Bush and his colleagues showed a reasonable agreement with the experiments of Noh and Fernando (1993), that is, a particle cloud initially descends in the form of a thermal and then transforms to a swarm of individual particles that settle independently of the background ambient.

2.2 Liquid-Liquid Immiscible interface

Past experimental studies on the impingement jets in an immiscible interface were mostly about gas-liquid interfaces (Banks and Chandrasekhara, 1962; Cheslak et al., 1696; Evans et al., 1996; Qain et al., 1996) and less attention has been paid to liquid-liquid immiscible interfaces.

Friedman and Katz (1999) investigated the structures of a diesel fuel and water interface impinged with a water jet for a broad range of Richardson ($R_i=D_p(\rho_2-\rho_1)/\rho_2 U_p^2$) and Reynolds ($R_e=\rho_2 U_p D_p/\mu_2$) numbers where D_p is the pipe diameter, U_p is the average pipe velocity, ρ_1 is fuel density, and ρ_2 and μ_2 are water density and viscosity, respectively. They identified four distinct flow regimes depending upon the aspect ratio which is the ratio of deformation height and water jet diameter ($AR=h_1/D_i$) and Richardson number at the interface. It was also found that the transition between regimes was found to be exclusively R_i and to a lesser extend R_e dependent, whereas the onset of droplet formation was dependent on both R_i and R_e.

Webster and Longmire (2001) examined the behaviour of glycerin-water jets flowing into immiscible ambient. Two fluid combinations were studied with similar density ratios (ρ_j/ρ_o=1.18) where ρ_j and ρ_o are the jet and ambient fluid density but different viscosity ratios (μ_j/μ_o=0.152, 0.0077). They found that the forcing frequency and the viscosity ratio between fluids had a strong effect on the flow regime and pinch-off characteristics.

The dynamics of negatively buoyant jets in a homogenous immiscible ambient liquid was experimentally studied by Geyer et al. (2011). They injected a jet of dyed water into a rapeseed oil ambient to determine different flow behaviors based on non-dimensional parameters such as $R_e=\rho_w U_w D/\mu_w$, $R_i=Dg'/u_w^2$ and $W_e=\rho_w u^2{}_w D/\gamma$ where the subscript w stands for water, D is diameter of the nozzle, γ is the interfacial tension coefficient, and g' is the reduced gravity. Four different flow regimes were found as very stable, oscillatory, smooth, and wavy. It was also found that R_i is the most dominant parameter to determine the maximum penetration height of the buoyant jets, while the flow behavior was found to be mainly controlled by R_e and W_e.

2.3 Sediment-Laden Jets in Liquid

Literature search located a number of studies, experimentally and numerically, on the behavior of sediment-laden jets in ambient fluid.

Nicolas (2002) conducted an experimental study of gravity-driven jets of dense suspensions falling in a stagnant miscible liquid. He observed four different flow regimes referred to as stable jet, unstable jet with blobs formation, spiral jet with dispersion, and atomized jet. Particle Reynolds number, $R_p=(d_p/d_o)R_o$ was found to be a suitable criterion to characterize the flow behavior as well as the dispersion phenomenon where d_p/d_o is the tube-to-particle diameter ratio and R_o is the Reynolds number at the nozzle outlet. The tube diameters d_o were ranging from 4 to 8 mm to form a jet. He found that a capillary-like instability with formation of blobs and dispersion of the jet particles occur when a particle Reynolds number is over unity. He also found that the hydrodynamics bonds between particles are strong enough to keep the jet in a cylindrical shape. He compared the shape of a liquid-into-liquid jet (dyed glycerol into salted water) to a suspension jet (polystyrene particles into water) and observed cylindrical and very stable shape for the liquid-into-liquid jet and found that the contrast of viscosity cannot explain the suspension jet instability.

Cai et al. (2012) studied the sand jet behavior in a non-Newtonian viscoplastic fluid. They investigated deformation regimes of sand jets by depositing circular sand jets vertically into viscoplastic fluids, known as Laponite gel. They found various regimes such as dripping, jetting, and mixing for sand jets. These regimes were proportional to the impact velocity, size of the jet, and viscosity of the fluid. For less viscous gel, they found that when the inertial force dominates the viscous force ($R_{ep}>1$), the cylindrical sand jet mixes with viscous fluid; otherwise, the cylindrical shape of the sand jets is maintained while the sands travel in the viscous fluid.

Moreover, for the fluid with high viscosity, they observed that the sand jet settles in the form of drops.

Hall et al. (2010) presented experimental measurements of particle velocity and concentration within sand and slurry jets in quiescent water. They measured sand-phase velocity and concentration of slurry jets with small particle size (D_{50}=206 μm). They also investigated the dynamics of sand and slurry jets with an initial sand volume fraction of c_o=0.6. The initial volumetric concentrations of slurry jets varied from 0.055 to 0.124. Nozzle diameters of d_o=6.1 and 10.3 mm, and d_o=15.5 and 9 mm were used to form sand jets and slurry jets, respectively. The concentration and velocity were found to have self-similar Gaussian profiles. It was found that the centerline sand concentration decayed with a −5/3 power relation and the centerline particle velocity decayed with a rate of −1/3, similar to a single-phase plume. They found that the terminal velocity varied depending on sand mass flux and the spreading rates of the jets varied with the particle Froude number $F_r=u_o/[gd_o(\rho_s-\rho_w)/\rho_w]$ where ρ_s and ρ_w are the density of sand and water, respectively, d_o is the jet diameter, u_o is the average velocity at the water surface and g is the gravitational acceleration.

Azimi et al. (2011) conducted a Computational Fluid Dynamics modeling to investigate the effect of particle size on the characteristics of sand jets in water. Sand phase axial velocity and concentration in different locations obtained from the numerical simulation were compared with and was in a good agreement with experimental measurements of Hall et al. (2010). It was found that the turbulent kinetic energy of the water phase decreases with increasing particle size. Far away from the nozzle, the maximum water phase turbulent kinetic energy of the sand jet with 210-μm particle size was found to be 6.7 and 11.5% higher than the sand jets with particles sizes of 460- and 780-μm, respectively.

Chapter 2 Literature Review

The behavior of sand jet front and its associated fluid motion for a wide range of nozzle diameter and sand particle size was studied by Azimi et al. (2012a). Two series of experiment were conducted to study the effect of nozzle diameter (series A) and particle size (series B). For first series, four nozzle sizes were used with nominal diameters of 2, 3, 4.75, and 10 mm to study the effect of nozzle size. Fine blasting sand particles with a D_{50} of 206 μm and density of ρ_p=2540 kg/m3 were used in these experiments. The sand particle sizes were considered uniform. For series B, sand particles with a density of ρ_p=2540 kg/m^3 passed through a series of sieves ranging from 125 to 589 μm and three classes were identified. The frontal shape of the jet was classified according to their R_{ep}. They found that for R_{ep}<10 jet acts as particle thermal, for R_{ep}~10, particles form a bowl shape and finally for R_{ep}>10, a narrow frontal head was observed due to the faster rate of the jet penetration in water. The analysis of the frontal velocity of the sand jets showed that larger particles produced higher frontal velocities. This velocity was found to be a function of nozzle diameter and particle size. They also observed that the velocity ratio (u_f/u_∞) drops continuously after releasing from the nozzle and reaches a plateau at x/d~200 which is called particle cloud fall velocity $u_{f\infty}$. For small particle sizes, the jet front terminal velocity was as large as 5 times of the individual settling velocity. The effect of particles on the frontal velocity of turbulent jets was found to be negligible close to the nozzle. However, along with the jet axis, it was found that when the larger particle sizes were used, the particle cloud settling velocity became larger.

The characteristics of slurry jets in water were numerically investigated by Azimi et al. (2012b). Prediction of the main characteristics of the jet such as axial and radial velocities, and particle concentration were found to be in a good agreement with laboratory measurements. They also studied the effect of sand particles on slurry jet spreading rate, axial velocity decay, decay of

concentration and turbulence properties, and the results were compared with the corresponding single-phase water jets and plumes. It was found that the width of slurry jets grows linearly from the nozzle up to a certain distance and then the growth rate became non-linear. At particle volume concentrations larger than 2.4% or with particle sizes larger than 505 μm, the spreading rate of sand phase was found to be only about one third of that of the water phase. Empirical formulations were also proposed to describe the effects of controlling parameters on the axial velocity decay of slurry jets.

2.4 Release Height and Release Angle

In gravity-driven particle flow, the initial velocity of particles is controlled by the density difference between sand particles and the ambient, as well as the ratio of the nozzle size to the particle diameter d_o/D_{50}. In addition, the initial velocity of sand particles can be controlled by adjusting the release height and release angle. In land reclamation and dredging, it is common to release sand particles from a certain height above the water surface, vertically or obliquely (Zhao et al., 2012; Moghadaripour et al., 2017a, 2017b). Under these conditions, sand particles accelerate as they fall through the air and gain significant momentum before impacting the water surface suggesting the hydrodynamics of particle clouds can be significantly influenced by the air release height as well as release angle. Most recent research studies assessed the underwater release of sediments in both stagnant and cross-flow ambient conditions (Rugabber, 2000; Gu and Li, 2004; Gensheimer et al., 2012); however, the effect of air release height and release angle has not been completely studied.

Zhao et al. (2012) investigated the impact of air release height on the underwater behavior of sediment thermals in a stationary body of water. A constant of 8.4 g of dry glass beads with the density of 2500 kg/m^3 and the median diameter of 0.51 mm was released through a cylindrical

container with the diameter of 20 mm. The L/d_o ratio of their experiments was 0.5 and the release height ranged from 20 mm to 100 mm. Three different phases of motion were observed for the evolution of sediment clouds: initial acceleration phase, self-preserving phase, and dispersive phase which found to resemble the behavior of particle clouds released without initial momentum into stagnant water studied by Rahimipour and Wilkinson (1992). It was found that although increasing the air release height accelerated the transition between the phases, the growth rate of the thermal within the self-preserving phase had no dependency on the air release height.

Cai et al. (2010) studied the behaviour of circular sand jets from three nozzles with diameters of 19.2, 31.1, and 63.8 mm and sand with median sizes of 0.21, 0.38, and 0.52 mm in air. Dry sand was released from a conical hopper and the sand was maintained over a depth more than 0.4 m above the bottom of the hopper during all the experiments. They approximated the initial sand jet velocity as $0.68(gd_o)^{0.5}$ where d_o is the nozzle diameter. In all experiments, the front velocity increased continuously with distance from the nozzle. The particle size did not affect the speed of the front jet. It was also reported that the velocity of the jet front was related to the travel distance x using the V^2-V_o^2=2gx equation. A uniform velocity distribution was observed for the sand jet because diameter of the sand jet did not spread due to interaction with air. For the steady-state velocity, it was found that the sand followed the same trend as the frontal velocity. Moreover, the diameter of the sand jet decreased while traveling in the jet direction until it reached to a constant at about $120d_o$ from the nozzle.

Moghadaripour et al. (2017a) carried out laboratory experiments to study the effects of aspect ratio L/d_o, particle size D_{50}, release angle θ, and release height h on the dynamics of oblique particle clouds in stagnant water. Particle size and release height were normalized to form Stoke number S_t and release number η, respectively. Four different release angles of θ=15˚, 30˚, 45˚, and 60˚ and

three different release numbers of η=8.5, 13.2, and 17 were selected to consider the effects of release angle and release height, respectively. It was found that the maximum horizontal displacement of the cloud front occurred at $3 \leq t/T \leq 5$ where t is evolution time and T is characteristic time scale, and it was independent of the aspect ratio. It was also observed that the trajectories of all particle clouds followed similar trend with no dependency on the aspect ratio. They proposed an exponential equation to simulate the trajectory of oblique particle clouds. It was found that the model predictions were in a better agreement for particle clouds with larger release angles of θ=45˚ and 60˚ and higher L/d_o.

2.5 Solid Phase in Immiscible Liquids

Other recent experiments focused on the dynamics of solid spheres (Aristoff and Bush, 2008; Tan et al., 2016; and Tan and Thomas, 2018) and sand jets (Mohammadidinani et al., 2017; Azimi, 2019) entering into a two-layer system of immiscible fluids.

The evolution of oily sand jets and cloud formation using different oil layer thicknesses, nozzle diameters, and sand masses was investigated by Mohammadidinani et al. (2017). They observed that the Reynolds number and the normalized oil thickness play the most important roles in the evolution of oily sand jets. The thin layer of oil forms sand clusters as a result of sand passing through the oil layer. The oil layer eventually ruptures due to the release of entrapped air bubbles and the existing shear stress in the boundary of sand clusters. Three different bursting mechanisms – rear bursting, multiple bursting, and bifurcation bursting – were identified. It was found that the bursting type is directly related to the magnitude of the Reynolds number, whereas bursting time can be correlated with the Richardson number. The presence of an oil layer reduces the initial velocity of particle clouds so they can be treated as a damper in the system.

Tan and Thomas (2018) studied the influence of an upper layer liquid on the phenomena and cavity formation associated with the entry of solid spheres into a stratified two-layer system of immiscible liquids. Various flow phenomena were generated based on the impact velocity called deep seal, shallow seal, oil trail, and vortex cloud. Shallow seal (cavity pinching off close to the water surface) was observed for the entry of steel sphere at a relatively high velocity in to a two-layer oil-water system. It was found that further increases in the impact velocity of the sphere led to the shallow seal occurring immediately after the sphere entry, resulting in the formation of relatively small cavities and did not experience the deep seal (cavity pinching off at significant depth below the water surface). They also defined the shallow seal transition velocity u_{ss} as the impact velocity above which the shallow seal appears with respect to the Bond number ($B_o=\rho_o g D^2/\sigma$) and Webber number ($W_e=\rho_o u_{ss}^2 D/\sigma$) of the oil layer where ρ_o and σ are density and surface tension of oil, respectively, D is sphere diameter, and g is acceleration due to gravity.

The motion of particle clouds in viscous fluids was experimentally investigated by Azimi (2019). The rear separation was observed for particle clouds and was classified into partial, moderate, and complete separation. It was found that the time and the location of rear separation were linearly correlated with the aspect ratio L/d_o. It was also observed that the secondary separation of particle clouds occurred for $L/d_o \geq 35$. The cloud width was found to grow with an increasing aspect ratio; however, it never reached the spreading rate of particle cloud in water.

3 Dimensional Analysis

The motion of vertical and oblique sand jets passing through an immiscible layer is controlled by properties of the background fluids, physical characteristics of sand particles, and initial release conditions. Predicting the fate of the instantaneously released sediments in stratified oil-water system requires knowledge of how various physical factors contribute to the formation process of sediment clouds. Frontal width and velocity of sand jets passing through the oil-water interface can be formulated as:

$$w,u_f = f_1\left(m,d_o,h,\theta,u_o,\rho_w,\rho_{oil},\rho_s,\mu_w,\mu_{oil},D_{50},h_{oil},c_o,g,t\right) \tag{3.1}$$

where m is the mass of sand particles, d_o is the inner diameter of nozzle, h is the air release height, θ is the release angle, u_o is the velocity of sand particles after the interface, ρ_w, ρ_{oil}, and ρ_s are the densities of water, oil and sand particles, respectively, μ_w and μ_{oil} are the dynamic viscosities of water and oil, respectively, D_{50} is the mean particle size where 50% of particles are greater than D_{50}, h_{oil} is the thickness of oil layer, c_o is the initial volumetric concentration of particles, g is the acceleration due to gravity, and t is time.

A narrow range of particle size (i.e., 0.250 mm$\leq D_{50} \leq$0.297 mm) was used in this study to reduce the number of unknown variables. The selected range of particle sizes is within the average particle size range being used in the literature. Mass of sand particles m can be converted into a length scale L, where L is the length of the pipe filled up with sand particles to form an aspect ratio of L/d_o (Moghadaripour et al., 2017a, b; Mohammadidinani et al., 2017) and can be formulated as:

$$L = \frac{4m}{c_o \pi \rho_s {d_o}^2} \tag{3.2}$$

Chapter 3 Dimensional Analysis

For certain particle size, the frontal velocity of turbulent thermals is a function of buoyancy B and distance from the water surface to the front of particle cloud y (Batchelor, 1954; Morton et al. 1956) with a scaling relationship described as:

$$u_f \sim B^{1/2} y^{-1} \tag{3.3}$$

A length scale l can be introduced using the particle settling velocity of individual sand particles u_∞ to include the effect of particle size D_{50} as:

$$l = \frac{B^{1/2}}{u_\infty} \tag{3.4}$$

Similarly, a time scale T can be used to normalize the evolution time as:

$$T = \frac{B^{1/2}}{u_\infty{}^2} \tag{3.5}$$

where the terminal settling velocity of individual particles can be estimated using Stokes formula as:

$$u_\infty = \frac{g(\rho_s - \rho_w) D_{50}{}^2}{18\mu_w} \tag{3.6}$$

Particle settling velocity is a non-linear function of particle size which can also be estimated by either using an empirical equation (Dietrich 1982) or Haywood tables (Holdich 2002).

The velocity of sand particles at the nozzle exit can be related to nozzle diameter using the orifice equation $u_n=c_1(gd_o)^{1/2}$ where c_1 is a constant coefficient. Cai et al. (2010) proposed a coefficient of 0.68 for $d_o/D_{50}>40$ and 0.6 for $d_o/D_{50}<40$. In the study conducted by Rao et al. (2008) a value of 0.74 was reported for c_1. The free-falling velocity of a single particle ignoring the drag force is given by $u_g=(2gh)^{1/2}$ where h is the air release height. Considering the structure of free-falling velocity of a single particle and assuming that the air release height plays an important role in the frontal velocity of sand jets, a non-dimensional air release height can be formed as:

$$\eta = \frac{2gh}{u_n^{\,2}} \tag{3.7}$$

The defined non-dimensional air release height can be described as a function of air release height and nozzle diameter as:

$$\eta = f_2(h, d_o^{\,-1}) \tag{3.8}$$

Based on dimensional analysis, Reynolds number R can be defined to describe the balance between the inertia and viscous forces. Effect of Reynolds number on characteristics of jet flows was found to be significant (Webster et al., 2001; Nicolas, 2002; Azimi et al., 2012a; Azimi et al., 2012b). Reynolds number can for oily sand jets be formed as:

$$\mathrm{R} = \frac{u_i d_o (\rho_s - \rho_{oil})}{\mu_{oil}} \tag{3.9}$$

Considering air resistant, the impact velocity of sand particles could be formulated as $u_i = c_2 u_g$ where c_2 is a constant. Using the free-falling velocity of a single particle to express the impact velocity of sand particles in Eq. (8), indicates that Reynolds number can be expressed as a function of air release height and nozzle diameter as:

$$\mathrm{R} = f_3(h^{1/2}, d_o) \tag{3.10}$$

Therefore, by grouping controlling parameters in Eq. (1), dynamics of oily sand jets can be studied using the following non-dimensional parameters as:

$$w, u_f = f_5\left(\frac{t}{T}, \frac{L}{d_o}, \eta, \mathrm{R}\right) \tag{3.11}$$

4 On the motion of vertical sand jets in stagnant immiscible liquids*

4.1 Experimental Setup

Experiments were performed in a 0.4 m square glass-walled tank with 1 m height in the hydraulic laboratory at Lakehead University. The experimental tank was filled with tap water with a temperature of T=23±0.5 °C, density of ρ_w=997.5 kg/m^3, and dynamic viscosity of μ_w=0.9321×10^{-3} Pa.s. The water in the tank was maintained at a constant level with a depth of 0.87 m for all experiments, using a drain valve. The water surface was covered with a 0.03 m layer of canola oil, h_{oil}, to form an immiscible layer. Density and dynamic viscosity of canola oil used in this research were measured by a Sigma 700 tensiometer (Biolin Scientific, Finland) and were ρ_{oil}=908 kg/m^3, and μ_{oil}=56.8×10^{-3} Pa.s, respectively.

A schematic view of the experimental setup and the coordinate system is depicted in Fig. 4.1. A steel pipe which was secured by an adjustable joint frame was held vertically above the tank and a brass nozzle having different diameters was attached to the bottom of the pipe. The pipe was aligned with the centre of the tank to avoid any boundary effect on the evolution of sand jets. A quasi-instantaneous sliding plug was adopted to simulate a point release of sand particles and to minimize the jet disturbance and the release error. Sand particles were poured uniformly-distributed in the pipe and were released instantaneously by sliding the plug. The release height from the oil layer surface h was adjusted at 0.2, 0.4 and 0.6 m using the adjustable frame. Three nozzle sizes with a nominal diameter of 8, 12 and 16 mm were used in these experiments. Sieve analysis was employed to select sand particles. The collected particles from two sieve sizes of D_{50}=0.250 mm (i.e., sieve #60) and 0.297 mm (i.e., #50) were mixed and used in this study with a nominal diameter of 0.275 mm. The uniformity coefficient of particles was calculated for the particle sample with a value of 1.31. Sand particles were considered uniform since the geometric

*A part of this chapter was submitted to the International Journal of Multiphase Flow

standard deviation $\sigma_g=D_{84}/D_{50}=D_{50}/D_{16}$ was smaller than 1.35 (Breusers and Raudkivi, 1991). The sand particles had a density of ρ_s=2540 kg/m^3, and an averaged unpacked sand concentration of c_o=0.6. Different masses of dry sand particles ranging from 5 to 30 g were selected to form a wide range of L/d_o ratio from 1.02 to 19.59. Experimental details and non-dimensional parameters are listed in Table 4.1.

Three minutes of relaxation time was allowed between each experiment to dampen oil-water interface fluctuations. During the relaxation time, all the oil and water droplets from the previous experiment were settled; thus, there was no memory impact on the next experiment. Since a small amount of oil was dragged by sand particles during the experiments, the thickness of oil layer was measured after each test, and a suitable volume of oil was added to keep the oil layer at the original level.

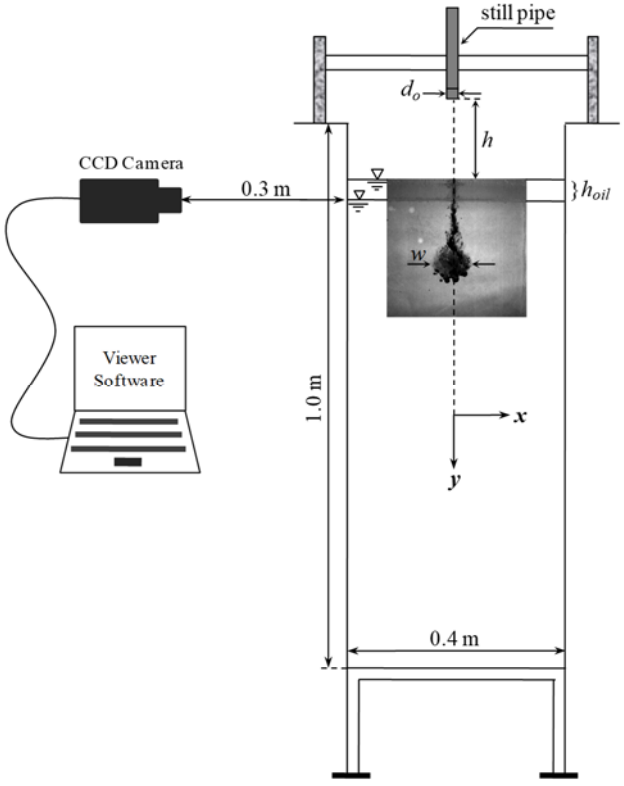

Figure 4.1 Schematic of the Experimental setup and coordinate system

Table 4.1 Experimental details of vertical sand jets passing through immiscible interface

Test no.	h (m)	d_o (mm)	m (g)	L (m)	L/d_o	u_n[a] (m/s)	R	η
1	0.2	8	5	0.065	8.16	0.19	433	108.1
2	0.2	8	8.5	0.111	13.88	0.19	433	108.1
3	0.2	8	10	0.131	16.33	0.19	433	108.1
4	0.2	8	12	0.157	19.59	0.19	433	108.1
5	0.2	12	10	0.058	4.84	0.23	649	72.1
6	0.2	12	15	0.087	7.26	0.23	649	72.1
7	0.2	12	20	0.116	9.67	0.23	649	72.1
8	0.2	12	25	0.145	12.09	0.23	649	72.1
9	0.2	16	5	0.016	1.02	0.27	865	54.1
10	0.2	16	10	0.033	2.04	0.27	865	54.1
11	0.2	16	15	0.049	3.06	0.27	865	54.1
12	0.2	16	30	0.098	6.12	0.27	865	54.1
13	0.4	8	5	0.065	8.16	0.19	612	216.3
14	0.4	8	8.5	0.111	13.88	0.19	612	216.3
15	0.4	8	10	0.131	16.33	0.19	612	216.3
16	0.4	8	12	0.157	19.59	0.19	612	216.3
17	0.4	12	10	0.058	4.84	0.23	918	144.2
18	0.4	12	15	0.087	7.26	0.23	918	144.2
19	0.4	12	20	0.116	9.67	0.23	918	144.2
20	0.4	12	25	0.145	12.09	0.23	918	144.2
21	0.4	16	5	0.016	1.02	0.27	1223	108.1
22	0.4	16	10	0.033	2.04	0.27	1223	108.1
23	0.4	16	15	0.049	3.06	0.27	1223	108.1
24	0.4	16	30	0.098	6.12	0.27	1223	108.1
25	0.6	8	5	0.065	8.16	0.19	749	324.4
26	0.6	8	8.5	0.111	13.88	0.19	749	324.4
27	0.6	8	10	0.131	16.33	0.19	749	324.4
28	0.6	8	12	0.157	19.59	0.19	749	324.4
29	0.6	12	10	0.058	4.84	0.23	1124	216.3
30	0.6	12	15	0.087	7.26	0.23	1124	216.3
31	0.6	12	20	0.116	9.67	0.23	1124	216.3
32	0.6	12	25	0.145	12.09	0.23	1124	216.3
33	0.6	16	5	0.016	1.02	0.27	1498	162.2
34	0.6	16	10	0.033	2.04	0.27	1498	162.2
35	0.6	16	15	0.049	3.06	0.27	1498	162.2
36	0.6	16	30	0.098	6.12	0.27	1498	162.2

[a] Velocity at nozzle exit was calculated based on $u_n=c_1(gd_o)^{1/2}$ where c_1=0.68 for d_o/D_{50}>40 and 0.6 for $d_o/D_{50}\leq 40$

Two different types of light sources were employed for boundary detection and recording of sand jet evolution. The background ambient was illuminated using continuous laser light sheets with a thickness of 3 mm, a power of 1 w, and a wavelength of 532 nm (Laserwave, G2000, China). The laser sheets were launched from the sides to illuminate the jet. For boundary detection and jet width measurement, a 500 w T3 halogen bulb was placed behind the backside wall of the tank which was covered with a sheet of white paper. The evolution of sand jets passing through the oil-water interface was recorded using a high-speed camera (Photron-FASTCAM, 1024PCI-100KC) with a resolution of 1024×1024 pixels. The camera was equipped with a 15-55 mm AF-S Nikkor, 1:3.5-5.6 GII (Nikon, Japan) lens to capture images. Raw images were captured with a frame rate of 250 frames/second and a shutter speed of 0.004 sec. Photron FASTCAM Viewer software was used to collect the images. The camera lens was located at the oil-water interface level and perpendicular to the tank with a distance of 0.3 m. The area of interest was a rectangle of 0.25 m × 0.20 m and located below the water surface. Obtained images were turned to negative for better visualization. Images were imported to AutoCAD to determine frontal width and velocity of sand jets. Horizontal and vertical rulers were placed in the tank to detect any image distortion. Also, the rulers were used as scales to scale the images and measure the displacement and the width of sand jets.

4.2 Experimental Results

4.2.1 Characteristics of sand jets in air

Fig. 4.2 shows the dependence of the frontal velocity of sand jets in the air u_i on the air release height h. Provided that the drag force is negligible, the sand particles will have an acceleration of g, thus $u_i=gt$, and the velocity of jet front will be related to the air release height as $u_i=(2gh)^{1/2}$ which is equal to the free-falling velocity of the single particle neglecting air resistance u_g

(represented with solid line in Fig. 2). Our observation revealed that the frontal velocity of sand jets was affected by the drag force and was found to be $0.95u_g$ for the air release height ranging from 0.2 to 0.6 m. It could be explained by the fact that the porosity of particles caused the air resistance not to be ignorable and reduced the frontal velocity by 5% compared to u_g. It was found that increasing the mass flow rate of particles had no impact on the frontal velocity of sand jets in the air. Observations by Cai et al. (2010) showed that the jet front was being accelerated with negligible air resistance and the size of the sand particles did not appear to affect the velocity of the jet front.

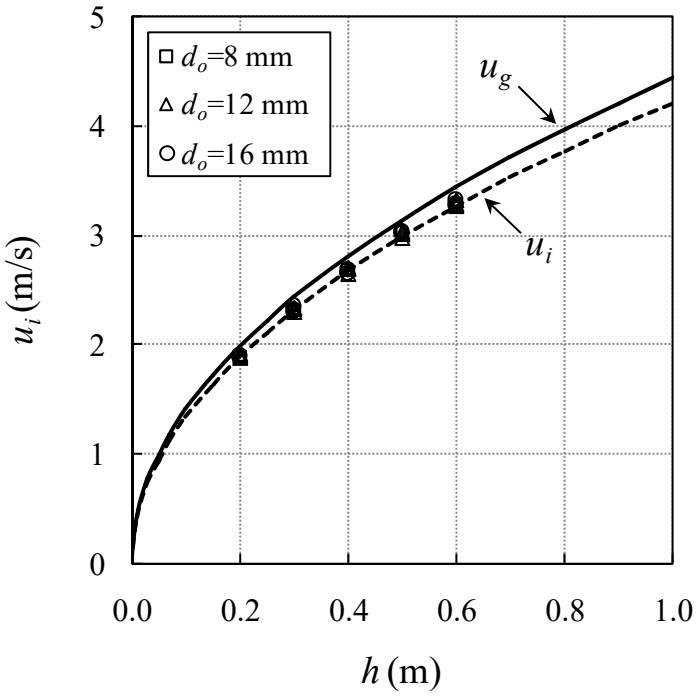

Figure 4.2 Relationship between frontal velocity of sand jet in the air and release height

The relationship between the mass flow rate of sand particles and the nozzle size is shown in Fig. 4.3. The mass flow rate of particles from an orifice under the gravitational conditions is

dependent on the orifice diameter and independent of the particle head if the height is large enough (Ogata et al., 2001). Beveloo et al. (1961) introduced an empirical equation for circular orifice as:

$$\dot{m} = 0.538\rho_b\left(d_o - 1.4D_{50}\right)^{5/2}\sqrt{g} \tag{4.1}$$

where ρ_b is the bulk density of the powder and g is the acceleration due to gravity. In this study a narrow range of particle size was used; therefore, the effect of particle size was excluded from the calculation of mass flow rate and Eq. (9) was rewritten as:

$$\dot{m} = 0.538\rho_b\left(d_o\right)^{5/2}\sqrt{g} \tag{4.2}$$

which was found to be in a better agreement with the present measurements with the average error of ±3%.

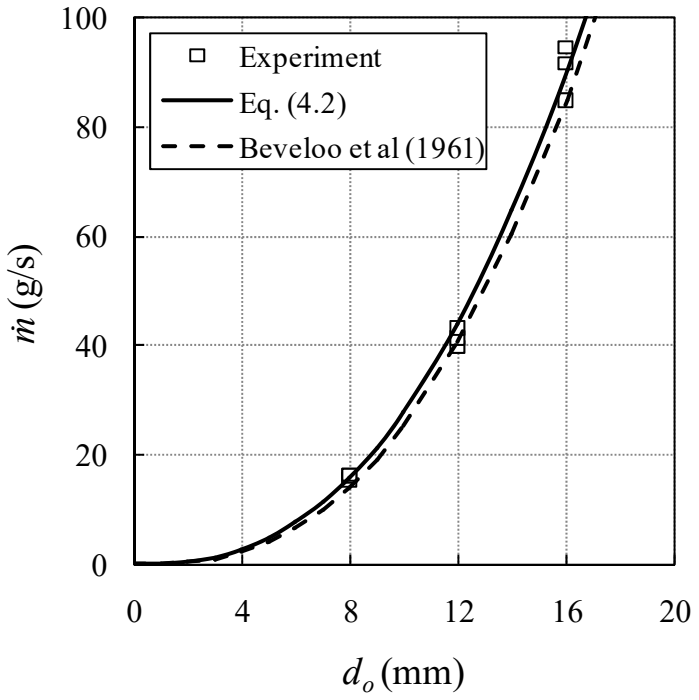

Figure 4.3 Relationship between mass flow rate of sand jet and nozzle diameter

Chapter 4 On the motion of vertical sand jets in stagnant immiscible liquids

It is important to understand at which diameter sand jets penetrate the oil layer. Once this diameter is determined, it can be used to calculate shear stress in the oil layer. Observations by Cai et al. (2010) on sand jets in air revealed contractions near the nozzle exits whereas no obvious spreading was observed in the far field. However, Ogata et al. (2001) found that powder jet in air diffuses with the mean angle of 1° far from the nozzle exit. This diffusion is very small relative to that for a single-phase turbulent jet, which is between 12° and 15°. Fig. 4.4 shows the relationship between the nozzle diameter d_o and the diameter of sand jet in air d_j. As can be seen, the diameters of sand jets in air were found to be smaller than the nozzle diameters. Experimental observation indicated that a linear formulation could appropriately describe the relationship between the sand jet diameter in air and the nozzle diameter as

$$d_j = 0.5 d_o - 0.813 \tag{4.3}$$

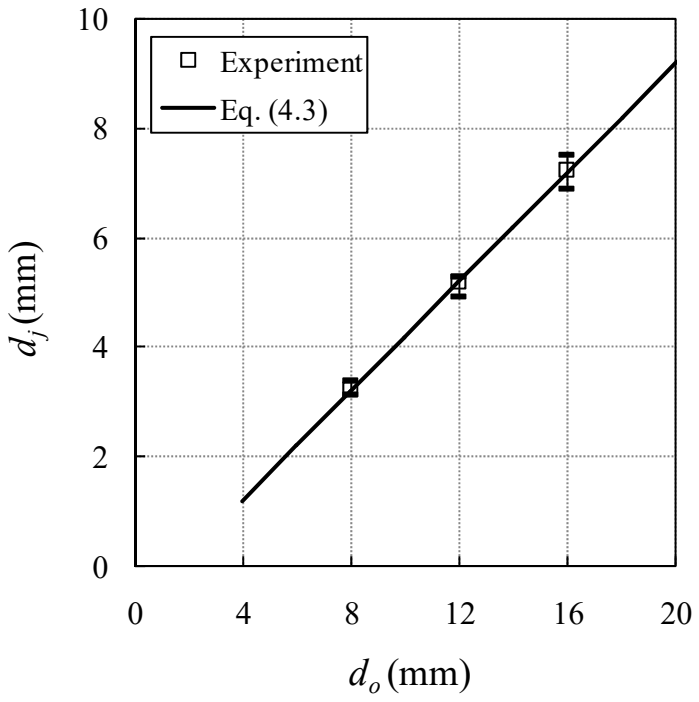

Figure 4.4 Relationship between diameter of sand jet in the air and nozzle diameter

Overbars shown in Fig. 4.4 indicated the uncertainty for measurements of sand jets in air in this study. No change in the jet diameter was observed in the range of air release height in this study within the experimental error.

4.2.2 Evolution of oily sand jets

The effects of nozzle diameter d_o, air release height h, and aspect ratio L/d_o on the evolution of oily sand jets passing through the immiscible interface are studied in this section using image analysis technique. A non-dimensional time scale t^* was defined to study the transitional effects of jets evolution where at t^*=1 all particles passed through the oil layer. This time scale was measured using images captured by the high-speed camera. The number of images from the beginning of a test to the image showing all particles are in water was counted to determine t^*.

Each image shows a time lag of 4×10^{-3} s from the onset of release. Fig. 4.5 illustrates the evolution of oily sand jets released from three different nozzle diameters d_o =8, 12, and 16 mm with a constant air release height of h=0.2 m for the largest aspect ratio L/d_o for each nozzle size (i.e., 19.59, 12.09, and 6.12). For d_o =8 mm (Fig. 4.5a), a bar-shape jet was formed at the early stage of evolution t^*<0.06. It was followed by destabilization of oily sand jets and hook formation in the jet front as a result of velocity difference between sand particles in air and the frontal head in water for 0.06<t^*<0.25. Formations of the bar- and hook-shape are consistent with observations of Nicolas (2002) and Mohammadidinani et al. (2017). The current results showed that the momentum introduced by the air released height accelerated the transition of the bar-shape to hook-shape pattern compared to Mohammadidinani et al.'s (2017) observations. Measurements of Zhao et al. (2012) showed a faster transition between two initial phases of the formation of sediment thermals in water as the air release height increased. A torsion front with an unstable sinuous-path tail was observed for 0.25<t^*<0.75 due to buoyancy difference. These instabilities

resulted in air bubbles escape from the tail part of oily sand jets. As particles descended further (t^*>0.75), a thin layer of oil covering sand particles was ruptured and the jet front was divided into a number of encapsulated clusters of particles with air bubbles. No cloud bursting was observed for the evolution of oily sand jet released from a nozzle of d_o =8 mm.

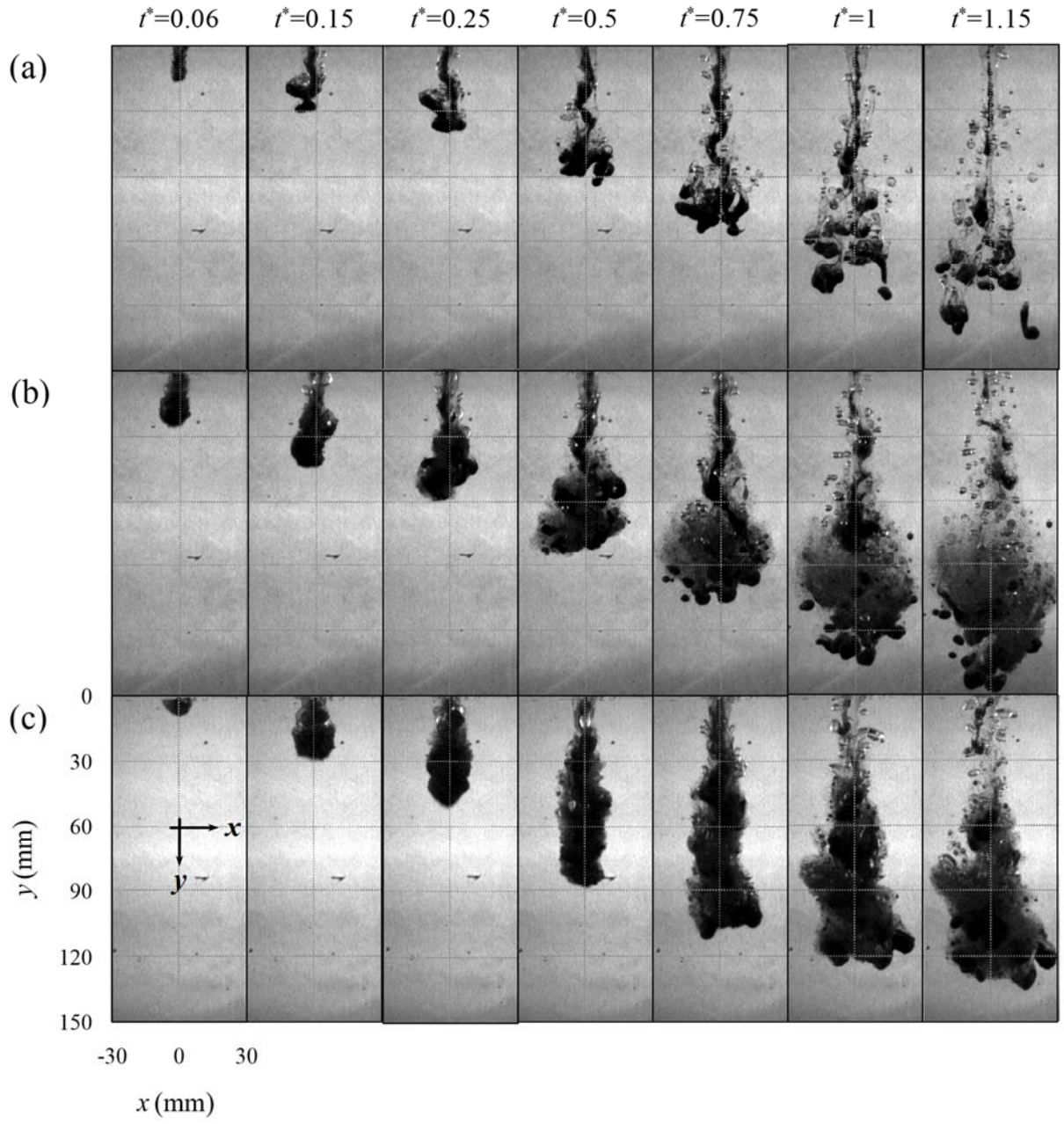

Figure 4.5 Effect of nozzle diameter on the evolution of oily sand jets for h=0.2 m at different non-dimensional time scale t*: (a) d_o=0.008 m; (b) d_o=0.012 m; and (c) d_o=0.016 m

Fig. 4.5b shows the evolution of oily sand jet for d_o =12 mm and h=0.2 m. It can be clearly observed that the oily sand jet expanded while it was surrounded by a thin cover of oil layer (t^*<0.15) and started to burst and disperse laterally as it moved downward (0.15<t^*<0.5). A physical interpretation is that a bigger nozzle diameter accelerates the onset of turbulence of ambient fluid and generates higher shear stress between the oil layer and the surrounding water, resulting in a rupture of oil layer covering sand particles and a burst of particle cloud. Consequently, sand particles descended as a mixture of individual particles and encapsulated groups of particles with air bubbles (t^*>0.75). Similar to d_o =8 mm, a sinuous-path tail was observed for 0.25<t^*<0.75 whereas no hook-shape pattern occurred.

The evolution of oily sand jet for d_o =16 mm and h=0.2 m is shown in Fig. 4.5c. As can be seen, the oil layer covering sand particles was ruptured at the very beginning stage of the evolution. It can be explained by the fact that the jet was fast enough (shear flow was large enough) not to allow the oil layer to encapsulate sand particles. As a result, the peripheral particles were torn away from the dense suspension and the jet descended with almost uniform concentration. Moreover, lateral dispersion was less significant due to a larger momentum resulting from bigger nozzle size than that of d_o=12 mm. Contrary to former cases (d_o=8 and 12 mm), no tailing stem was formed for the evolution of oily sand jets for d_o =16 mm and fewer air bubbles were observed to be escaping from the jets.

Fig. 4.6 shows the effect of air release height on the evolution of oily sand jets for d_o=0.012 m at two different non-dimensional time scales t^*=0.5 and 0.75. Some cloud bursting was observed when sand particles were released from a height of h=0.2 m (Fig. 4.6a). In this case, sand particles descended as a mixture of encapsulated clusters of particles and individual particles. As the air release height increases, sand particles gain more momentum as they pass through the immiscible

interface. Therefore, the effects of the excess momentum overcome the impact of the oil layer resistance. In this condition, oily sand jets evolve like steady buoyant thermals and the sediment concentration becomes dilute (Fig. 4.6b and 4.6c. In addition, the higher air release elevation, the more instabilities and air bubble escape from the tailing section. It can clearly be observed that the overall growth of suspension jets was independent of the air release height within the experimental variations which is consistent with observations of Zhao et al. (2012) on the effect of air release height on the growth rate of the sediment thermals in water. One could explain it by the fact that the additional kinetic energy induced from the higher release height is mostly dissipated to rupture oil layer covering sand particles. Consequently, there is no energy left to have an impact on the overall growth of sand jets.

The effect of aspect ratio L/d_o on the evolution of oily sand jets was considered and no significant changes were observed but for the smallest aspect ratio with the value of L/d_o=1. In this case, the aspect ratio was not large enough to create jets as sand particles leave the nozzle exit. As a result, all the sand particles hit the oil surface, pass through the oil layer, and enter the water ambient as a cumulative mass. Fig. 4.7 depicts the evolution of oily sand jet for L/d_o=1 at different non-dimensional time scale t^*. As can be seen, particles descended as a single cluster in water. As the cluster traveled further in the tank, an oil layer was formed behind the cluster. The oil layer was stretched until it was ruptured from the rear of the cluster at t^*=3 which was found to be the commencement of air bubble escape from the rear of the cluster. This could be compared with the deep seal phenomenon observed by Tan and Thomas (2018) for the entry of solid spheres into a stratified two-layer system of immiscible liquids.

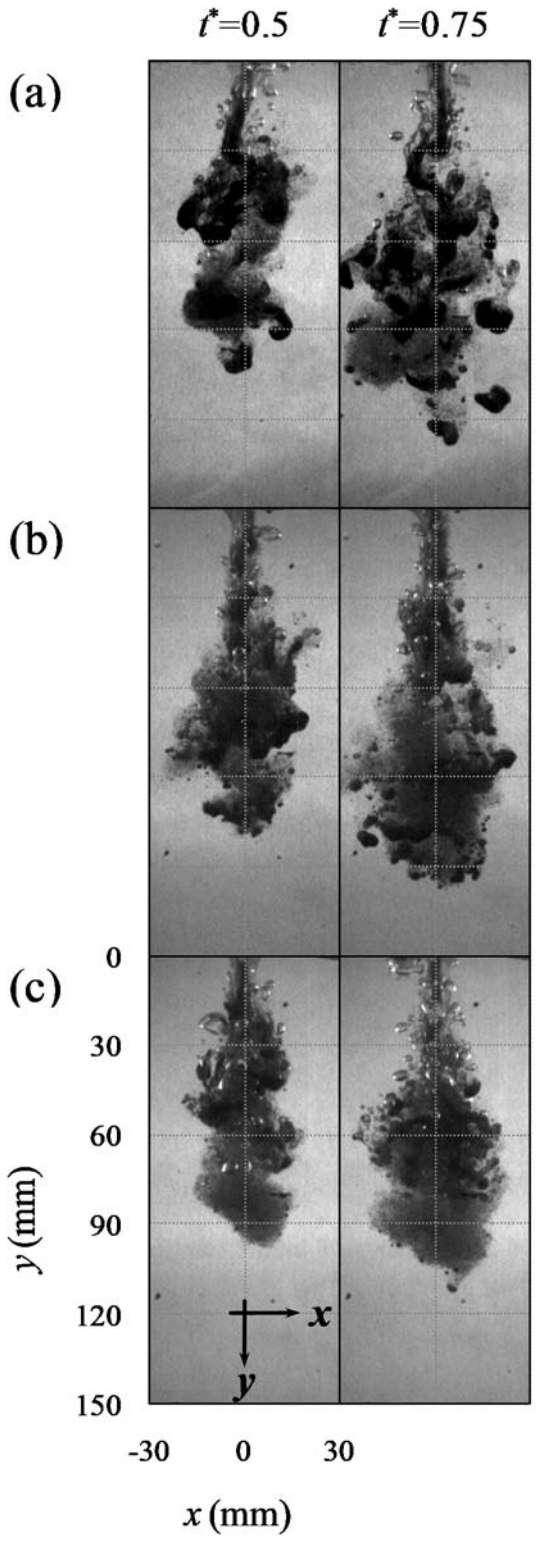

Figure 4.6 Effect of air release height on the evolution of oily sand jets for d_o =0.012 m at different non-dimensional time scale t^*: (a) h=0.2 m; (b) h=0.4 m; and (c) h=0.6 m.

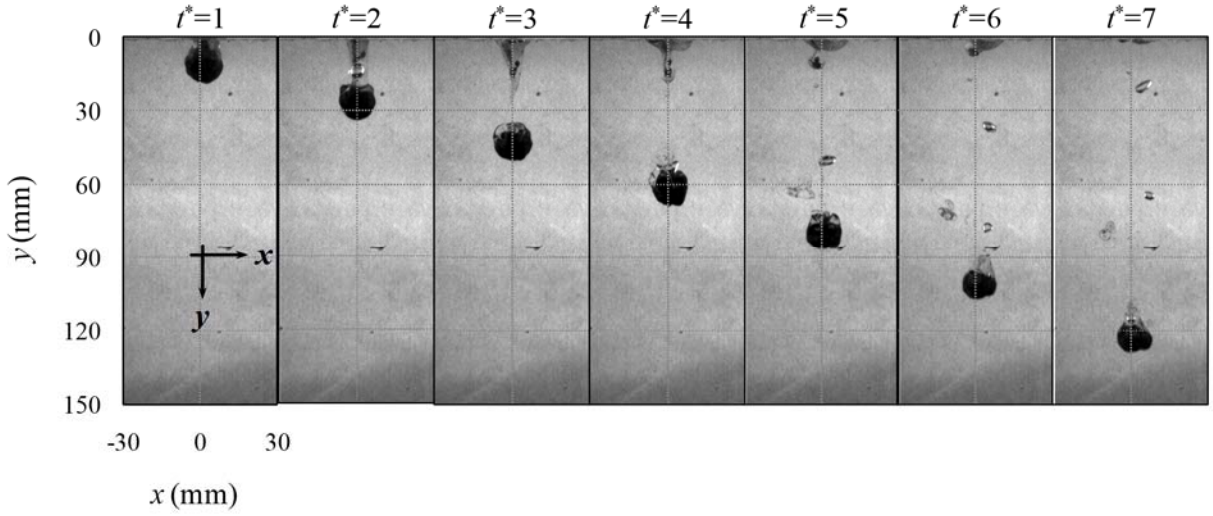

Figure 4.7 Evolution of oily sand jet for L/d_o=1 at different non-dimensional time scale t^*

4.2.3 Frontal width and velocity

The effects of initial parameters on the variation of the frontal width of oily sand jets are also considered in this section. Fig. 4.8 shows the effect of nozzle diameter on the growth of the frontal width of oily sand jets along the axis of the jets for m=10 g. Both the frontal width w and the distance from the water surface x were normalized by the nozzle diameter d_o. The growth rate of single-phase water jets which are pure momentum-driven flows (Turner, 1969) and the growth rate of thermals of heavy salt which represent pure buoyancy-driven flows (Lee and Chu, 2003) were included in Fig. 4.8 for comparison. Fig. 4.8a shows the variations of the normalized frontal width of oily sand jets discharging from 0.2 m height. As can be seen, nozzle size had no significant impact on the spreading rate of oily sand jets. Some instabilities were observed for y/d_o<6, but for y/d_o>6 the normalized frontal width increased linearly with y/d_o with the growth rates similar to single-phase buoyant thermals. Fig. 4.8b shows the growth of the normalized frontal width of oily sand jets issuing from a height of 0.4 m. As can be seen, the spreading rate increased by increasing

the nozzle diameter. For smaller nozzle size (L/d_o=16.3), the width rose linearly with y/d_o with a rate of 0.375 which was equal to the growth rate of pure buoyancy-driven flows. By increasing the nozzle size, the growth rate increased and reached 0.5 and 0.6 for d_o=12 mm (L/d_o=4.8) and d_o=16 mm (L/d_o=2.0), respectively. The excess momentum gained as a result of higher mass flow rate led to rupture of the oil layer surrounding sand particles and resulted in increasing the growth rate of the normalized width of oily sand jets. Similar to the former cases, irregularities were observed for y/d_o<6 as a result of fluctuations of the oil-water interface.

The effect of air release height on the variation of the frontal width of oily sand jets for L/d_o=16.3 is demonstrated in Fig. 4.9. For both shorter release heights (η=108.1 and 216.3) the normalized frontal width of oily sand jets revealed growth trends similar to single-phase buoyant thermals whereas, for the highest elevation (η=324.4), the spreading rate increased and reached 0.45. A physical interpretation is that sand particles gain more momentum as they are released from a higher elevation. This enhances instability of oily sand jets as they pass through the oil-water interface which results in enhancement of the growth rate of the normalized frontal velocity of oily sand jets. Mohammadidinani et al. (2017) reported that the spreading rates of oily sand jets were located between the growth rates of single-phase water jets and thermals of heavy salt for the release height of h≈0. Moghadaripour et al. (2017b) observed that the spreading rates of the normalized width of particle clouds in water were independent of the air release height for the particle size and the aspect ratio range studied in this paper.

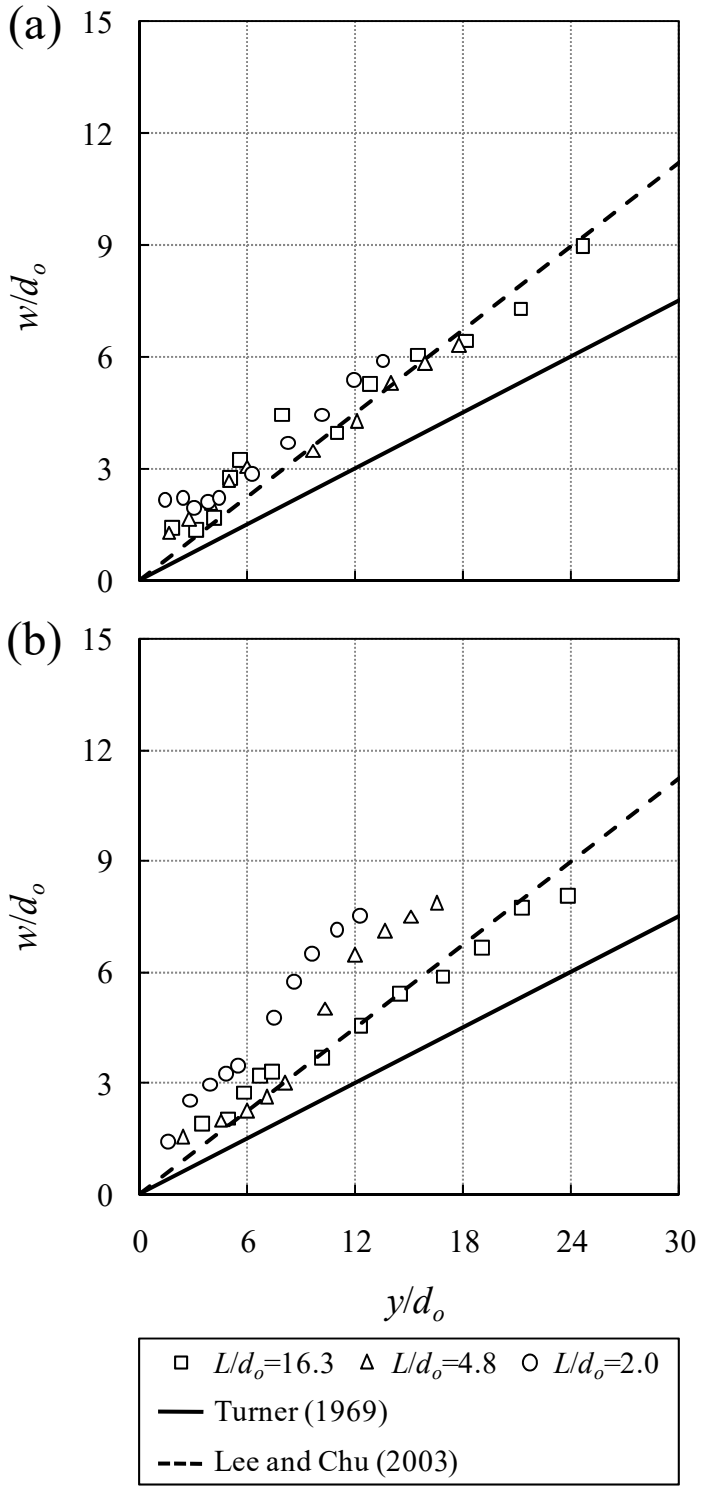

Figure 4.8 Effect of nozzle diameter on variation of normalized width of oily sand jets w/d_o with normalized distance y/d_o for m=10 g: (a) h=0.2 m; (b) h=0.4 m

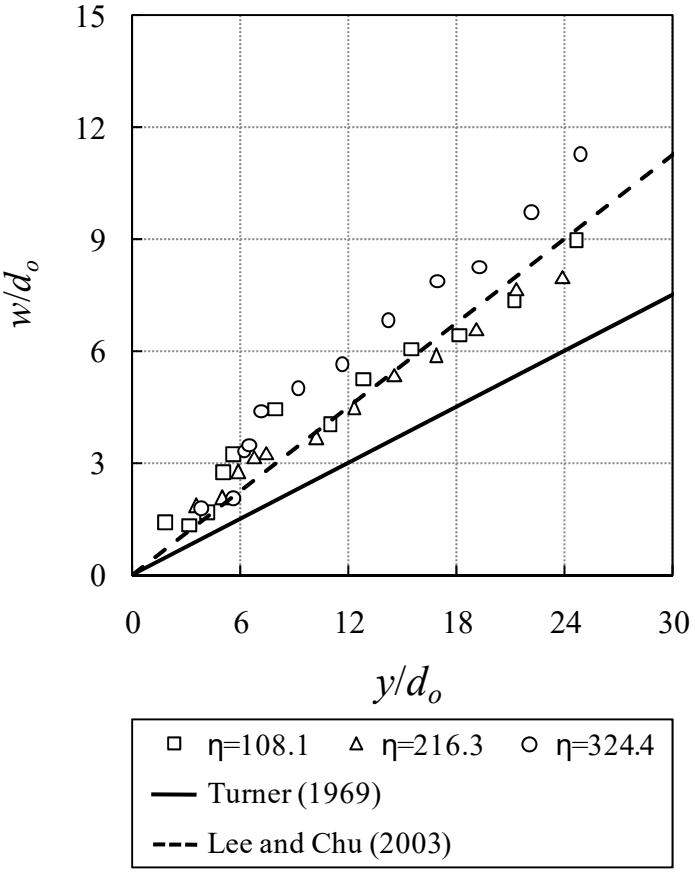

Figure 4.9 Effect of air release height on the variation of normalized width of oily sand jets w/d_o with normalized distance y/d_o for L/d_o=16.3

Variation of the frontal velocity of oily sand jets with the evolution time is shown in Fig. 4.10. The frontal velocity u_f was normalized with the initial velocity of sand jet in water u_o and the evolution time was normalized with the characteristic time scale T presented in chapter 3. Fig. 4.10a shows the variation of the normalized frontal velocity with the normalized time for jets issuing from an 8 mm nozzle at different release heights of h=0.2, 0.4, and 0.6 m. As can be seen, the normalized frontal velocity radically decreased and reached 0.4 times of its initial value at t/T=0.03 for all release heights. For h=0.2 m, no more drop in the normalized frontal velocity was observed after t/T=0.03, whereas the normalized frontal velocity decelerated with small gradient for the higher release elevations and reached a plateau 0.2 times of the initial value at t/T=0.06.

Doubling the air release height from 0.2 m to 0.4 m caused the normalized frontal velocity to reach a plateau two times later which roots in having higher kinetic energy as a result of issuing from higher elevation. On the other hand, by increasing the discharge height to 0.6 m, the change in the behavior of the normalized frontal velocity was not significant. It can be interpreted by the fact that the excess kinetic energy due to the higher discharge height was consumed during the rupturing process of oil layer encapsulating sand particles. Similar results were also observed for discharging sand particles from a 12 mm nozzle in Fig. 4.10b. Observations of Mohammadidinani et al. (2017) showed that the frontal velocities of oily sand jets in this regime decreased linearly with time and reached the minimum value of 0.75 u_o at $t/T \approx 0.05$ and then linearly accelerated due to the release of trapped air inside the frontal head which was caused by frontal detachment and multiple bursting. By comparing the results of Figs. 4.10a and b, it could be concluded that the normalized frontal velocity was not proportional to the nozzle size. Uncertainties were observed during the measurement of the frontal velocities of oily sand jets released from a 16 mm nozzle. Therefore, those calculations were excluded from this section.

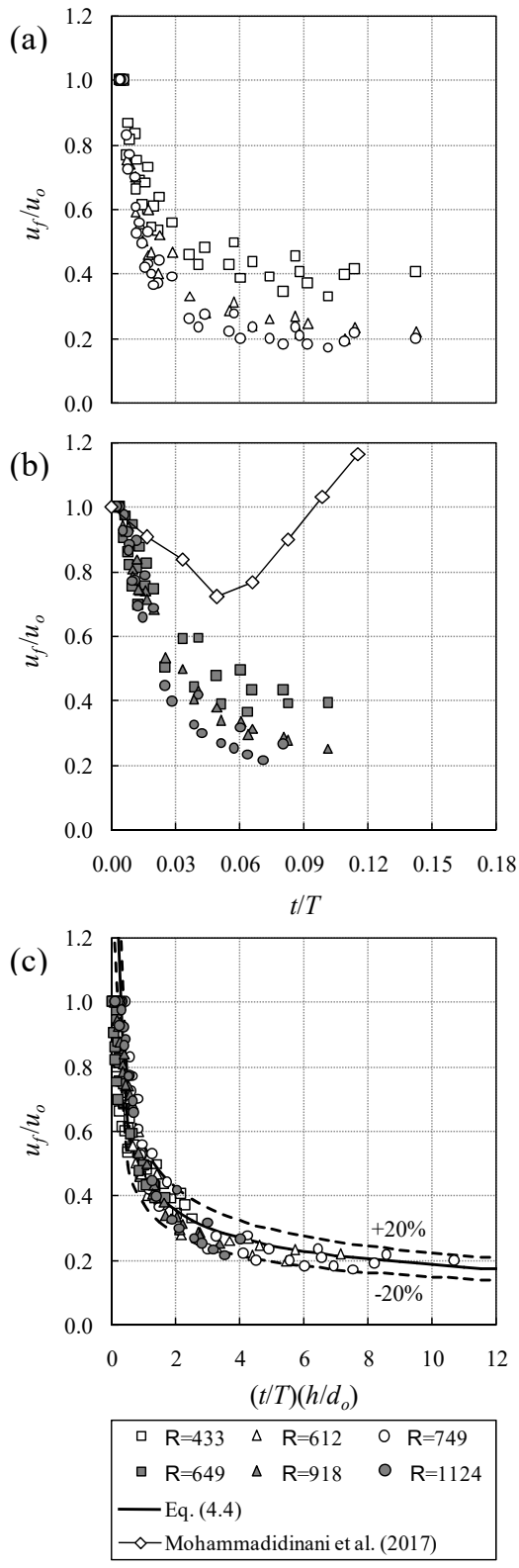

Figure 4.10 Variation of normalized frontal velocity u_f/u_o with normalized time t/T: (a) d_o=0.008 m; (b) d_o =0.012 m. Dashed lines show the ±20% variations

Accurate estimation of frontal velocities is needed for oily sand jets evolution and design processes. Experimental observations indicated that the normalized frontal velocity could be appropriately described by

$$\frac{u_f}{u_o} = 0.843\left[\eta\left(\frac{t}{T}\right)\right]^{-0.4} \tag{4.4}$$

with the regression coefficient of correlation R^2=0.912. Fig. 4.10c shows the presented formula within ±20% variations. Results pointed out that the effect of aspect ratio on the variation of the frontal velocity of oily sand jets was negligible. Once oily sand jets are formed, the motion of sand jets is mostly governed by the interaction between the covering oil layer and the surrounding ambient water. Therefore, the aspect ratio plays a less important role in the variation of frontal velocity. Observations of Moghadaripour et al. (2017b) reported that frontal velocity of particle cloud in stagnant water increases with increasing L/d_o.

A literature search indicates that the terminal velocity of sand particles u_∞ is a practical parameter for better understanding the variation of the frontal velocity. As it was mentioned in chapter 3, the terminal settling velocity of individual particles in water is a function of particle size, particles and water densities, and dynamic viscosity of water. Since only one particle size was used in this study, u_∞ has a constant magnitude. The velocities of sand jet front issued from 8 mm and 12 mm nozzles were normalized with the settling velocity of particles, and variations of the normalized frontal velocity with t/T were depicted in Fig. 4.11a and b, respectively. As can be seen from Fig 4.11a, at the early stage, the frontal velocity of sand jets increased with increasing the air release height due to higher impact energy at the interface layer. The ratio of the jet frontal velocity to the particle settling velocity close to the water surface was found to be 20, 35, and 40 for air release heights of 0.2, 0.4, and 0.6 m, respectively. The effect of impact energy became less pronounced as sand jets moved downward and dissipated at $t/T\approx0.04$. The frontal velocity reached

a plateau equal to $8u_\infty$ almost after t/T=0.06. For the jets issued from a 12 mm nozzle (Fig. 4.11b), the u_f/u_∞ ratio at the early stage found to be higher than that of an 8 mm nozzle owing to the higher initial velocity at the nozzle exit. As a result, the effect of impact energy lasted longer and faded away at $t/T\approx$0.06 which is almost the moment that the frontal velocity reached the plateau ten times of the particle settling velocity. Considering the variation of the normalized frontal velocity along the jet axis points out that the frontal velocity discharging from smaller nozzles reached the plateau regime faster compared to bigger nozzles which is in a good agreement with the results obtained by Azimi et al. (2012a).

Fig. 4.12 shows the variations of the normalized velocity u_f/u_∞ with y/d_o for sand jets released from 8 and 12 mm nozzles. The variations of the velocity for sand jets discharged from a 16 mm nozzle were eliminated from Fig. 4.12 due to uncertainties observed while measuring the frontal velocities. Prediction curves of sand jet frontal velocities with y/d_o from experimental study of Azimi et al. (2012a) for $L/d_o\approx\infty$ and Moghadaripour et al. (2017b) for $0.8<L/d_o<15$ described by Eq. (4.5) and (4.6), respectively, were included for comparison.

$$\frac{u_f}{u_\infty} = -\frac{1}{4}\left(\frac{D_{50}}{d_o}\right)^{-0.75} \ln\left(\frac{y}{d_o}\right) + \left(\frac{D_{50}}{d_o}\right)^{-0.55} \tag{4.5}$$

$$\frac{u_f}{u_\infty} = 9.4\left[\frac{y}{d_o}\left(\frac{L}{d_o}\right)^{-0.5}\right]^{-0.61} \tag{4.6}$$

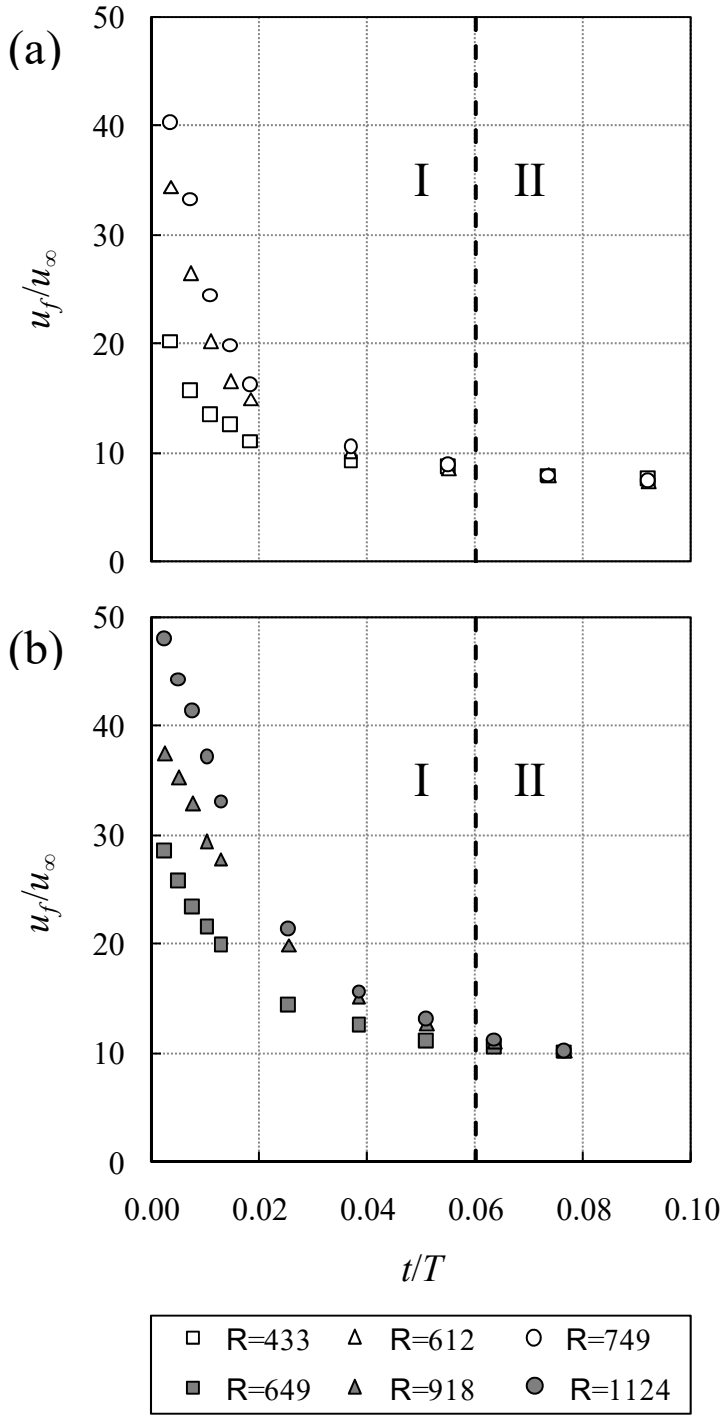

Figure 4.11 Variation of normalized frontal velocity u_f/u_∞ with normalized time t/T: (a) d_o=0.008 m; (b) d_o=0.012 m

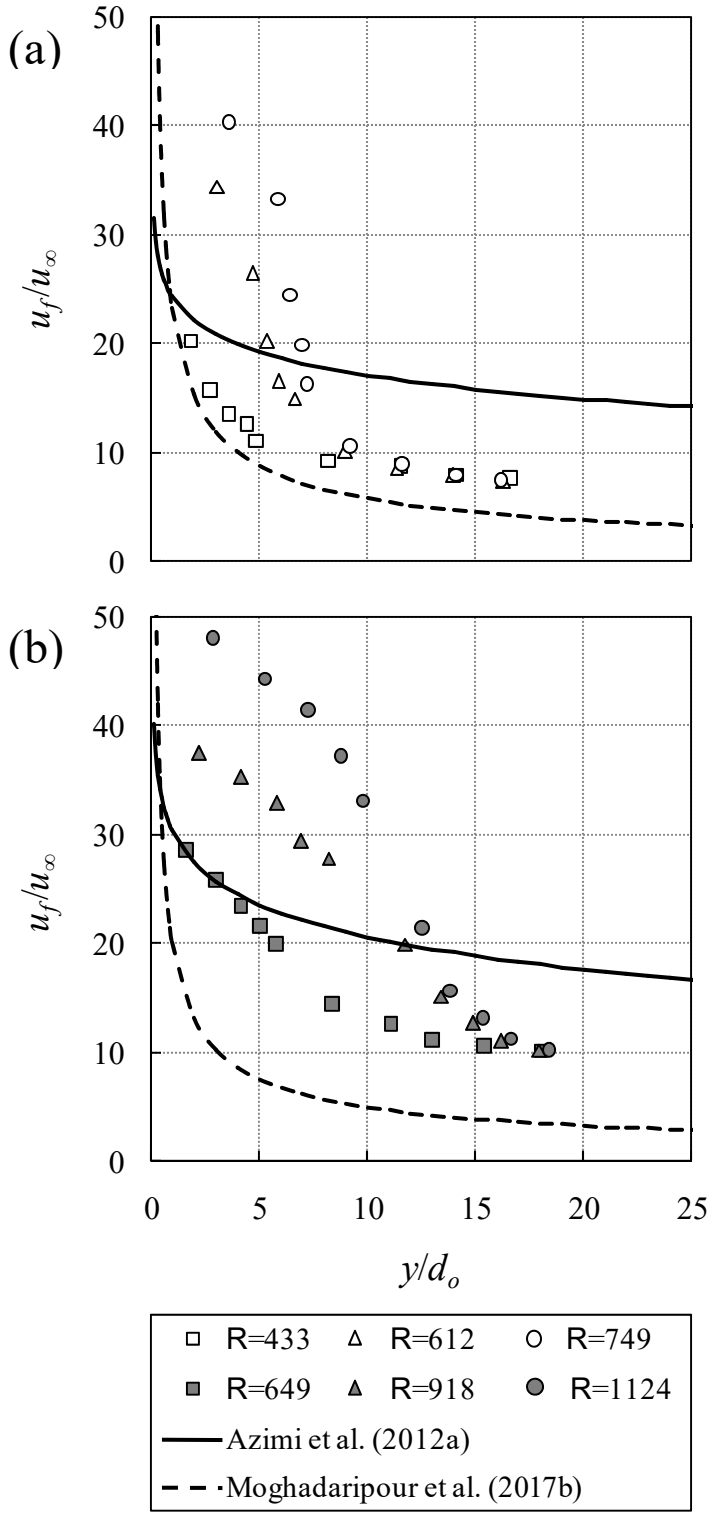

Figure 4.12 Variation of normalized frontal velocity u_f/u_∞ with y/d_o: (a) d_o=0.008 m; (b) d_o=0.012 m

As can be seen, at the early stage, frontal velocities of oily sand jets for higher air release heights (i.e., 0.4 and 0.6 m) were higher than the frontal velocities of continuous sand jets since higher air release heights result in higher initial velocities. As jets travel further in the ambient water, the gained energy is consumed and frontal velocities of oily sand jets fall under the frontal velocities of continuous sand jets. As it was mentioned in section 4.2.2, during this period, sand particles descend either as a number of encapsulated clusters of particles or as a mixture of individual particles and encapsulated groups of particles. In both cases, owing to the group effect between particles, oily sand jets descend with a velocity that is much faster than the particle settling velocity which was found to be $8u_\infty$ for the former case and $10u_\infty$ for the latter one. Azimi et al. (2012a) indicated a group settling velocity of $5u_\infty$ for $L/d_o \approx \infty$, while Moghadaripour et al. (2017a) reported $1.3u_\infty$ for $0.8<L/d_o<40.1$.

4.2.4 Shear stress and drag coefficient

As it was mentioned in section 4.2.1, sand jets penetrate the oil layer with a diameter of d_j. Therefore, the motion of sand jets passing through the oil layer can be approximated with a semi-cylindrical figure with a diameter of d_j and a length of h_{oil}. Newton's second law could be applied to formulate force imbalances equation with the change of momentum rate. A schematic of force balance at the oil layer is illustrated in Fig. 4.13a where ρ_m represents the density of the mixture of oil and sand particles as $\rho_m=[c_o\rho_s+(1-c_o)\rho_{oil}]$ where c_o is the initial sand concentration, A_j is the cross-sectional area of the cylinder, F_g is the gravitational force, F_D is the drag force, and τ is the shear stress due to the friction between the oil layer and sand particles passing through and resulting in the skin friction drag force F_τ.

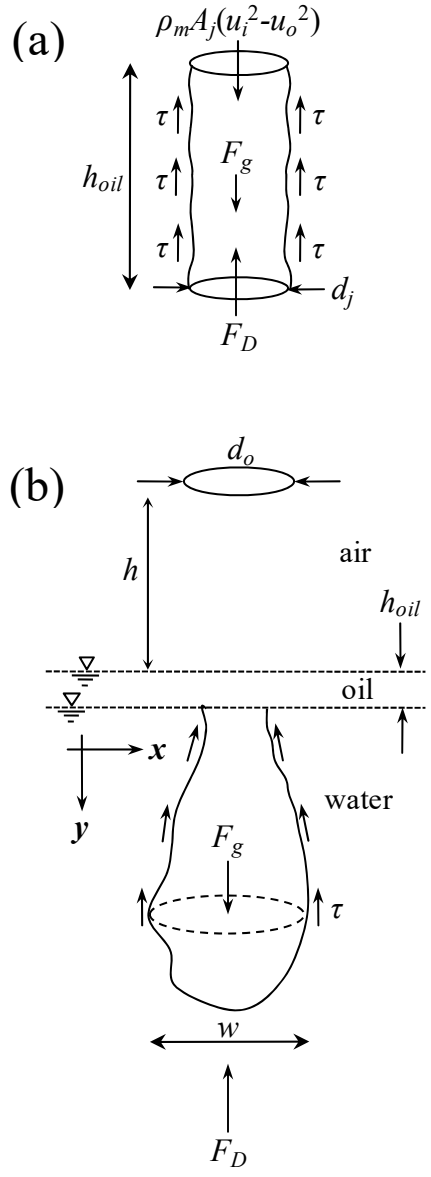

Figure 4.13 Schematic of force balance of sand jets (a) at the oil layer, (b) at the early stage of evolution

Exerted forces can be written as:

$$F_g = \dot{m}tg = \left(0.538\,\rho_b (d_o)^{5/2}\sqrt{g}\right)(tg) \tag{4.7}$$

where ρ_b is the bulk density of sand particles as $\rho_b=c_o\rho_s$ and $\dot{m}$ is the mass flow rate of sand particles.

$$F_D = c_o \frac{\pi d_j^2}{4} h_{oil} \rho_{oil} g \tag{4.8}$$

$$F_\tau = \pi d_j h_{oil} \tau \tag{4.9}$$

Thus, Newton's second law for a group of sand particles passing through the oil layer can be formulated as:

$$\rho_m A_j (u_i^2 - u_o^2) = \sum F = F_g - F_D - F_\tau \tag{4.10}$$

where the left-hand side of Eq. (4.10) represents the momentum change of sand jets penetrating the oil layer.

The variation of shear stress induced by sand particles passing through the oil layer is shown in Fig. 4.14. The skin friction force was calculated using the momentum equation (Eq. (4.10)), and the shear stresses were approximated from Eq. (4.9). Fig. 4.14a shows the effects of Reynolds number on the variation of shear stress in the oil layer for all experiments in this study. As can be seen, the magnitude of shear stress is directly related to Reynolds number. Eq. (3.10) showed a direct relationship between Reynolds number and initial parameters, air release height and nozzle, diameter as $R \sim h^{1/2} d_o$. Sand particles discharged from either a higher elevation or a bigger nozzle have higher momentum as they hit the oil surface which results in higher shear stress in the oil layer. Observation indicated that nozzle size plays a more important role in the variation of shear stress in the oil layer compared to air release height. For example, by doubling the nozzle diameter from 8 to 16 mm, shear stress grew 2.1 times, whereas it increased 1.75 times as the air release height was doubled. It can be physically interpreted by the fact that bigger nozzle size results in both higher impact velocity and higher mass flow rate. However, higher air release elevation only increases the impact velocity and does not affect mass flux. Therefore, the growth rate of

momentum and as a result, the growth rate of shear stress is more affected by nozzle diameter than that of air release height.

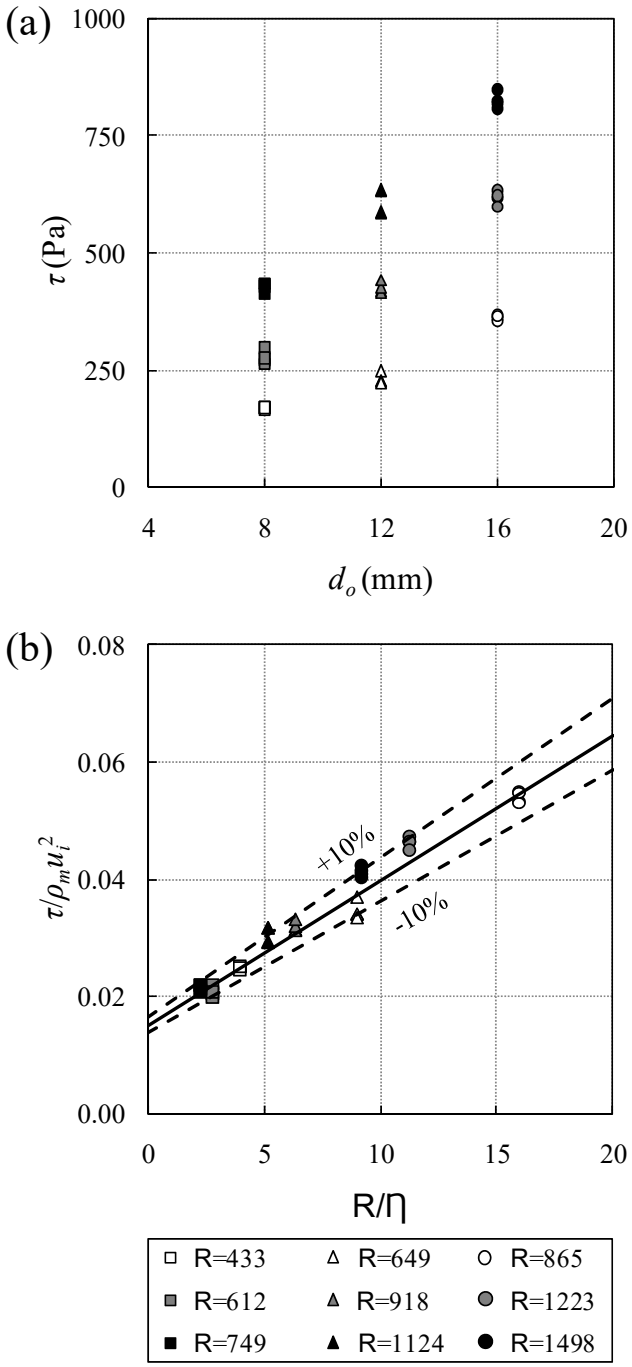

Figure 4.14 Variation of (a) shear stress in the oil layer with Reynolds number (b) normalized shear stress in the oil layer with R/η ratio

Variation of the normalized shear stress is shown in Fig. 4.14b. Shear stress was normalized with $\rho_m u_i^2$ where ρ_m is the density of the mixture of sand particles and oil and u_i is the impact velocity. The ratio between non-dimensional parameters R and η which both are functions of nozzle size and air release height (Eqs. (3.7) and (3.10)) was found to be an appropriate parameter to study the variation of the normalized shear stress. As can be seen in Fig. 4.14b, the normalized shear stress linearly increased with R/η ratio. Predictions of the normalized shear stress with the RMS method were within ±10%.

A schematic of force balance at the early stage of evolution is shown in Fig. 4.13b. The forces exerted on the encapsulated sand particles are the gravitational force F_g, the drag force F_D, and the skin friction drag force F_τ due to the friction between the oil layer and encapsulated particles. The rate of momentum change can be calculated knowing the frontal velocity and the frontal area of sand jet u_f and A_f, respectively. The momentum equation can be formulated for the initial stage of sand jets as:

$$\rho_n (A_j u_o^2 - A_f u_f^2) = \sum F = F_g - F_D - F_\tau \tag{4.11}$$

where $\rho_n=[c_o\rho_s+(1-c_o)\rho_w]$ is the density of the mixture of water and sand particles. The drag and the skin friction drag forces for the early stage of evolution can be written as:

$$F_D = c_o \frac{\pi d_j^2}{4} y \rho_w g \tag{4.12}$$

$$F_\tau = A_s \tau \tag{4.13}$$

where A_s is the side surface area of the sand jets which was measured using boundary detection technique. Fig. 4.15a shows the effect of air release height on variations of shear stress with time for the initial stage of sand jets for d_o=16 mm and m=30 g. As can be seen, the estimated early stage shear stress linearly increased with time for different air release heights. Mohammadidinani

et al. (2017) reported that the average shear stress considerably decreased with y/d_o. They also found that higher initial momentum results in higher shear stress. However, the results obtained in this study revealed that higher initial momentum due to higher air release height does not necessarily result in higher shear stress. As can be seen, the average shear stress decreased by doubling the air release height from 0.2 to 0.4m and increased as the release altitude was elevated from 0.4 to 0.6 m. It could be explained by the differentiation of evolution pattern. The larger momentum which was gained by doubling the release elevation from 0.2 to 0.4 led to lateral dispersion of oily sand jets. As a result, the side surface area of the sand jets expanded; therefore, the average shear stress decreased. On the other hand, lateral dispersion of oily sand jets released from a 0.6 m height was found to be less significant due to surplus momentum. The frontal velocities were large enough not to let the oily sand jets expand laterally. Therefore, the increment of the side surface area of oily sand jets was less remarkable which resulted in the growth of the average shear stress.

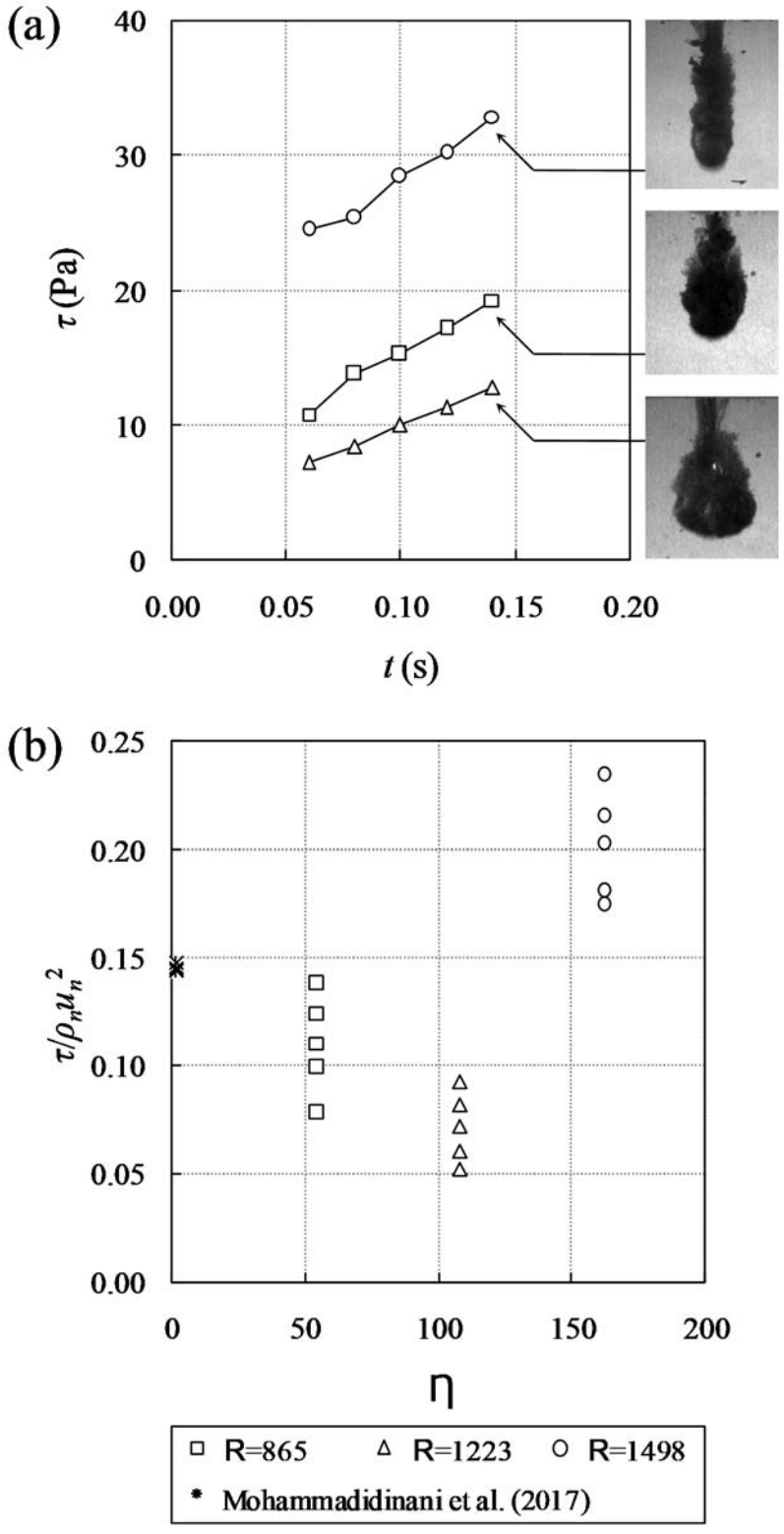

Figure 4.15 Variation of the average shear stress of oily sand jets along the axis of the jets at the early stage evolution for d_o=16 mm and m=30 g

To show the non-linear correlation between the air release height and the average shear stress, variations of the normalized shear stress with η was plotted in Figure 4.15b. The average shear stress was normalized with $\rho_n u_n^2$. For oily sand jets with zero release height (i.e., η=0) Mohammadidinani et al. (2017) reported a constant value for the normalized shear stress as $\tau/(\rho_n u_n^2)=0.14\pm0.01$. Figure 4.15b shows that, the minimum shear stress is for jets with 0.4 m release height with a value of $\tau/(\rho_n u_n^2)=0.072\pm0.02$.

The particle drag coefficient plays a key role, as a hydrodynamic parameter, in the modeling and design of multiphase processes especially when entrained with solid particles. From a hydrodynamic point of view, the fundamental aspects of solid-liquid multiphase flow are inter-phase interaction and intra-phase interaction. Inter-phase interaction between the fluid phase and the particulate phase is manifested mainly in the drag force exerted on the particles by the fluid ambient and the transfer of momentum from one phase to another. The average drag coefficient of sand jets passing through immiscible fluids can be estimated using a momentum equation. The average drag force F_D acts on the surrounding fluids of a particle cloud and can be estimated by balancing the net force and momentum flux as

$$F_B - F_D = \frac{d(mu_f)}{dt} = \frac{d(\rho_s V_o u_f)}{dt} = \rho_s V_o \frac{du_f}{dt} \tag{4.14}$$

where $F_B=(\pi d_o^2/4)Lc_o(\rho_s - \rho_w)g$ is the buoyancy force and $V_o=m/c_o\rho_s$ is the initial volume of sand particles in the pipe. The average drag force on each particle f_D can be approximated by dividing the drag force to the total number of particles N as

$$f_D = \frac{\pi}{6}\frac{F_D}{V_o} D_{50}^3 \tag{4.15}$$

Using $f_D=1/2\rho_w C_d A_p u_f^2$ as the classical formulation for drag force where $A_p=\pi D_{50}^2/4$ is the projected frontal area of individual sand particles to predict the drag coefficient and assuming that particle separation is insignificant during the motion, the drag coefficient can be calculated as:

$$C_d = \frac{\pi F_D D_{50}^3}{3\rho_w u_f^2 V_o A_p} \tag{4.16}$$

Several correlations for drag coefficient have been proposed over a wide range of Reynolds number in the literature. The empirical equation of Schiller and Neumann to calculate the drag coefficient of individual spherical particles falling down in stagnant water (Clift et al., 1978; wörner, 2003) is one of the most widely used one expressed as:

$$C_d = \frac{24}{\mathsf{R}_\mathsf{p}}(1 + 0.15\mathsf{R}_\mathsf{p}^{0.687}) \tag{4.17}$$

where $\mathsf{R}_\mathsf{p}=\rho_w u_\infty D_{50}/\mu$ is the particle Reynolds number ranging from 0.1 to 800 which explains the effect of particle inertia over the ambient viscosity. Engelund and Hansen (2010) formulated the drag coefficient of sand and gravel as:

$$C_d = \frac{24}{\mathsf{R}_\mathsf{p}} + 1.5 \tag{4.18}$$

Sphericity of particles φ which is the ratio of the surface of a sphere having the same volume as the particle and the actual surface area of the particle, was taken into account by Chien (1994) on estimation of the drag coefficient for low range of particle Reynolds number ($\mathsf{R}_\mathsf{p}<5000$) and the sphericity ratio of $0.2\leq\varphi\leq1$ as:

$$C_d = \frac{30}{\mathsf{R}_\mathsf{p}} + 67.3e^{(-5\varphi)} \tag{4.19}$$

Moghadaripour et al. (2017a) proposed a linear model for the variations of the drag coefficient for a constant particle size with Stokes number of $S_t=0.22$ as:

$$C_d = \left[\frac{1}{15}\left(\frac{L}{d_o}\right)^{-\frac{5}{9}}\right]\left(\frac{y}{d_o}\right) \tag{4.20}$$

where y is vertical distance from cloud front to the nozzle exit. It was found that the average drag coefficient increased as the L/d_o ratio decreased. The average drag coefficient of sand jets passing through an immiscible interface was calculated using Eq. (4.16). Variations of the average drag coefficient with particle Reynolds number in log-log scale were plotted in Fig. 4.16a. This figure shows the effect of L/d_o and η on the drag coefficient of oily sand jets issued from an 8 mm nozzle. Variations of the drag coefficient of natural particles (Julien, 2010), the estimated average drag coefficient of particles for slurry jets (Azimi et al., 2012b) and particle clouds (Moghadaripour et al., 2017a), and the average drag coefficient of particle clusters (Azimi, 2019) were also plotted for comparison. As can be seen, the average drag coefficient of oily sand jets was considerably smaller than the values of C_d for individual particles. This discrepancy could be explained by the fact that the velocity of oily sand jets released from an 8 mm nozzle was found to be as high as eight times of the particle settling velocity u_∞ once it reached a plateau regime (see Fig. 4.11b). A direct correlation was observed between C_d and L/d_o which was in a good agreement with observations of Azimi (2019). It was also found that the average drag coefficient rose with increasing η. Fig. 4.16b reveals that the calculated drag coefficient of oily sand jets is comparable to the C_d estimations of Chien (1994).

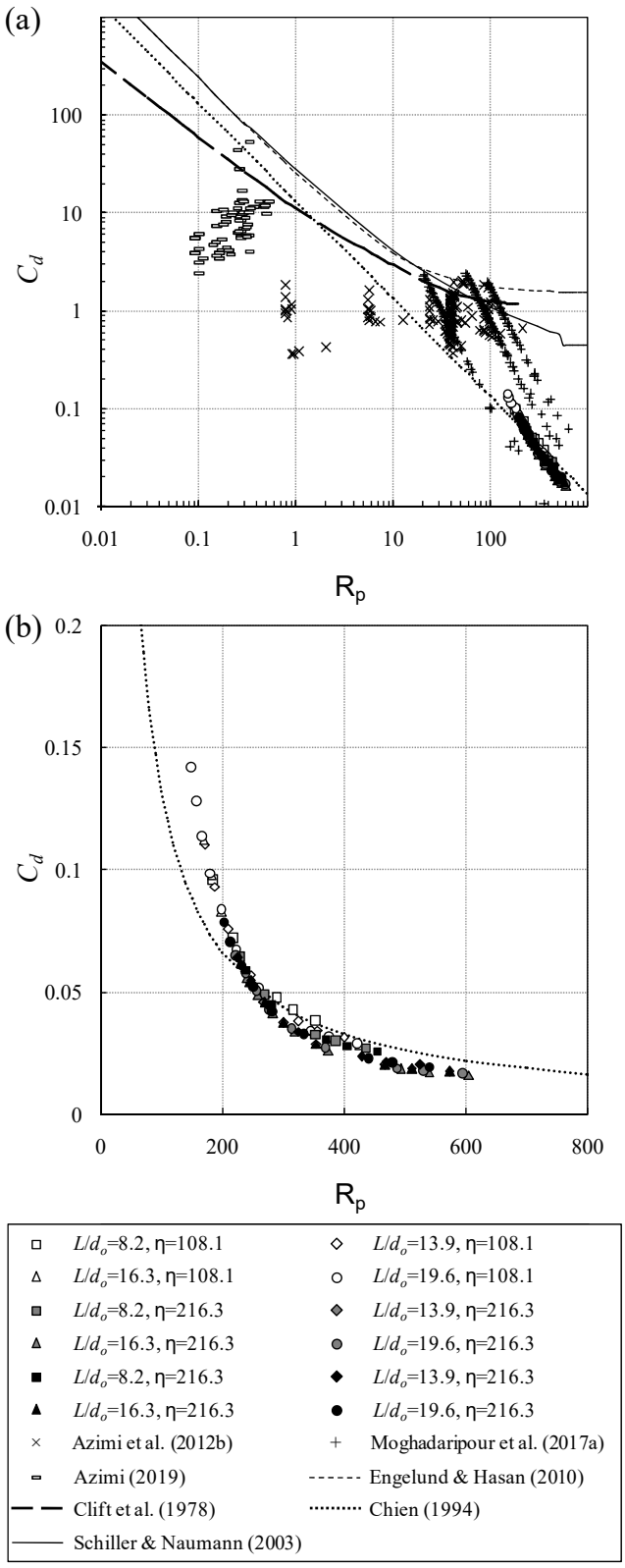

Figure 4.16 Variation of drag coefficient C_d of oily sand jets with particle Reynolds number R_p for d_o=8 mm

Chapter 4 On the motion of vertical sand jets in stagnant immiscible liquids

Acknowledgments

The work presented in this chapter was supported in part by NSERC Discovery grant No. 421785. I would like to thank our undergraduate students (Graham Havers, Rohail Khan, Dillon Simms, and Mateo Tobon) for their help in conducting part of the laboratory experiments.

5 On the motion of oblique sand jets in stagnant immiscible liquids

5.1 Experimental Setup

Experiments were conducted in a rectangular glass-walled tank of 1.6 m long, 0.8 m wide, and 0.8 m height in the hydraulic laboratory at Lakehead University. The experimental tank was filled with tap water with a temperature of T=23±0.5 °C, density of ρ_w=997.5 kg/m^3, and dynamic viscosity of μ_w=0.9321×10^{-3} Pa.s. The water in the tank was maintained at a constant level with a depth of 0.65 m for all experiments, using a drain valve. The water surface was covered with a 0.015 m layer of canola oil, h_{oil}, to form an immiscible layer. Density and dynamic viscosity of canola oil used in this research were measured by a Sigma 700 tensiometer (Biolin Scientific, Finland) and were ρ_{oil}=908 kg/m^3, and μ_{oil}=56.8×10^{-3} Pa.s, respectively.

A schematic view of the experimental setup and the coordinate system is depicted in Fig. 5.1. Three different pipe sizes with inner diameters of d_o=8, 10, and 14 mm were used in these experiments. Three angle of release θ=30˚, 45˚, and 60˚ were chosen. Oblique pipes were located 3 mm above the oil surface to eliminate oil contact with and clogging the nozzle, and to minimize air entrainment. The pipes were aligned with the centre of the tank to avoid any boundary effect on the evolution of oblique sand jets. Sand particles were evenly poured in a funnel and were released instantaneously from above the oil surface using a rubber plug. Sieve analysis was employed to select sand particles. The collected particles from two sieve sizes of D_{50}=0.250 mm (i.e., sieve #60) and 0.297 mm (i.e., #50) were mixed and used in this study with a nominal diameter of 0.275 mm. The uniformity coefficient of particles was calculated for the particle sample with a value of 1.31. Sand particles were considered uniform since the geometric standard deviation $\sigma_g=D_{84}/D_{50}=D_{50}/D_{16}$ was smaller than 1.35 (Breusers and Raudkivi, 1991). The sand particles had a density of ρ_s=2540 kg/m^3, and an averaged unpacked sand concentration of c_o=0.6.

Different masses of dry sand particles ranging from 2.5 to 30 g were selected to form a wide range of L/d_o ratio from 1.5 to 24.5. Experimental details and non-dimensional parameters are tabulated in Table 5.1.

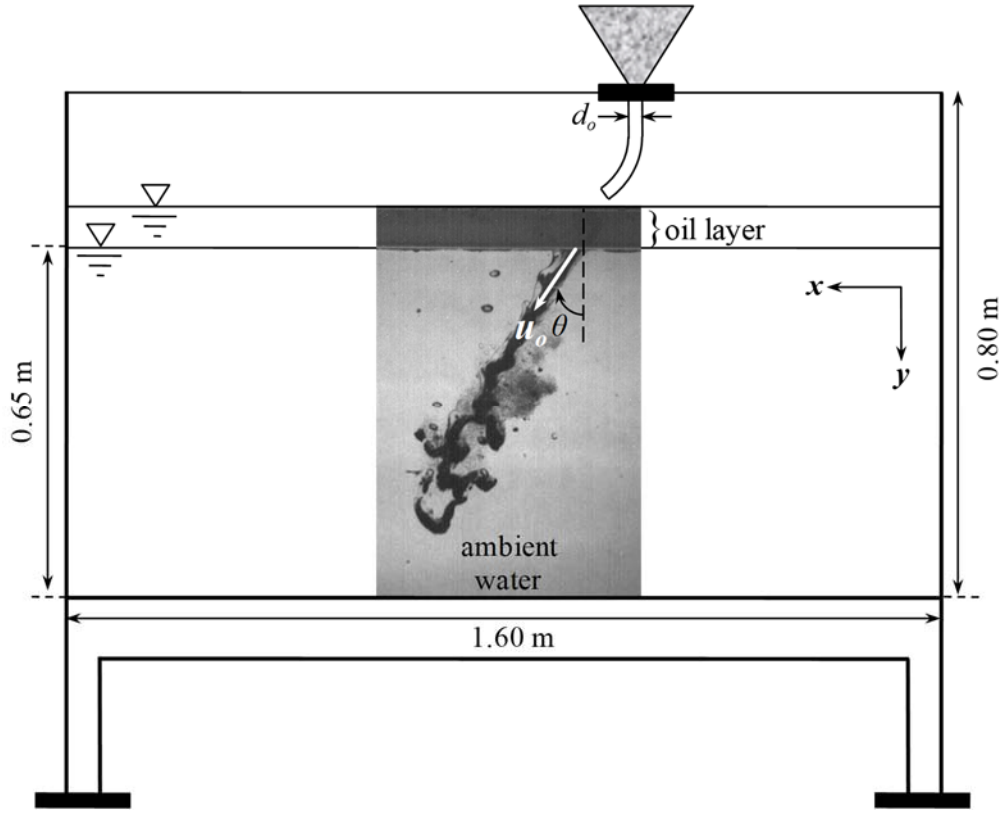

Figure 5.1 Schematic of experimental setup and coordinate system

Three minutes of relaxation time was allowed between each experiment to dampen oil-water interface fluctuations. During the relaxation time, all the oil and water droplets from the previous experiment were settled; thus, there was no memory impact on the next experiment. Since a small amount of oil was dragged by sand particles during the experiments, the thickness of oil layer was measured after each test, and a suitable volume of oil was added to keep the oil layer at the original level.

Table 5.1 Experimental details of oblique sand jets passing through immiscible interface

Test No.	d_o (m)	θ (degree)	m (gr)	L (m)	L/d_o	R
1	0.008	30	2.5	0.033	4.1	38.6
2	0.008	30	5	0.065	8.2	38.6
3	0.008	30	10	0.131	16.3	38.6
4	0.008	30	15	0.196	24.5	38.6
5	0.008	45	2.5	0.033	4.1	38.6
6	0.008	45	5	0.065	8.2	38.6
7	0.008	45	10	0.131	16.3	38.6
8	0.008	45	15	0.196	24.5	38.6
9	0.008	60	2.5	0.033	4.1	38.6
10	0.008	60	5	0.065	8.2	38.6
11	0.008	60	10	0.131	16.3	38.6
12	0.008	60	15	0.196	24.5	38.6
13	0.01	30	5	0.042	4.2	54.0
14	0.01	30	10	0.084	8.4	54.0
15	0.01	30	15	0.125	12.5	54.0
16	0.01	30	20	0.167	16.7	54.0
17	0.01	45	5	0.042	4.2	54.0
18	0.01	45	10	0.084	8.4	54.0
19	0.01	45	15	0.125	12.5	54.0
20	0.01	45	20	0.167	16.7	54.0
21	0.01	60	5	0.042	4.2	54.0
22	0.01	60	10	0.084	8.4	54.0
23	0.01	60	15	0.125	12.5	54.0
24	0.01	60	20	0.167	16.7	54.0
25	0.014	30	5	0.021	1.5	89.4
26	0.014	30	10	0.043	3.0	89.4
27	0.014	30	20	0.085	6.1	89.4
28	0.014	30	30	0.128	9.1	89.4
29	0.014	45	5	0.021	1.5	89.4
30	0.014	45	10	0.043	3.0	89.4
31	0.014	45	20	0.085	6.1	89.4
32	0.014	45	30	0.128	9.1	89.4
33	0.014	60	5	0.021	1.5	89.4
34	0.014	60	10	0.043	3.0	89.4
35	0.014	60	20	0.085	6.1	89.4
36	0.014	60	30	0.128	9.1	89.4

Two different types of light sources were employed for boundary detection and recording of sand jet evolution. The background ambient was illuminated using continuous laser light sheets with a thickness of 3 mm, a power of 1 w, and a wavelength of 532 nm (Laserwave, G2000, China). The laser sheets were launched from the sides to illuminate the jet. For boundary detection and jet width measurement, a 500 w T3 halogen bulb was placed behind the backside wall of the tank which was covered with a sheet of white paper. The evolution of sand jets passing through the oil-water interface was recorded using a high-speed camera (Photron-FASTCAM, 1024PCI-100KC) with a resolution of 1024×1024 pixels. The camera was equipped with a 15-55 mm AF-S Nikkor, 1:3.5-5.6 GII (Nikon, Japan) lens to capture images. Raw images were captured with a frame rate of 250 frames/second and a shutter speed of 0.004 sec. Photron FASTCAM Viewer software was used to collect the images. The camera lens was located at the oil-water interface level and perpendicular to the tank with a distance of 0.35 m. The area of interest was a rectangle of 0.50 m × 0.30 m and located below the water surface. Obtained images were turned to negative for better visualization. Images were imported to AutoCAD to determine frontal width and velocity of sand jets. Horizontal and vertical rulers were placed in the tank to detect any image distortion. Also, the rulers were used as scales to scale the images and measure the displacement and the width of sand jets.

5.2 Experimental Results

5.2.1 Evolution of oblique sand jets

The effects of release angle θ and nozzle diameter d_o on the evolution of oblique sand jets passing through the immiscible interface are studied in this section using image analysis technique. Fig. 5.2 shows the evolution of oblique sand jets issued from an 8 mm nozzle for the non-dimensional time range of $0.2 \leq t/T \leq 1.4$, the release angles of θ=30˚, 45˚, and 60˚, respectively, and

the largest aspect ratio (i.e., L/d_o=24.5). For θ=30˚ (Fig. 5.2a), a cane-shape jet was formed at the early stage of evolution $t/T \leq 0.4$ due to buoyancy difference. It was followed by the growth of the front and body of the cane with some instability in the front section as the jet moved downward in the water ambient ($0.4 \leq t/T \leq 0.8$). Formation of the cane-shape front is consistent with the hook-shape formation observed by Nicolas (2002) and Mohammadidinani et al. (2017) whereas no bar-shape occurred prior to cane formation as it was observed by Nicolas (2002) and Mohammadidinani et al. (2017). A torsion front was observed for $t/T \geq 0.8$ resulted in detachment of the oily sand jet front at t/T=1.2. The detachment of oily sand jet front could be explained by the fact that the body of the jet behaves as an oblique jet having momentum in both vertical and horizontal directions while the jet front behaves like a buoyant thermal which its motion is controlled by buoyancy and gravitational forces. As a result, the forces exerted on the oil layer covering the jet front overcome surface tension of the oil layer and the jet front detaches from the jet. Detachment of jet front at the late evolution time is consistent with observations of Mohammadidinani et al. (2017). After front detachment, the jet descended further as a single encapsulated cluster of particles without oil layer rupture. It can be interpreted by the fact that the small portion of sand particles which interlock with the oil layer and form a channel through which dry particles can flow in a straight line downward into the ambient, do not have enough energy to exceed surface tension of the oil layer. Therefore, the oblique jet settles while being covered by a thin layer of oil.

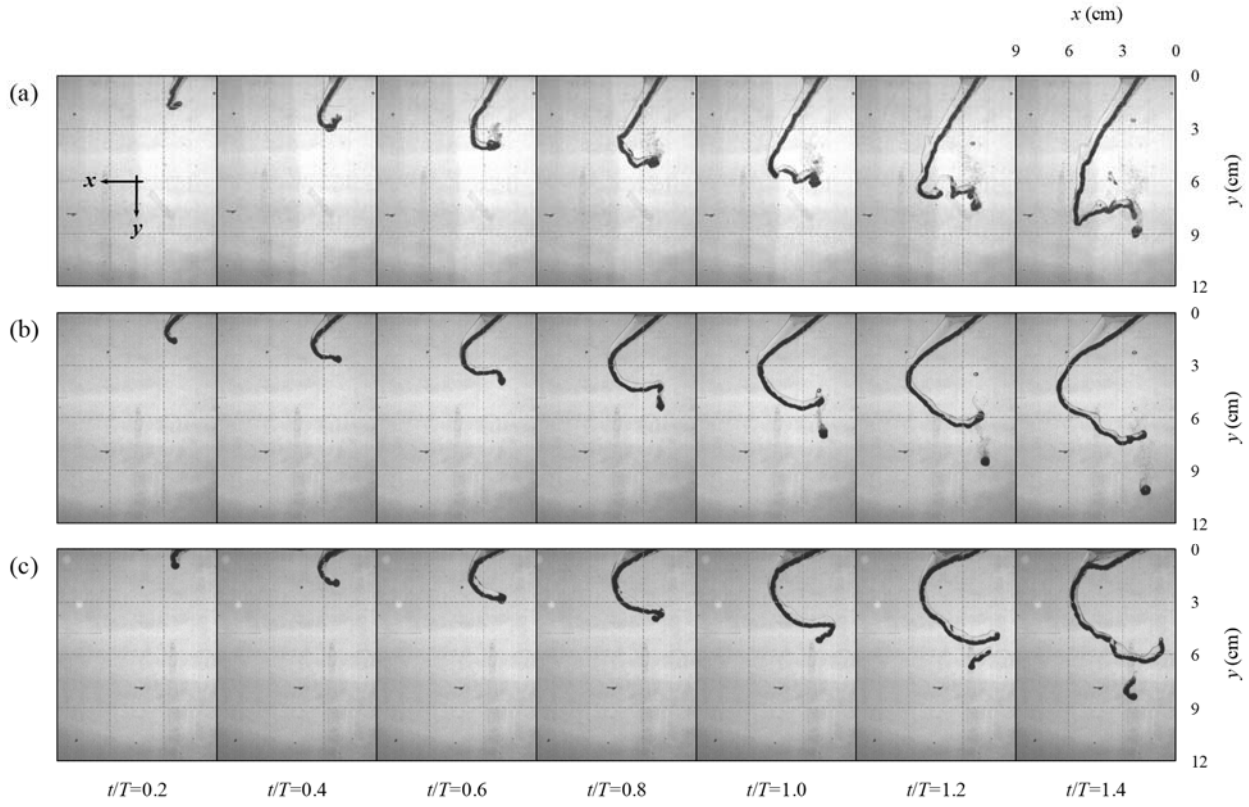

Figure 5.2 Effect of release angle on the evolution of oblique oily sand jets for d_o=0.008 m at different non-dimensional time t/T: (a) θ=30˚; (b) θ=45˚; and (c) θ=60˚

Fig. 5.2b and c show the evolution of oily sand jet for released from a nozzle of d_o=8 mm for θ=45˚ and 60˚, respectively. It can be clearly seen that the general evolution of sand jets (e.i., cane formation and front detachment) are similar to the former case (e.i., θ=30˚) with bigger front curves and shorter body length compared to that of θ=30˚. By incresing the release angle, the jet velocity in x direction increases while decreases in y direction. Therefore, the jet penetrates more in x direction whereas less in y direction compared to tha of θ=30˚. As a result, the length of the jet's body becomes shorter as the release angle increases. Having more velocity (momentum) in x direction while the jet front being governed by buoyancy and gravitational forces leads into the growth of frontal curvature. All in all, the bigger release angle, the bigger front curve and the

shorter body length. Similar to θ=30˚, after the front detachment, the jets descended further as a single encapsulated cluster of particles without rupturing the oil layer.

By comparing the evolution of vertical oily sand jets released from an 8 mm nozzle presented in chapter four and the evolution of oblique oily sand jets released from the same nozzle size, it can be concluded that a bar-shape jet was formed at the early stage of evolution for vertical jets while no bar-shape occurred for the evolution of oblique jets. In Addition, for vertical jets, sand particles settled either as a number of encapsulated clusters of particles or as a mixture of individual particles and encapsulated groups of particles depending of the release height; however, oblique jets moved downward as a single cluster of particles after the front detachment independent of the release angle.

The evolution oblique sand jets released from a nozzle of d_o=10 mm for the non-dimensional time range of $0.2 \leq t/T \leq 1.2$, the release angles of θ=30˚, 45˚, and 60˚, respectively, and the aspect ratio of L/d_o=16.7 shown in Fig. 5.3. As can be seen in Fig. 5.3a, a bar-shape jet front and cloud bursting were observed at the early stage of evolution ($t/T \leq 0.4$) for θ=30˚. Contrary to d_o=8 mm, no hook formation was observed for the evolution of oily sand jet issued from a 10 mm nozzle. A torsion front occurred for $t/T \geq 0.4$ due to buoyancy difference, which resulted in front detachment and air bubble escape. An unstable sinuous-path tail and rear bursting arose from instabilities in the jet front as sand particles descended further. Consequently, sand particles descended as a mixture of individual particles and encapsulated groups of particles with air bubbles.

By increasing the release angle to θ=45˚ and 60˚ (Figs 5.3b and c), it can be clearly observed that an unstable hook-shape front was formed at the early stage of evolution ($t/T \leq 0.4$) compared to the bar-shape front formation for the former case (i.e., θ=30˚). One could explain it by the fact that the larger momentum in horizontal axis induced from the larger release angle results in the jet

front to be more interacted by the momentum and buoyancy sources at the same time. Therefore, a hook-patern forms in the jet front. Similar to the former case (i.e., θ=30˚), A torsion front occurred for $t/T \geq 0.4$ due to buoyancy difference, which resulted in front detachment and air bubble escape. An unstable sinuous-path tail and rear bursting arose from instabilities in the jet front as sand particles settled and sand particles descended as a mixture of individual particles and encapsulated clusters of particles with air bubbles.

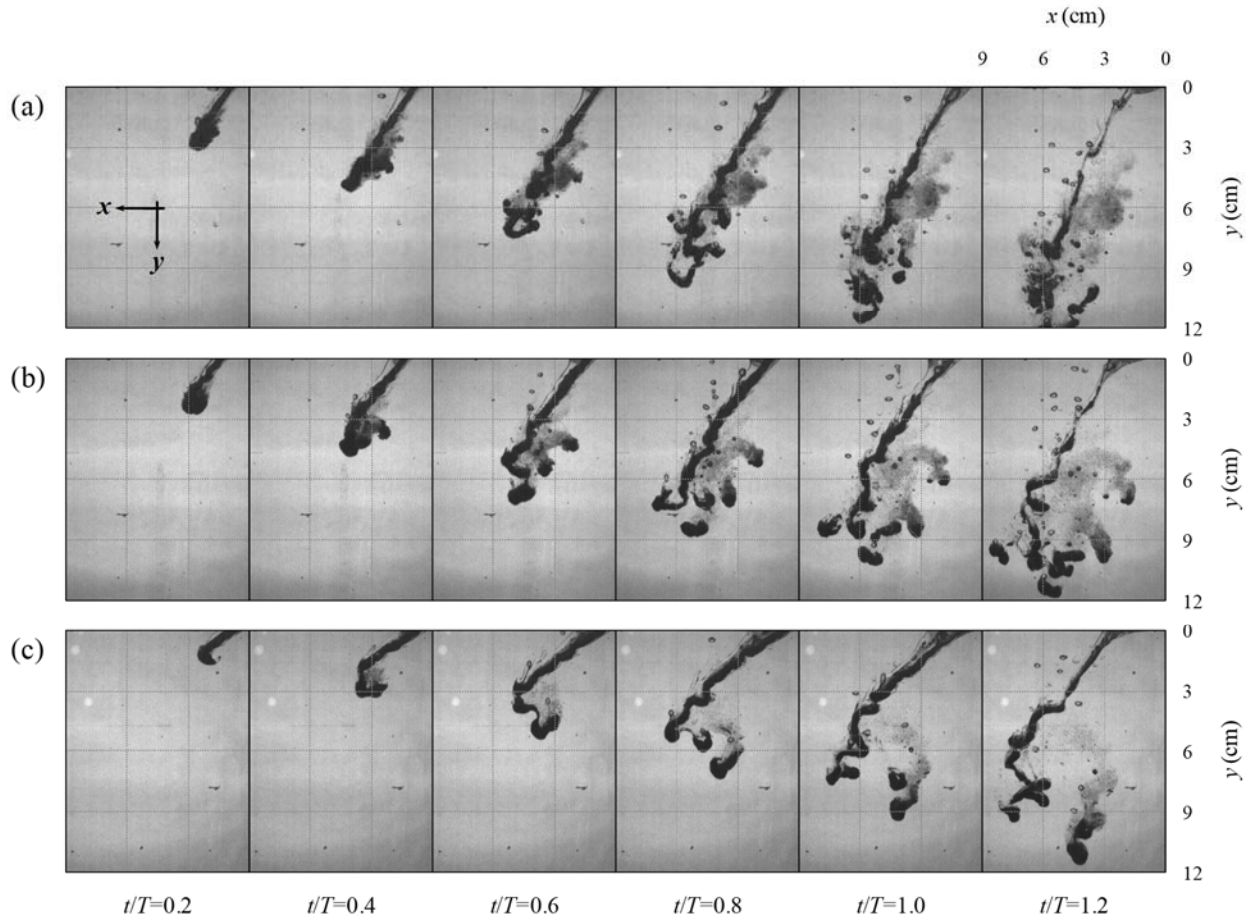

Figure 5.3 Effect of release angle on the evolution of oblique oily sand jets for d_o=0.010 m at different non-dimensional time t/T: (a) θ=30˚; (b) θ=45˚; and (c) θ=60˚

Fig. 5.4 shows the evolution of oblique sand jets issued from a 14 mm nozzle for the non-dimensional time range of $0.2 \leq t/T \leq 1.2$, the release angles of θ=30˚, 45˚, and 60˚, respectively, and the ratio of L/d_o=9.1. As can be seen, the evolution of oblique sand jets resulted from a nozzle of d_o=14 mm nozzle is similar to that of a 10 mm nozzle while more cloud bursting was observed. It could be explained by the fact that for bigger nozzle sizes, a larger portion of sand particles interlock with the oil layer to form a channel through which dry particles can directly move downward in to the water ambient having a higher initial velocity according to the orifice equation (i.e., $u_n=c_1(gd_o)^{1/2}$). Therefore, more cloud bursting would occur as the covering oil layer ruptures.

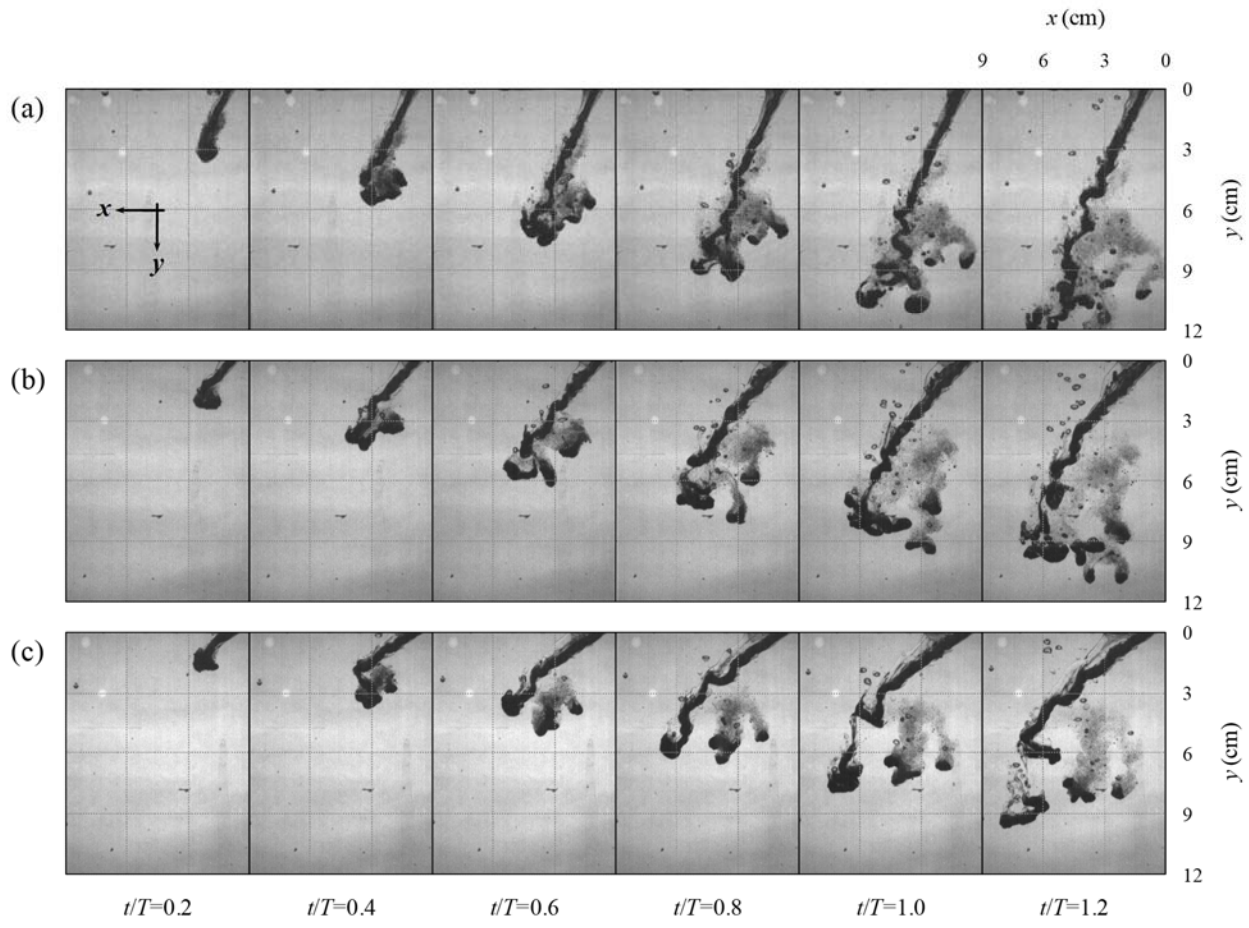

Figure 5.4 Effect of release angle on the evolution of oblique oily sand jets for d_o=0.014 m at different non-dimensional time t/T: (a) θ=30˚; (b) θ=45˚; and (c) θ=60˚

5.2.2 Initial Velocity and Frontal width

It is important to understand at which velocity, u_o, oblique sand jets pass through the oil layer and enter the ambient water. Once this velocity is determined, it can be used to study the variation of frontal velocity. Fig. 5.5 shows variation of the initial velocity of oblique oily sand jets u_o with mass of sand particles m. The initial velocity was normalized by the initial velocity of sand particles at the nozzle exit u_n. mass of sand particles was converted to lenght scale L and the lenght scale was normalized by the nozzle diameter to form the L/d_o aspect ratio. It was observed that the normalized initial velocity showed a direct relationship with the aspect ratio for all the experiments. It could be explained by the fact that by increasing the mass of sand particles, there is more force (i.e., $F=mg$) pushing the frontal sand particles as they are released from the releasing pipe and passed through the oil layer. Therefore, the frontal sand particles entre into the ambiet having more velocity as the release mass increases. It was also obsereved that for different release angles the normalized initial velocity inceased by incresing the nozzle diameter from d_o=8 mm to d_o=10 mm; however, the normalized initial velocity for sand particles released from the 14 mm nozzled did not increased compared to that of the 10 mm nozzle. A physical interpretation is that for the smallest nozzle size (i.e., d_o=8 mm) sand particles fill the entire cross-sectional area of the release pipe while passing through the pippe. Therefore, the excess friction between the sand particles and the pipe's inner wall lowers the initial momentum of the sand particles. On the other hand, for larger nozzle sizes (i.e., d_o=10 and 14 mm) the cross-sectional area of the pipe is not fully filled with sand particles. As a result, sand partilces gain more momentum as they exit the pipe.

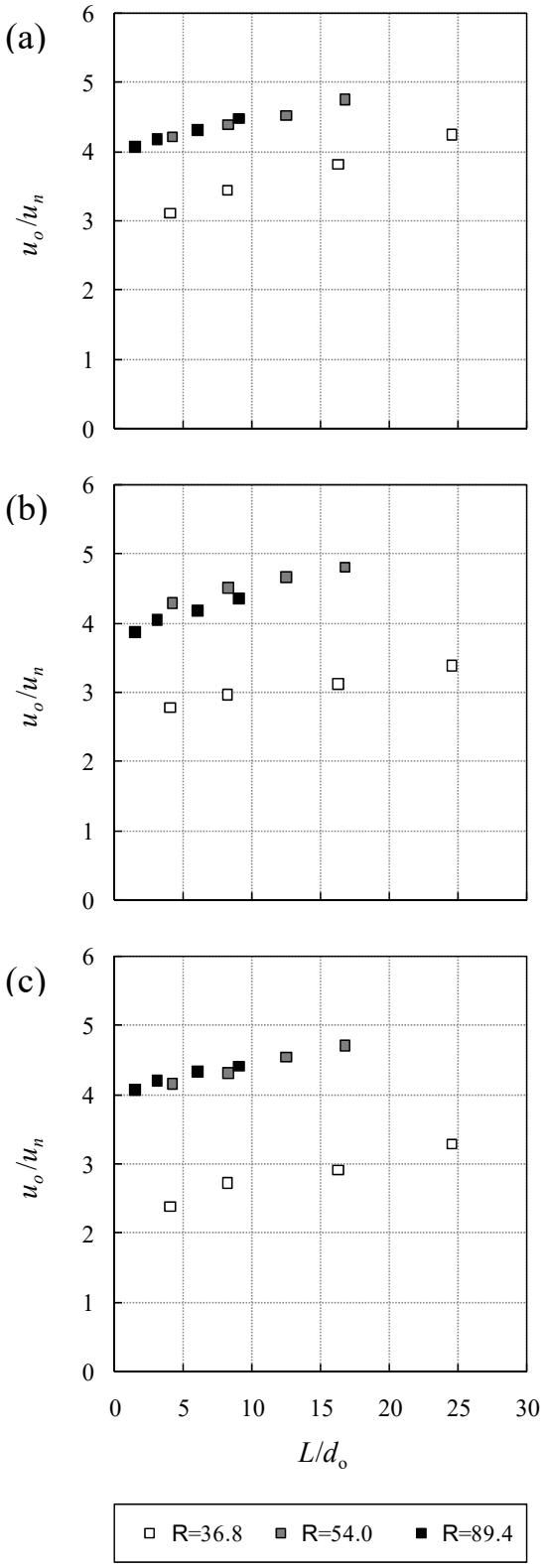

Figure 5.5 Variation of normalized initial velocity u_o/u_n with aspect ratio L/d_o: (a) θ=30˚; (b) θ=45˚; and (c) θ=60˚

Variations of the frontal width of oblique oily sand jets are also studied in this section. Figs. 5.6 and 5.7 show the growth of the frontal width of sand jets with evolution time for d_o=8 and 14 mm, respectively, at different release angles. The frontal width w_f was normalized by the normalized by the nozzle diameter d_o and the evolution time t was normalized by the characteristic time scale T presented in chapter 3. As can be seen in Fig. 5.6, the normalized frontal width grew linearly with the normalized time although some instabilities were observed for θ=45˚ and L/d_o=8.2. It was also found that the growth rate of the normalized frontal width had a direct relationship with the aspect ratio for all release angles.

By increasing the nozzle diameter to d_o=14 mm, the increment of the normalized frontal width revealed a different pattern. The frontal width grew linearly and reached a plateau at the normalized time ranging from 0.3 to 0.4 for different cases (see Fig. 5.6). Similar to the former case (i.e., d_o=8 mm), the spreading rate of the normalized frontal width was proportional to the aspect ratio for all release angles. Some irregularities were observed for θ=60˚ and L/d_o=3.0, though.

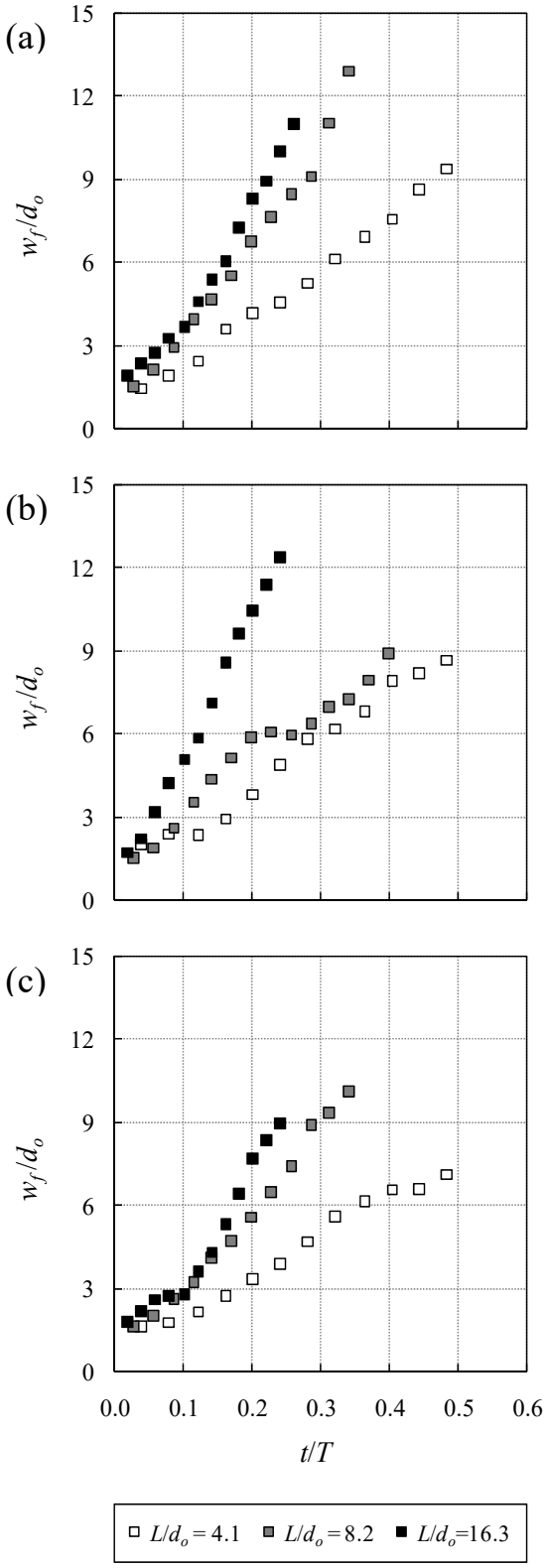

Figure 5.6 Variation of normalized frontal width w_f/d_o with normalized time t/T for d_o=0.008 m: (a) θ=30˚; (b) θ=45˚; and (c) θ=60˚

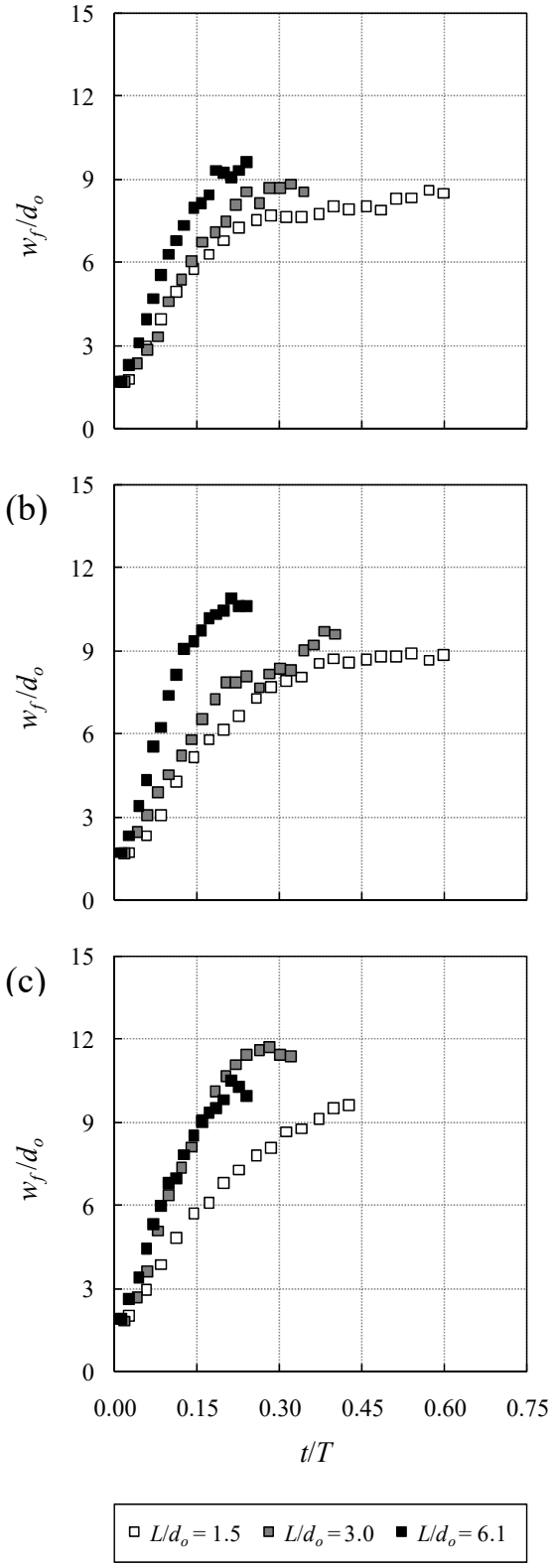

Figure 5.7 Variation of normalized frontal width w_f/d_o with normalized time t/T for d_o=0.014 m: (a) θ=30˚; (b) θ=45˚; and (c) θ=60˚

5.2.3 Trajectory of Oblique Jets

Trajectory of oblique oily sand jets was measured by locating the centre of frontal head during the motion. Fig. 5.8 shows the effect of aspect ratio on trajectory of oblique jets released from a nozzle of d_o=8 mm. Variation of the normalized horizontal displacement x/d_o with the normalized depth y/d_o were plotted for initial release angles of θ=30˚, 45˚, and 60˚, respectively. The trajectory curves of oblique particle clouds in stagnant water investigated by Moghadaripour et al. (2017a) were included in Fig 5.8 for comparison. As can be seen, the horizontal and vertical displacements of oblique jets for each release angle followed a same trend and were independent of the aspect ratio, which is consistent with observations of Moghadaripour et al. (2017a) on the independency of the trajectory of oblique particle clouds on the aspect ratio close to the nozzle exit for $x/d_o \leq 8$. As it was mentioned in section 5.2.1, jets released from smaller nozzle size do not have enough momentum to overcome the surface tension of the covering oil layer and to result in rupture of oil layer. Therefore, sand particles entre the ambient while being covered by the dragged oil layer surface and penetrate through the channel formed by the oil layer. In other word, dry particles can flow in a straight line downward into the ambient while there is no interaction between sand particles and the ambient water.

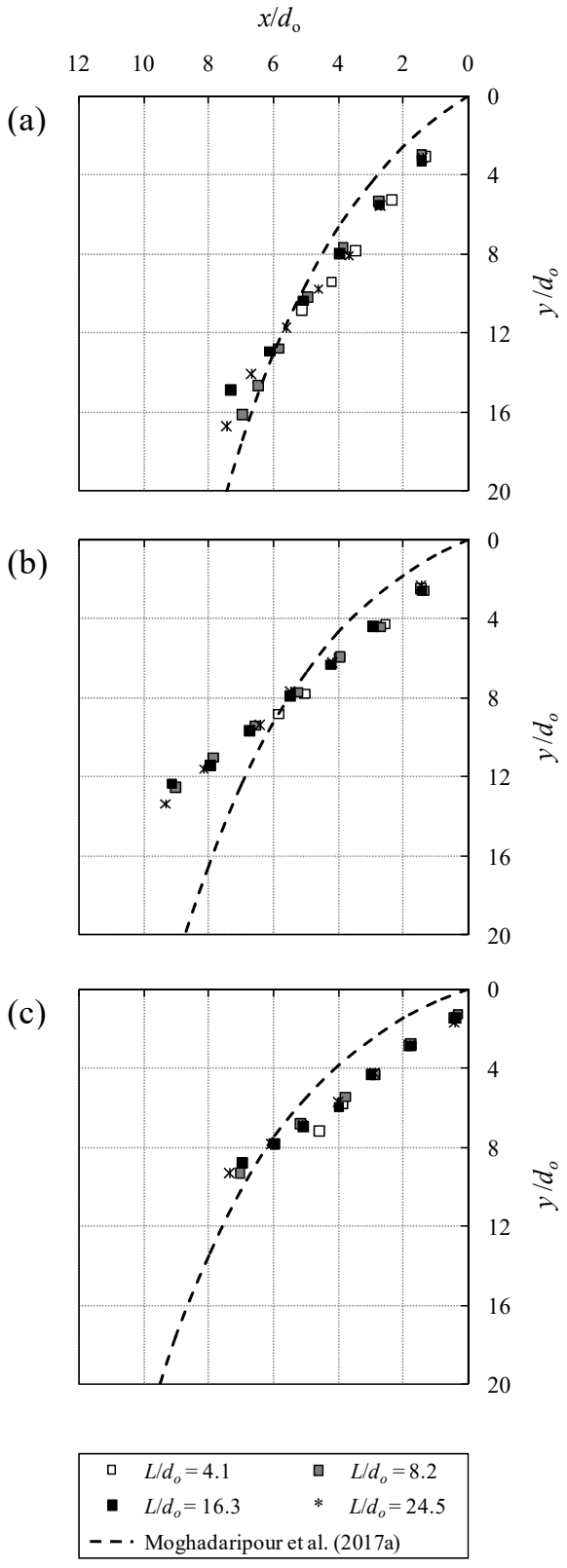

Figure 5.8 Effect of aspect ratio L/d_o on trajectory of oblique sand jets for d_o=0.008 m: (a) θ=30˚; (b) θ=45˚; and (c) θ=60˚

The effect of aspect ratio on trajectory of oblique jets released from a 10 mm nozzle is shown in Fig. 5.9. It was aforementioned in section 5.2.1 that cloud bursting occurs at the early stage evolution of oblique sand issued from a nozzle of d_o=10 mm. As a result, trajectory of sand jets is influenced by interaction between the sand particles and ambient water and ambient flow entrainment. It was observed that despite to the smaller nozzle diameter (i.e., d_o=8 mm), the trajectory curves are controlled by the aspect ratio. As mentioned in section 5.2.2, the initial velocity of oblique jets increases as the aspect ratio increases. Therefore, Sand jets with small aspect ratios have less momentum than that of larger aspect ratios. The horizontal momentum transfers from sand particles to the ambient water and particles reach to a point where there is no momentum left in horizontal direction. At this point, oblique jets with small L/d_o values reach the fall out point earlier than jets with larger L/d_o values.

Effect of initial release angle on trajectory of oblique oily sand jets for d_o=8 mm is shown in Fig. 5.10. The trajectory curves formulated by Moghadaripour et al. (2017a) were included in Fig. 5.10 for comparison. As can be seen, sand jets with release angle of θ=30˚ penetrated less in the horizontal direction as they reached the fall out point due to less momentum in x direction. Jet trajectory for larger release angles (i.e., θ=45˚ and 60˚) followed same patterns close to the water surface for $y/d_o \leq 8$ (i.e., $t \approx 0.5$ s) and started to fall out for θ=45˚ at $y/d_o \geq 8$ while penetrated in horizontal direction for θ=60˚ due to exceed momentum.

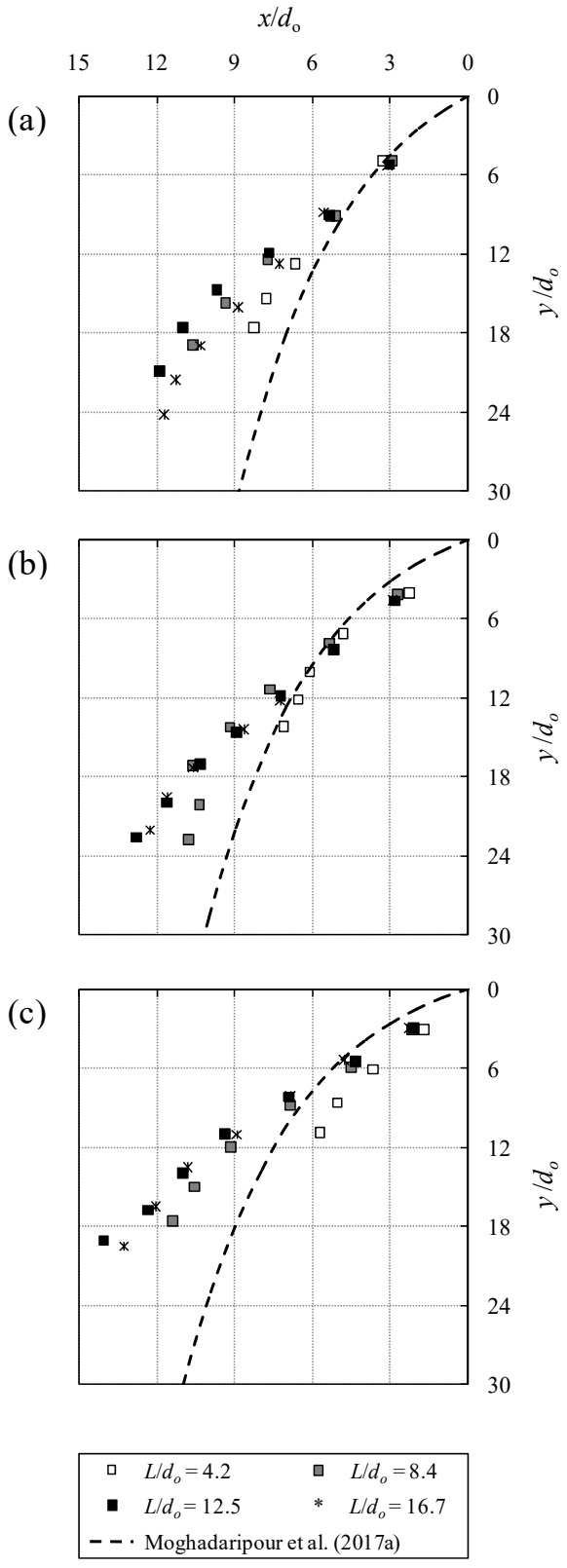

Figure 5.9 Effect of aspect ratio L/d_o on trajectory of oblique sand jets for d_o=0.010 m: (a) θ=30˚; (b) θ=45˚; and (c) θ=60˚

Effect of release angle on trajectory of sand jets released from d_o=10 mm is plotted in Fig. 5.11. Some irregularities were observed for smaller aspect ratio (see Fig. 5.11a). Jets with release angles of θ=30˚ and 45˚ revealed similar behaviour for L/d_o=12.5 while penetrated more in horizontal direction for θ=60˚. However, for larger aspect ratio value of L/d_o=16.7 Jets with release angles of θ=30˚ and 45˚ followed same patterns close to the water surface for $y/d_o \leq 8$ and started to fall out of θ=30˚. Similar to the former case (L/d_o=12.7), jets with release angle of θ=60˚ penetrated more in x direction compared to that of θ=30˚ and 45˚.

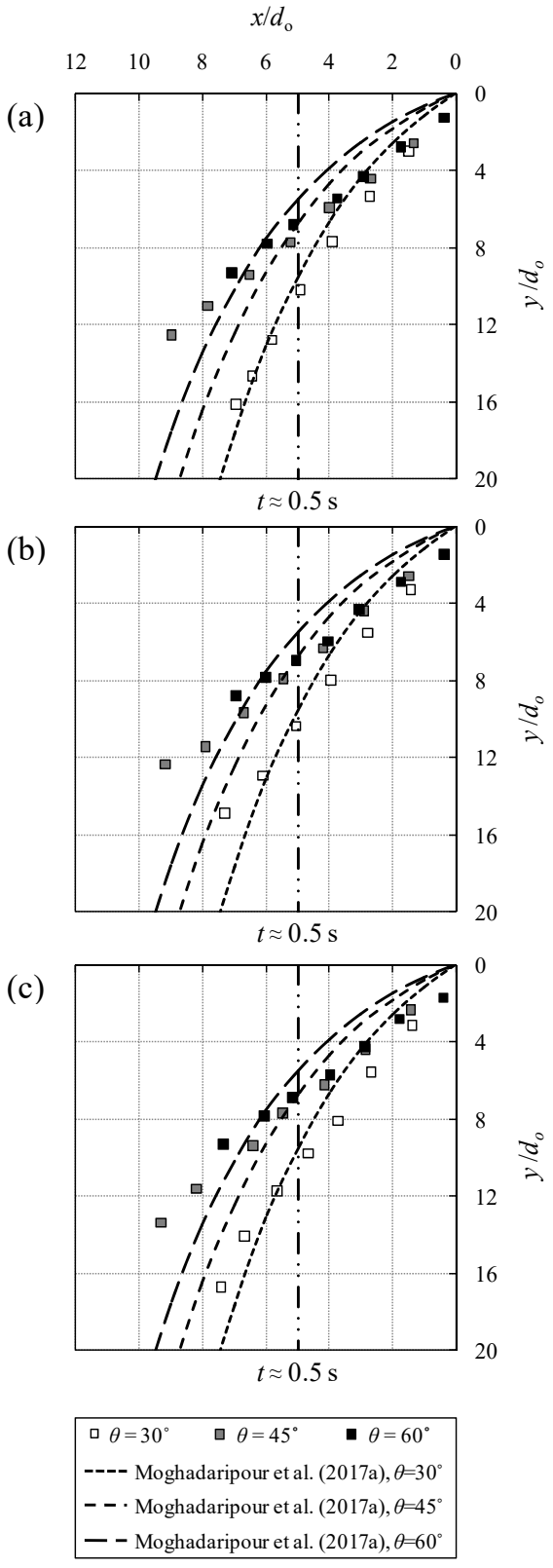

Figure 5.10 Effect of release angle θ on trajectory of sand jets for d_o=0.008 m: (a) L/d_o=8.2; (b) L/d_o=16.3; and (c) L/d_o=24.5

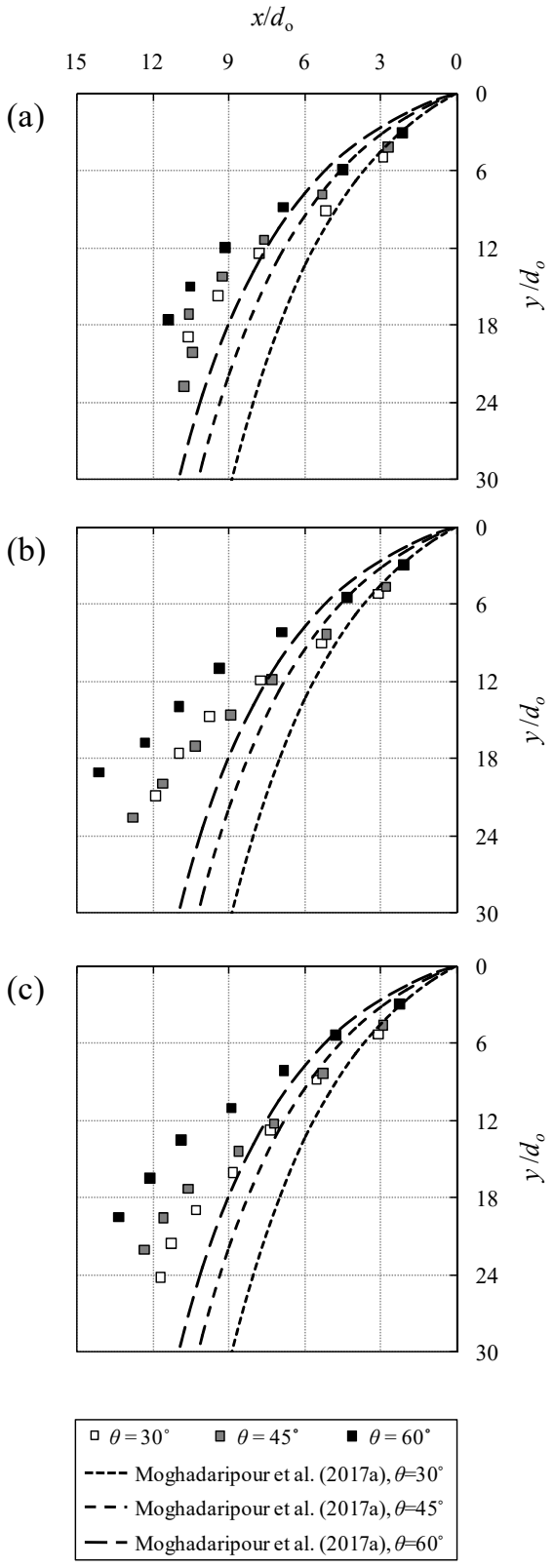

Figure 5.11 Effect of release angle θ on trajectory of sand jets for d_o=0.010 m: (a) L/d_o=8.4; (b) L/d_o=12.5; and (c) L/d_o=16.7

Chapter 5 On the motion of oblique sand jets in stagnant immiscible liquids

Acknowledgments

The work presented in this chapter was supported in part by NSERC Discovery grant No. 421785. I would like to thank our undergraduate students (Brock Vandenbrand, Benjamin White, Godfrey Mwenelupembe, and Daniel Grigoriu) for their help in conducting part of the laboratory experiments.

6 General conclusions and recommendations for future research

6.1 General Conclusions

In the preceding chapters, comprehensive experimental studies and analysis were presented on the motion of sand jets passing through stagnant immiscible liquids.

In chapter 4, the evolution oily sand jet released from various release heights was investigated. Effects of the characteristics of sand jets in air such as mass flow rate, sand impact velocity, and jet diameter on the evolution of oily sand jets were also investigated. A total of 36 experiments were carried out to study the effect of nozzle diameter, air release height, and mass of sand particles. In order to study the effect of air release height, three different air release heights of h=0.2, 0.4, and 0.6 m were used. Air release height was normalized to form non-dimensional air release height as η. Three different nozzle diameters of d_o=8, 12, and 16 mm and masses of sand particles ranging from 5 g to 30 g were chosen to study the effect of nozzle diameter and mass of sand particles, respectively. Nozzle size and mass of sand particles were grouped to form wide range of non-dimensional parameter L/d_o from 1 to 19.6. A non-dimensional time scale t^* was presented to study the evolution of oily sand jets. Following results were concluded:

- Jet diameter in air was directly correlated with the nozzle diameter.
- The frontal velocity of sand jets in air was 5% less the falling velocity of particles for the air release height ranging from 0.2 m to 0.6 m.
- The overall behaviour and flow regimes could be better explained in the space frame, whereas a time frame is suitable to correlate data and develop semi-empirical formulations for predictions of frontal velocity.
- Nozzle diameter was found to be the most important parameter in the evolution of oily sand jets.

- Formation and air bubbles escape were directly related to the air release height.
- The overall growth of suspension jets was found to be independent of the air release height.
- L/d_o ratio had no significant impact on the evolution of oily sand jets but for the smallest aspect ratio with the value of L/d_o=1.
- Nozzle size had no significant impact on the spreading rate of oily sand jets for air release height of h=0.2 m and the normalized frontal width increased linearly with y/d_o with the growth rates similar to single-phase buoyant thermals, whereas for air release height of h=0.4 m the spreading rate increased by increasing the nozzle diameter.
- For both shorter release heights (η=108.1 and 216.3), it was found that the normalized frontal width of oily sand jets grew like single-phase buoyant thermals and the spreading rate increased for the highest release height and reached 0.45.
- The effect of air release height and on variations of the frontal velocity with time was studied. It was found that the effect of impact energy became less pronounced as sand jets moved downward and dissipated at $y/d_o \approx 17$.
- The shear stress between sand particles and the oil layer was computed using a momentum equation. It was found that both release height and nozzle diameter have a significant impact on the magnitude of shear stress, while the effect of sand mass is less significant.
- A linear equation was developed to describe the correlation between the normalized shear stress and the controlling parameters with ±10% variations.
- The average shear stress between particles and the ambient was found to be non-linearly correlated with the release height.

- The average drag coefficient of oily sand jets in the early stage of evolution was found to be smaller than the predictions of classical drag formulas in a steady-state condition. However, far from the nozzle where oily sand jets reached the semi-steady condition, the computed drag coefficient became comparable with predictions of the classical drag models.

In chapter 5, the evolution oblique oily sand jet released from various release angles was investigated. A total of 36 experiments were carried out to study the effect of nozzle diameter, release angle, and mass of sand particles. In order to study the effect of release angle, three different release angles of θ=30˚, 45˚, and 60˚ were used. Three different nozzle diameters of d_o=8, 10, and 14 mm and masses of sand particles ranging from 2.5 g to 30 g were chosen to study the effect of nozzle diameter and mass of sand particles, respectively. Nozzle size and mass of sand particles were grouped to form wide range of non-dimensional parameter L/d_o from 1.5 to 24.5. The evolution time t was normalized by the characteristic time scale T to study the evolution of oblique oily sand jets. Following results were concluded:

- Nozzle diameter was found to be the most important parameter in the evolution of oily sand jets.
- No cloud bursting was occurred for evolution of oblique jets released from the smallest nozzle diameter and sand jets descended as a single cluster of particles.
- For bigger nozzle sizes, similar pattern was observed for evolution of sand jets: settling as a mixture of encapsulated clusters of particles and individual sand particles.
- Release angle and aspect ratio did not have significant impact on the general formation of oblique oily sand jets.
- The normalized initial velocity had a direct relationship with L/d_o ratio.

- The normalized initial velocity increased by increasing the nozzle diameter from 8 mm to 10 mm for all release angles, whereas no increment occurred as the nozzle diameter increased from 10 mm to 14 mm.
- the growth rate of the normalized frontal width was proportional to the aspect ratio for all release angles.
- The normalized frontal width grew linearly for d_o=8 mm, whereas reached a plateau at the normalized time ranging from 0.3 to 0.4 for d_o=14 mm.
- For d_o=8 mm, the horizontal and vertical displacements of oblique jets for each release angle followed a same trend and were independent of the aspect ratio, however, the trajectory curves are controlled by the aspect ratio for d_o=10 mm.

6.2 Recommendation for Future Research

This research can be developed in several ways such as:

- Studying the effect of particle size on the on the evolution of oily sand jets. Particle size is on of the parameters that can have significant impact on axial velocity and frontal width of sand particles passing through immiscible interface
- Investigating the effect of oily layer thickness on the characteristics of oily sand jets since in this research the oil layer thickness was kept constant
- Computing the centroid of mass for oblique oily sand jets
- Analysing the behaviour of dragged oil layer during the evolution of oily sand jets
- Calculating shear stress and drag coefficient for oblique oily sand jets.

Notation

The following symbols were used in this thesis:

A_f = frontal cross-sectional area of sand jets, m^2

A_j = cross-sectional area of sand jets in oil layer, m^2

A_s = side surface area of sand jets, m^2

B = buoyancy, m^4/s^2

c_o = initial volumetric concentration of sand particles, vol/vol

c_1 = coefficient

c_2 = coefficient

C_d = drag coefficient

d_o = nozzle diameter, mm

d_j = diameter of sand jets in air, mm

D_{50} = particle size, mm

F_B = buoyancy force, N

f_D = average drag force per particle, N

F_D = drag force, N

F_g = gravitational force, N

F_τ = friction force, N

g = acceleration due to gravity, m/s^2

h = air release height, m

h_{oil} = oil layer thickness, mm

l = characteristic length scale, m

L = length of sand particles in release pipe, m

m = sand mass, g

$\dot{m}$ = mass flux, m/s

R = Reynolds number

R_p = particle Reynolds number

t = time, s

t^* = non-dimensional time scale

T = characteristic time scale, s

u_o = initial velocity of oily sand jets in water, m/s

u_f = frontal velocity of oily sand jets in water, m/s

u_g = free falling velocity, m/s

u_i = impact velocity, m/s

u_n = initial velocity of sand particle at nozzle exit, m/s

u_∞ = terminal velocity of sand particles in water, m/s

w = width of oily sand jets front, m

x = horizontal penetration of sand jets in water, m

y = vertical distance of sand jets from water surface, m

η = non-dimensional air release height

μ_{oil} = dynamic viscosity of oil, kg/m s

μ_w = dynamic viscosity of water, kg/m s

θ = release angle, degree

ρ_b = bulk density of sand particles, kg/m^3

ρ_m = mixture density of oil and sand particles, kg/m^3

ρ_n = mixture density of water and sand particles, kg/m^3

ρ_{oil} = density of oil, kg/m^3

ρ_s = density of sand particles, kg/m^3

ρ_w = density of water, kg/m^3

τ = shear stress, Pa

φ = sphericity

References

Aristoff, J. M. and Bush, J.W. M., (2008). "Water entry of small hydrophobic spheres." *J. Fluid Mech.* 619, 45–79.

Azimi, A. H., Zhu, D. Z., and Rajaratnam, N., (2011). "Effect of particle size on the characteristics of sand jet in water." *J. Eng. Mech.*, 137 (12), 822–834.

Azimi, A. H., Zhu, D. Z., and Rajaratnam, N., (2012a). "Experimental study of sand jet front in water." *Int. J. Multiphase Flow*, 40, pp. 19-37.

Azimi, A. H., Zhu, D. Z., and Rajaratnam, N., (2012b). "Computational investigation of vertical slurry jets in water." *Int. J. Multiphase Flow*, 47, pp. 94-114.

Azimi, A.H., Zhu, D. Z., and Rajaratnam, N. (2014). "An experimental study of subaqueous sand deposition from slurry wall jets." *ASCE, Journal of Engineering Mechanics*, 140(2), pp. 296-314.

Azimi, A. H., (2019). "Experimental investigation on the motion of particle cloud in viscous fluids." *ASME, Journal of Fluids Engineering*, 141(3), 031202, 14 p.

Baines, W. D., (1975). "Entrainment by a plume or jet at a density interface." *J. Fluid Mech*, 68, 309–320.

Banks, R. B., and Chandrasekhara, D. V., (1962). "Experimental investigation of the penetration of a high velocity gas jet through a liquid surface." *J. Fluid Mech.*, 15, 13–34.

Batchelor, G. K. (1954). "Heat convection and buoyancy effects in fluids." Q. J. R. Meteorolog. Soc., 80(345), 339–358.

Breusers, H. N. C., Raudkivi, A. J., (1991). "International Association for Hydraulic Research." Scouring, Balkema, Rotterdam, Netherlands.

Bush, J. W. M., Thurber, B. A., and Blanchette, F., (2003). “Particle clouds in homogeneous and stratified environments.” *J. Fluid Mech.*, 489, 29–54.

Cai, J., Zhu, D. Z., and Rajaratnam, N. (2012). “Observations on sand jets in viscoplastic fluids.” *Theoretical & applied mechanics letters*, 2, 052001.

Cai, J., Hall, N., Elenany, M., Zhu, D. Z., and Rajaratnam, N. (2010). “Observations on sand jets in air.” *J. Eng. Mech*., 10.1061/(ASCE)EM.1943-7889.0000161, 1181–1186.

Cheslak, F. R., Nickolls, J., and Sichel, M., (1969). “Cavities formed on liquid surfaces by impinging gaseous jets.” *J. Fluid Mech.*, 36, 55–63.

Chien, S. F., (1994). “Settling Velocity of Irregularly Shaped Particles.” SPE Drill Completion, 9(4), pp. 281–289.

Ching, C. Y., Fernando, H. J. S. and Noh, Y., (1993). “Interaction of a negatively buoyant line plume with a density interface.” *Dyn. Atmos. Oceans*, 19, 367–388.

Clift, R., Grace, J.R., Weber, M.E., (1978). *Bubbles, Drops, and Particles*. Academic Press, New York, p. 380.

Cotel, A. J., Gjestvang, J. A., Ramkhelawan, N. N., and Breidenthal, R. E., (1997). “Laboratory experiments of a jet impinging on a stratified interface.” *Exp. Fluids*, 23, 155–160.

Cotel, A. J., and Breidenthal, R. E., (1997). “Jet detrainment at a stratified interface.” *J. Geophys. Res.*, 75, 23813–23818.

Deguen, R., Olson, P., and Cardin, P., (2011). “Experiments on turbulent metal-silicate mixing in a magma ocean,” *Earth Planet. Sci. Lett.*, 310(3–4), pp. 303–313.

Deguen, R., Landeau, M., and Olson, P., (2014). “Turbulent metal-silicate mixing, fragmentation, and equilibration in magma oceans,” *Earth Planet. Sci. Lett.*, 391, pp. 274–287.

Dietrich, W. E. (1982). “Settling velocity of natural particles.” *Water Resour. Res*., 18(6), 1615–1626.

Evans, G. M., Jameson, G. J., and Rielly, C. D., (1996). “Free jet expansion and gas entrainment characteristics of plunging liquid jet.” *Exp. Therm. Fluid Sci.*, 12, 142–149.

Friedman, P. D., and Katz, J., (1999). “The flow and mixing mechanisms caused by the impingement of an immiscible interface with a vertical jet.” *Phys. Fluids*, 11(9), pp. 2598–2606.

Gensheimer, R.J., Adams, E.E. and Law, A.W., (2012), “Dynamics of particle clouds in ambient currents with application to open-water sediment disposal.” *J. Hydraul. Eng.*, 139(2), pp.114-123.

Geyer, A., Phillips, J. C., Mier-Torrecilla, M., Idelsohn, S. R., and Onate, E., (2011). “Flow Behaviour of Negatively Buoyant Jets in Immiscible Ambient Fluid.” *Exp. Fluids.*, 52(1), pp. 261–271.

Giraut, F., Carazzo, G., Tait, S., Ferrucci, F., and Kaminski, E., (2014). “The Effect of Total Grain-Size Distribution on the Dynamics of Turbulent Volcanic Plumes.” *Earth Planet. Sci. Lett.*, 394, pp. 124–134.

Gu, J., Li, C.W., (2004). “Modeling instantaneous discharge of unsorted particle cloud in ambient water by an Eulerian-Lagrangian method.” *J. Hydraul. Res.*, 42(4), 399−405.

Hall, N., Elenany, M., Zhu, D. Z., and Rajaratnam, N., (2010). “Experimental Study of Sand and Slurry Jets in Water.” *J. Hydraul. Eng.*, 136(10), pp. 727–738.

Holdich, R. G. (2002). *Fundamentals of particle technology*, Midland Information Technology and Publishing, Shepsted, U.K.

Julien, P.Y., (2010). *Erosion and Sedimentation*. Cambridge University Press.

Larson, M., and Jonsson, L., (1994). “Mixing in a two-layer stably stratified fluid by a turbulent jet.” *J. Hydraul. Res.*, 32, 271–289.

Lee, J., and Chu, V. (2003). *Turbulent jets and plumes: A Lagrangian approach*. Kluwer, Dordrecht, The Netherlands.

Miller, W. G., Scott, J. D., and Sego, D. C., (2009). “Flume Deposition Modeling of Caustic and Noncaustic Oil Sand Tailings.” *Can. Geotech. J.*, 46(6), pp. 679–693.

Moghadaripour, M., Azimi, A. H., and Elyasi, S. (2017a). “Experimental Study of Oblique Particle Clouds in Water.” *Int. J. Multiphase Flow*, 91, pp. 193−213.

Moghadaripour, M., Azimi, A. H., and Elyasi, S. (2017b). “Experimental Study of Particle Clouds in Stagnant Water.” *ASCE, Journal of Engineering Mechanics*, 143(9), 04017082-1-17.

Mohammadidinani, N., Azimi, A. H., and Elyasi, S. (2017). “Experimental Investigation of Sand Jets Passing through Immiscible Fluids.” *ASME, Journal of Fluids Engineering*, 139(5), 051303, 13 p.

Morton, B. R., Taylor, G., and Turner, J. S. (1956). “Turbulent gravitational convection from maintained and instantaneous sources.” *Proc. R. Soc. Lond. Ser. A Math. Phys. Sci*., 234(1196), 1–23.

Nicolas, M., (2002). “Experimental Study of Gravity-Driven Dense Suspension Jets.” *Phys. Fluids*, 14(10), pp. 3570–3576.

Noh, Y., Fernando, H. J. S., and Ching, C. Y., (1992). “Flows induced by the impingement of a two-dimensional thermal on a density interface.” *J. Phys. Oceanogr.*, 22, 1207–1220.

Noh, Y., and Fernando, H. J. S. (1993). “The transition in the sedimentation pattern of a particle cloud.” *Physics of Fluids*, 5(12), pp. 3049-3055.

Noh, Y. (2000). “Sedimentation of a particle cloud across a density interface.” *Fluid Dyn. Res.*, 27, 129–142.

Ogata, k., Funatsu, K., Tomita, Y. (2001). “Experimental investigation of a free falling powder jet and the air entrainment.” *Powder Technology*, 115 (2001) 90-95.

Qian, F., Mutharasan, R., and Farouk, B., (1996). “Studies of interface deformations in single-and multilayered liquid baths due to an impinging gas jet.” *Metall. Mater. Trans.*, B 27, 911–920.

Rahimipour, H. and Wilkinson, D., (1992). “Dynamic behavior of particle clouds.” *Eleventh Australasian Fluid Mechanics Conference*, Vols 1 and 2, University of Tasmania, Hobart, Australia, 743-746.

Rajaratnam, N., and Mazurek, K.A. (2006). “An experimental study of sand deposition from sediment laden water jet.” *ASCE, J. Hydraulic Res*. 44(4), pp. 560-566.

Rao, K. K., Nott, P. R., and Sundaresan, S. (2008). *An introduction to granular flow*, Cambridge University Press, Cambridge, U.K.

Ruggaber, G.J., (2000). “The dynamics of particle clouds related to open-water sediment disposal.” *Ph.D. Thesis*, Department of Civil and Environmental Engineering, MIT, Cambridge, MA, 242 p.

Sheen, H. J., Jou, B. H., and Lee, Y. T., (1994). “Effect of particle size on a two-phase turbulent jet.” *Exp. Therm. Fluid Sci*., 8, 315–327.

Shy, S. S., (1995). “Mixing dynamics of jet interaction with a sharp density interface.” *Exp. Therm. Fluid Sci.*, 10, 355–369.

Tan, B. C.-W., Vlaskamp, J. H. A., Denissenko, P., and Thomas, P. J., (2016). “Cavity formation in the wake of falling spheres submerging into a stratified two-layer system of immiscible liquids.” *J. Fluid Mech.* 790, 33–56.

Tan, B. C.-W., and Thomas, P. J., (2018). "Influence of an upper layer liquid on the phenomena and cavity formation associated with the entry of solid spheres into a stratified two-layer system of immiscible liquids." *Phys. Fluids* 30, 064104.

W.A. Beveloo, H.A. Leniger, J. Van De Velde, Chem. Eng. Sci. 15 (1961) 260.

Webster, D. R., and Longmire, E. K. (2001). "Jet pinch-off and drop formation in immiscible liquid-liquid systems." *Exp. in Fluids*, 30, 47–56.

Wörner, M., (2003). *A compact introduction to the numerical modeling of multiphase flows*. Forschungszentrum Karlsruhe, p 38.

Zhao, B., Law, A.W., Eric Adams, E., Shao, D. and Huang, Z., (2012). "Effect of air release height on the formation of sediment thermals in water." *J. Hydraul. Res.*, 50(5), pp.532-540.

Appendix

A study of mound formation by discharging sand particles through oblique pipes in stagnant water*

Abstract

Laboratory experiments were performed to investigate the development of subaqueous sand deposition from oblique pipes in stagnant water. Effects of four nozzle diameters d_o=8, 10, 13, and 15 mm, four release angles θ=15º, 30°, 45º, and 60°, three released heights H=0.25, 0.50, and 1.00 m and a wide range of sand mass from 40 g to 450 g were evaluated to study the growth and development of sediment mound. The masses of sand particles ranged from 40 g to 450 g. 12laboratory tests (series A) with ten different particles masses were performed to study the mound formation and its development. Another 12 tests (Series B) were carried out to study the shape of deposition. It was found that the initial parameters can alter the shape of deposition. Five different shape patterns were observed named as circular, ellipse, circular-ring, ellipse-ring, and pear-shaped. Formations of the first four shapes were identified by prediction of the scour hole and study the effect of controlling parameters. It was found that the nozzle size plays the most important role in shape formation and mound development. Release angle and release height were secondary important. Size of the scour hole in the middle of sediment deposition was predicted using engineering assumptions and available semi-empirical correlations in the literature. It was found that the existing formulations can accurately predict the size of the scour for large release angle (θ=60º). Semi-empirical formulations were developed to predict the deposition length,

*A part of this appendix was submitted to the International Journal of Sediment Research

width, height, and area. The existence of the pear-shaped deposition was tested using mass balance concept.

1. Introduction

Sediment deposition has many applications in engineering and environment such as artificial island construction, land development, marine bed capping and dredging (Shields et al., 1984; Tamai et al., 1991; Rajaratnam and Mazurek, 2006; Azimi et al., 2011, 2012a, b, 2014, 2015). In artificial island construction, sand is continuously discharged from barges into marine environments to develop an island foundation. Marine sediment capping is a technique which can be used to cover waste sediment disposal. The cover layer remains in place to prevent the spread of waste material in aquatic environment. Dredging is an act of removing silt and aggregates from the bottom of lakes, rivers and other water bodies. Dredged material is often required to be discharged in to specific disposal areas (Chin, 2012). Land development and reclamation operations are other applications of subaqueous sediment mounds (Gu and Huang, 2008; Bhuyian et al., 2010). A great example of land reclamation was the Kansai International Airport project studied by Tamai et al. (1991). Sediment deposition also occurs in construction of artificial beaches near shorelines and in tailing beach construction (Azimi et al., 2014). Sediment mounds are formed if sandy materials are discharged from the water surface. When waste materials are released into flowing water, deposition patterns are affected by the sediment and flow characteristics of the receiving water field (Gu and Huang, 2008; Bhuiyan et al., 2010).

Mound formation can be better predicted by understanding particle dynamics and mixing processes of particle cloud with ambient water (Noh and Fernando, 1993; Bush et al., 2003). Once particles are discharged into water it first forms a particle cloud and the cloud characteristics changes as particles descend downward. Accordingly, deposition pattern and mound formation are

affected by the shape of particle cloud when it collides with the bed. Experimental studies have been carried out to understand the dynamics and dispersion of particles once they are released into ambient water (Nakasuji et al., 1990; Buhler and Papantoniou, 2001; Rahimipour and Wilkinson, 1992; Bond and Johari, 2005; Kikkert et al., 2009; Zhao et al., 2012; Wang and Kikkert, 2014). Particle cloud is formed once particles are released into the ambient. Considering the mass of sediments m, sediments density ρ_s, and the mean size of particlesD_{50}, sediment motion can be categorized into a thermal regime and a particle-settling (i.e., swarm) regime (Fischer et al. 1979). Particle cloud is formed immediately after releasing particles (i.e., thermal motion), and it grows and spreads as it descends further downstream. Far from the point of release, particles set a distance between each other and particle-particle interaction becomes less significant and the cloud motion is governed by the balance between the buoyant force and the drag force on each particle (Fischer et al., 1979). In this condition, the cloud velocity is identified by a function of terminal settling velocity of individual particles (Noh and Fernando, 1993; Bush et al., 2003; Azimi et al. 2012a). Azimi et al. (2012a) found that in swarm regime the grouping effect of particles on frontal of sand jets is still exist and the frontal velocity of the cloud is around five times of the individual particle settling velocity.

Many research studies have been performed to study sediment deposition in quiescent water (Ruggaber, 2000; Bhuiyan, 2010; Azimi et al., 2014, 2015). Formation of sand mounds issued by vertical slurry jets was studied by Rajaratnam and Mazurek (2006). Two uniform sand particle sizes with mean diameters of 1.2 mm and 2.38 mm and a nozzle size of 12.7 mm were used to form circular slurry jets. The mound profile was approximated with a half-cosine equation with a reasonable accuracy. The effects of jet characteristics such as bed slope, particle size, and sediment concentration on the growth of sediment mound was experimentally studied by Azimi et al. (2014).

Appendix

Their study was focused on subaqueous deposition of sand particles from sediment-laden circular jets on horizontal and sloping beds. Three different flow regimes named as developing regime, spreading regime, and backup regime were identified. Empirical formulations were developed to predict the sizes of sediment deposition with time. Sediment deposition from horizontal submerged turbulent jets into an ambient was studied using both laboratory experiments and numerical modeling (Lane-Serff and Moran, 2005; Cuthbertson and Davies, 2008; Lee et al., 2013; Chan et al., 2014; Chan and Lee, 2016). These studies were mainly focused on presenting integral models to predict the structure of horizontal sediment-laden jets and near-source deposition patterns.

Mound formation by sand disposal in flowing water was studied Li and Ma (2001). They developed a three-dimensional numerical model to investigate the deposition pattern for sediment disposal in cross-flow ambient water. It was found that the deposition size is a function of buoyancy flux, sand mass flux, and the horizontal momentum flux of the flow. Based on their analysis, two different deposition patterns were observed and they were named as oblong and horseshoe-shaped deposition. The effects of sediment concentration, bed slope and flow discharge on sediment deposition of silty soils were experimentally studied by Beuselinck et al. (1998). Particles ranging from 2 to 63 μm were introduced to a sloping flume having a slop of 10% in the upper part and a slop of 2% in the lower part. They reported a threshold discharge after which the deposition rate reduced considerably. Bhuiyan et al. (2010) studied the growth of large sediment mounds in flowing water formed by continuous release of relatively large sand particles (i.e., 2.38 mm) from the water surface. Three different flow conditions with initial velocities of 0.205, 0.257 and 0.304 m/s were designed to investigate the growth of mound characteristic dimensions. A longitudinal mound profile was modeled by an exponential function. It was found that the growth of the width and area of the mound were faster than the height and the mound height increased

until it reached to the water surface. Scheffner (1996) proposed a methodology to predict long-term behaviour of deposited sediment such as fade and stability of the mound. Miller et al. (2002) conducted field studies to investigate the fate and long-term sediment characteristics of the mound.

In construction of artificial island and dredging, sand particles and dredging waste materials are usually introduced to water body in an angle with the water surface. In these cases, the dynamics of particle clouds can be significantly influenced by effects of the release angle and release height. Hydrodynamics of particle cloud in these conditions are recently studied by Moghadaripour et al. (2017a, b) indicating the significance of those parameters. The main objective of the present study is to investigate the resulted sediment deposition from particle clouds forming from different release angles and release heights from the water surface. In addition, most of experimental investigations on sediment depositions in the past have dealt with continuous release of sand particles to study sediment deposition development with time. However, the present study deals with sediment mound development using instantaneous release of various sand masses to model sediment disposal from barges. In this study, effects of sand mass m, nozzle diameter d_o, release angle θ, and release height H on formation and growth of sediment deposition are studied.

This paper is organized in 5 sections. In the following section, the underlying physics on mound formation are discussed using dimensional analysis. Experimental setup and the initial parameters are described in section 4. Section 4 discuss about the experimental results and provide semi-empirical models to predict mound development. Summary and conclusions of the present study are explained in section 5.

2. Dimensional Analysis

The characteristic length scales (i.e., length l, width w, and height h) and area A of a sediment deposition are controlled by the properties of the ambient, physical characteristics of particles, and

initial release conditions. Development of sediment deposition can be linked to those parameters as:

$$l, w, h, A = f_1\left(m, d_o, D_{50}, H, \theta, u_o, z, \rho_w, \rho_s, g, \mu\right) \quad \text{(A1)}$$

where m is the mass of sand particles, d_o is the inner diameter of nozzle, D_{50} is the mean particle size where 50% of particles are greater than D_{50}, H is the release height, θ is the release angle, u_o is the velocity of particle cloud at the nozzle exit, z is the depth of water from water surface to the bed, ρ_w and ρ_s are the densities of water and sand particles, respectively, g is the acceleration due to gravity, and μ is the dynamic viscosity of water. Using Bernoulli's equation, the velocity of particle cloud at the nozzle can be correlated with nozzle size in form of $u_o=(gd_o)^{0.5}$. Previous laboratory experiments in the field of sediment deposition indicated that the size of the sand mound can be correlated with the nozzle size (Rajaratnam and Mazurek, 2006, Azimi et al., 2014). Mass of sand particles passing through a pipe can be described as a length scale to show the length of the pipe L filled up with the corresponding mass m (Moghadaripour et al., 2017a, b; Mohammadidinani et al., 2017) and it can be defined as:

$$L = \frac{4m}{(1-n)\pi\rho_s d_o^{\,2}} \quad \text{(A2)}$$

Relatively narrow range of particle sizes has been used to study mound formation from continuous release of sand particles in the literature. Rajaratnam and Mazurek (2006) used D_{50}=1.2 and 2.38 mm, Bhuiyan et al. (2010) used D_{50}=2.38 mm and Azimi et al. (2014) used D_{50}=0.21, 0.42, and 0.54 mm. It was shown that the effect of particle size can be properly included in the time scale of mound development. For releasing a fix amount of sand mass, particle size changes the angle of repose of deposition which can potentially changes the mound height and the base area of the mound. A narrow range of particle size (i.e., 0.595 mm≤D_{50}≤0.707 mm) was used in

this study to reduce the number of unknown variables. The selected range of particle size is within the average particle size range being used in the literature.

Assuming constant particle size, the controlling parameters can be group together to reduce the number of unknowns to non-dimensional parameters as:

$$\frac{l}{d_o},\frac{w}{d_o},\frac{h}{d_o},\frac{A}{d_o^2}=f_2\left(\frac{u_o}{\sqrt{g\frac{(\rho_s-\rho_w)}{\rho_w}L}},\frac{\rho_w u_o L}{\mu},\frac{z}{H},\theta\right) \tag{A3}$$

An important non-dimensional parameter describing particle dynamics in this study known as Froude number $\mathsf{F_r}$ and it can be described as:

$$\mathsf{F_r}=\frac{u_o}{\sqrt{g'L}}\approx\frac{\sqrt{gd_o}}{\sqrt{g\frac{(\rho_s-\rho_w)}{\rho_w}L}}\approx\lambda_1\left(\frac{L}{d_o}\right)^{-1/2} \tag{A4}$$

Where $g'=g(\rho_s-\rho_w)/\rho_w$ is the reduced gravity and λ_1 is a constant with a value of 0.77 in this study. As it describes from Eq. (A4), the defined Froude number is a function sand mass and nozzle size as:

$$\mathsf{F_r}=f_3(m^{-1/2},d_o^{3/2}) \tag{A5}$$

Based on dimensional analysis Reynolds number $\mathsf{R_e}$ can be defined to describe the balance between the inertia and viscous forces as:

$$\mathsf{R_e}=\frac{u_o L}{\nu}\approx\lambda_2\left(\frac{L}{d_o}\right)(d_o)^{3/2} \tag{A6}$$

Where $\nu=\mu/\rho_w$ is the kinematic viscosity of water and λ_2 is constant with a value of $3.13\mathsf{x}10^6$. Eq. (A6) can be also described based on the initial parameters of sand mass and nozzle size as:

$$\mathsf{Re_p}=f_4(m,d_o^{-3/2}) \tag{A7}$$

Appendix

Shape and development of underwater mound formation can be studied in a non-dimensional form. Hence, Eq. (A1) can be written as:

$$\frac{l}{d_o},\frac{w}{d_o},\frac{h}{d_o},\frac{A}{d_o^{\,2}} = f_5\left(\mathsf{F_r},\mathsf{R_e},\frac{z}{H},\theta\right) \tag{A8}$$

In this study, Froude number varies from 0.04 to 0.27 and Reynolds number varies from 49,110 to 1,015,000 (see Table A1).

The extent to which a jet starts to behave as a plume can be predicted by the length scale of l_m (Fischer et al.,1979) defined as $l_m=M_o^{1/4}/B_o^{1/2}$ where $M_o=\rho_m/\rho_w(\pi d_o^2/4)u_o^2$ is the initial specific momentum flux of particle cloud, $B_o=g[(\rho_s-\rho_w)/\rho_w](\pi d_o^2/4)u_o$ and ρ_m is the density of the mixture defined as [$\rho_m=c_o\rho_s+(1-c_o)\rho_w$] where c_o is the initial sand concentration. The momentum length scale of l_m was 3.5, 3.12, 2.74 and 2.55 m for tests with d_o of 8, 10, 13, and 15 mm, respectively. The values of l_m indicate that all tests are in the jet-like regime and the effect of momentum dominates the buoyancy. In addition, the minimum equivalent pipe length filled out with sand particles using constant mass of 380 g in Eq. (A2) gives L=0.128 m which is comparable to the water depth z. This indicates that slurry jets is formed instead of detached particle clouds in most cases in this study.

Appendix

Table A1 Details of laboratory experiments and particle cloud characteristics for sediment deposition with D_{50}=0.65 mm and z=0.15 m

Test	d_o (mm)	θ (degree)	H (m)	u_o[a] (m/s)	η	u_w (m/s)	u_z (m/s)	L (m)	L/d_o	w' (m)
A1(B6)	10	30	0.25	0.21	10.5	0.106	0.32	0.288-3.24	28.8-324	0.052
A2	10	30	0.50	0.21	14.7	0.106	0.32	0.288-3.24	28.8-324	0.050
A3	10	30	1.00	0.21	20.8	0.106	0.32	0.288-3.24	28.8-324	0.048
A4(B8)	10	60	0.25	0.21	10.5	0.078	0.27	0.288-3.24	28.8-324	0.090
A5	10	60	0.50	0.21	14.7	0.078	0.27	0.288-3.24	28.8-324	0.086
A6	10	60	1.00	0.21	20.8	0.078	0.27	0.288-3.24	28.8-324	0.081
A7(B14)	15	30	0.25	0.26	8.5	0.164	0.32	0.128-1.44	8.5-96	0.048
A8	15	30	0.50	0.26	12	0.164	0.32	0.128-1.44	8.5-96	0.046
A9	15	30	1.00	0.26	17	0.164	0.32	0.128-1.44	8.5-96	0.044
A10(B16)	15	60	0.25	0.26	8.5	0.120	0.27	0.128-1.44	8.5-96	0.088
A11	15	60	0.50	0.26	12	0.120	0.27	0.128-1.44	8.5-96	0.084
A12	15	60	1.00	0.26	17	0.120	0.27	0.128-1.44	8.5-96	0.080
B1	8	15	0.25	0.19	11.7	0.083	0.25	4.74	592	---
B2	8	30	0.25	0.19	11.7	0.063	0.25	4.74	592	---
B3	8	45	0.25	0.19	11.7	0.083	0.25	4.74	592	---
B4	8	60	0.25	0.19	11.7	0.063	0.25	4.74	592	---
B5	10	15	0.25	0.21	10.5	0.106	0.32	0.288-3.24	28.8-324	0.042
B7	10	45	0.25	0.21	10.5	0.106	0.32	0.288-3.24	28.8-324	0.064
B9	13	15	0.25	0.24	9.2	0.140	0.31	1.79	138	0.043
B10	13	30	0.25	0.24	9.2	0.140	0.31	1.79	138	0.049
B11	13	45	0.25	0.24	9.2	0.152	0.31	1.79	138	0.062
B12	13	60	0.25	0.24	9.2	0.152	0.31	1.79	138	---
B13	15	15	0.25	0.26	8.5	0.120	0.27	0.128-1.44	8.5-96	0.042
B15	15	45	0.25	0.26	8.5	0.120	0.27	0.128-1.44	8.5-96	0.060

[a]Initial velocity was calculated based on $u_o=0.68(gd_o)^{1/2}$.

3. Experimental Setup

Experiments were conducted in a rectangular glass-walled tank of 1.60 m long, 0.80 m wide and 0.80 m high in the hydraulic laboratory at Lakehead University. The experimental tank was filled with fresh water with a temperature of T=23±0.5 °C and a water density of ρ_w=997.5 kg/m^3. The water in the tank was kept at a constant level with a depth of 0.65 m using a control valve. A false bed was constructed with a dimension of 0.72 m×0.42 m to adjust the depth of water from the surface to z= 0.15 m. The false bed was located at the centre of the tank to avoid any boundary effect on the motion of particles. Figure A1 shows the experimental setup and adopted coordinate

system. Silica sand particles were selected using sieve analysis. The collected particles from two sieve sizes of D_{50}=0.595 mm (i.e., sieve #30) and 0.707 mm (i.e., #25) were mixed and used in this study with a nominal diameter of 0.65 mm. The uniformity coefficient of particles $\sigma=(D_{84}/D_{16})^{0.5}$ was calculated for the particle sample with a value of 1.31. Based on Breusers and Raudkivi (1991) soil sample can be considered uniform if $\sigma\leq1.35$. The Silica sand particles had a density of ρ_s=2660 kg/m^{3}and an averaged unpacked sand concentration of c_o=0.6. Sand particles were evenly poured in a funnel and they were released instantaneously above the water surface using a robber plug.

Four different nozzle sizes with the inner diameters of d_o=8, 10, 13, and 15 mm were used for mound shape classification and further experiments were carried out for nozzle sizes of 10 and 15 mm for prediction of mound development. Nozzles were located at least 3 mm above the water surface to avoid water contact with sand particles and clogging the nozzle.12sets of experiments (i.e., Series A) were carried out to predict mound development with sand mass and in each test ten different masses of sand particles ranging from 40 g to 450 g were released from three various heights $H$of 0.25 m, 0.5 m and 1.0 m at two different angles of θ=30° and 60° respect to the vertical plane.16 experiments were conducted for a constant release height of H=0.25 m to study the effect of initial parameters on shape patterns of mounds (i.e., Series B). Details of laboratory experiments and non-dimensional parameters are listed in Table A1. Development of sediment depositions were recorded from top and side views using a highspeed camera (Photron−Fastcam, 1024PCI−100KC). Figure A2 shows the top-view images of sediment deposition patterns for a constant mass and release height. The obtained images were turned into negative for better visualization. Images were imported to AutoCAD to determine the mound's characteristic dimensions. After recording images, sediments were carefully removed from the false bed to

minimize water disturbance. Three minutes time lag was allowed between each experiment to dampen water surface fluctuations.

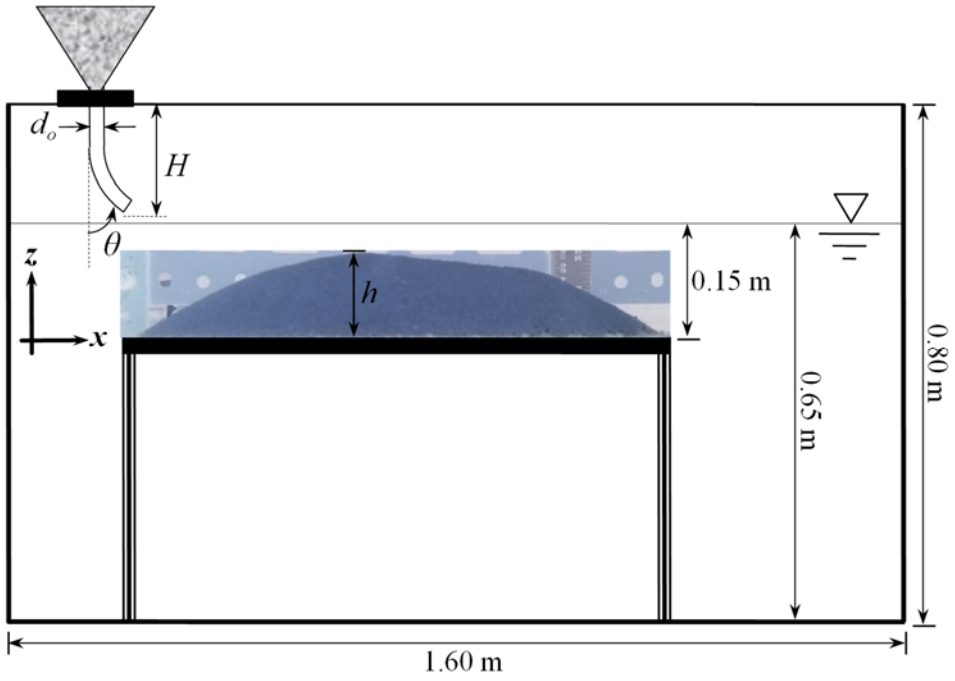

Figure A1 Schematic of the experimental setup and coordinate system

Following a short acceleration period, particles hit the bed and spread in both longitudinal and transverse directions and formed sediment deposition. Tests A3 (m=40 g, d_o=0.010 m, θ=30° and H=1.0 m) and A10 (m=450 g, d_o=0.015 m, θ=60° and H=0.25 m) were repeated for five times to measure the uncertainties of measurements. Measurement uncertainty of length and area were found to be higher than mound width with a variation of 3%-15% and 5%-7%, respectively. Mound width increased due to rolling of particles from mound height so clear edges was formed in both sides of the mound. This reduced measurement uncertainty of width to 0.5%-4%.

Appendix

4. Experimental Results

4.1 Shape of sediment deposition

16 experiments were performed to classify the shape of sediment mound while the release height and mass are constant. Four different nozzle sizes with the inner diameters of 8, 10, 13 and 15 mm with four various release angles of 15°, 30°, 45° and 60° were selected. In each test, 380 g of sand particles was released and the release height was constant at H=0.25. The water depth was also constant (z=0.15 m) forming the z/H ratio of 0.6. Figure A2 shows the sediment deposition of sand particles with different nozzle sizes and release angles. As can be seen, the deposition pattern is explicitly controlled by the nozzle size and the release angle. Using the obtained images, five distinct patterns were observed during the mound classification process which can be referred to as the circular, ellipse, circular ring, ellipse ring, and pear-shaped. The circle deposition pattern occurs when particles were released from a nozzle of 8 mm diameter and the release angle ranging from 15° to 45° (Figures A2a-A2c). As the release angle increases, the stream wise component of the initial momentum of sand particles becomes larger and this can push sand particles further away from the nozzle. So, the mound length becomes larger for test with a release angle larger than 45 degrees (see Figure A2d). As a result, an ellipse pattern starts to build up for all sand mounds with nozzle sizes of 8, 10, 13 mm and with θ=60^{o} (see Figures A2d, A2h, and A2i).

Appendix

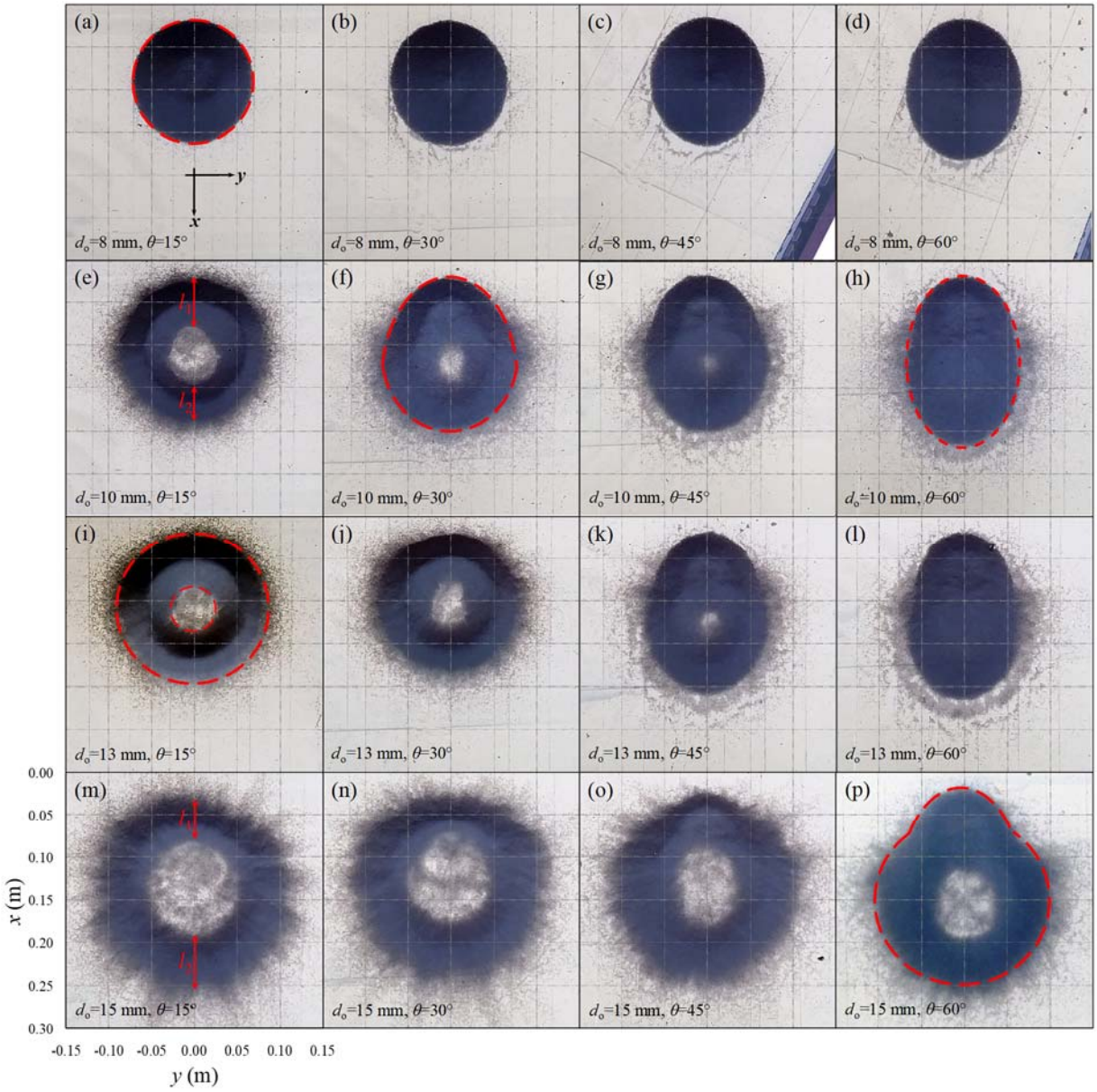

Figure A2 Effects of nozzle size and release angle on deposition patterns of sediment mounds for Series B experiments with a constant release height of H=0.25 m

Visual boundary views (i.e., dashed lines) for the circle and ellipse patterns are depicted in Figures A3a and A3h, respectively. Circular ring shapes were observed for tests with relatively larger nozzle sizes than 8 mm. The scour forms at the center of deposition may be the result of high velocity impact of sand particles with the bed which forms a crater. Similar deposition patters

were observed due to collision of a vortex ring in granular layer (Yoshida and Sano, 2014; Masuda et al., 2012; Munro et al., 2009). Depends on the release angle either circular ring or ellipse ring form (see Figures A2i and A2k). A pear-shaped deposition pattern forms in large release angle and large nozzle size. This deposition pattern can be seen in Figure A2p where d_o=15 mm and θ=60°. The pear-shaped pattern forms due to non-uniform sand concentration of oblique slurry jets and unbalanced distribution of kinetic energy after particle collision with the bed. These effects also control the mound thickness size of circular rings (i.e., l_1 and l_2) as shown in Figures A2e and A2m. Deposition pattern classification is summarized in Table A2.

As mentioned in the dimensional analysis section, the initial velocity as well as the initial energy of sand particles can be correlated with the size of the nozzle (i.e., $u_o \sim d_o^{1/2}$). Therefore, particles passing through a larger nozzle have higher velocity and therefore, higher kinetic energy. Considering that the particle grouping effect is similar for all cases, the rate of energy dissipation of particle clouds in water will be relatively similar for all particle clouds in Figure A2. Therefore, particles passing through larger nozzles have higher initial kinetic energy and the impact velocity of those tests with the bed becomes higher. Particle re-suspension can occur once the particles impact energy becomes larger than the energy losses due to impact. This may be the reason of large scour formation at the center of deposition as the nozzle size increases (see Figures A2e, A2i, and A2m).

Appendix

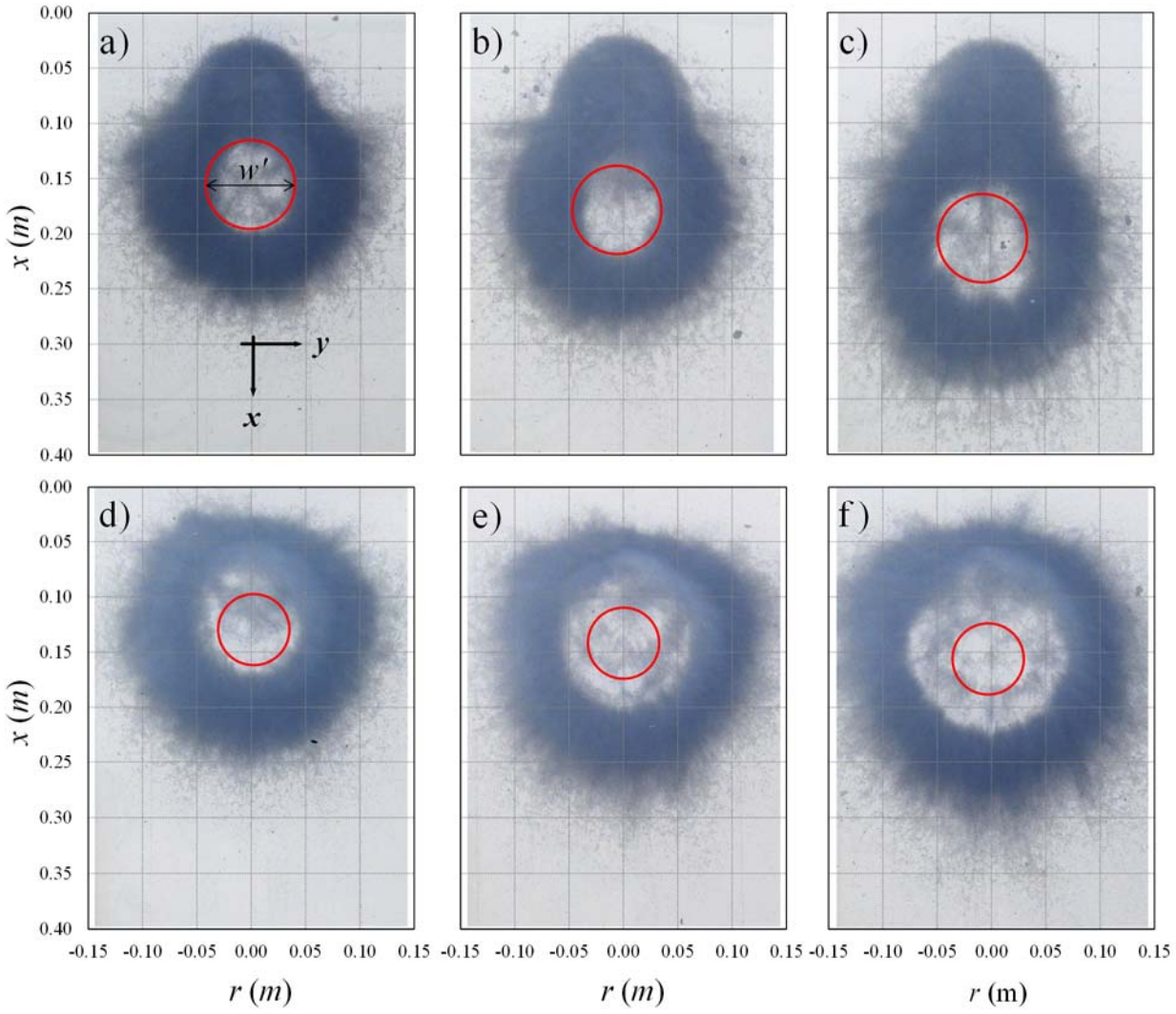

Figure A3 Effect of release height and release angle on formation of sediment mound for constant mass (m=380 g) and nozzle size (d_o=15 mm); a) θ=60°, H=0.25 m; b) θ=60°, H=0.5 m; c) θ=60°, H=1 m; d) θ=30°, H=0.25 m; e) θ=30°, H=0.5 m; f) θ=30°, H=1 m

In order to determine the formation of scour hole in the middle of sediment deposition impact velocities of water and sand particles at the bed location should be predicted. A comparison of those velocities with the terminal settling velocity of individual particles u_∞ determines the scouring condition. Julien (2010) classified the general flow of sediments in water in three zones of bed load, mixed load, and suspended load by comparison of the shear velocity u^* with the terminal settling velocity of individual particles. It was found that the bed load zone forms for

Appendix

$u_*/u_\infty<0.5$ and in this condition almost all particles roll on the bed and no suspended load exists in the flow. All sediments become suspended if the shear velocity becomes at least two times of the terminal settling velocity of individual particles. The mixed load occurs for $0.5<u^*/u_\infty<2$.

Table A2 Summary of pattern classification for sediment deposition

d_o (mm)	Release angle θ			
	15°	30°	45°	60°
8	Circle	Circle	Circle	Ellipse
10	Circular ring	Ellipse ring	Ellipse ring	Ellipse
13	Circular ring	Circular ring	Ellipse ring	Ellipse
15	Circular ring	Circular ring	Pear	Pear

Existence of deposition scour can be evaluated by assuming that the vertical velocity of slurry jets is comparable with the bed shear velocity. Two formulas are used to predict the velocity of water and sand particles in slurry jet flows. Azimi et al. (2012b) proposed a formula to predict the water-phase velocity of slurry jets at different distances from the nozzle for a relatively wide range of distances ($10\leq z/d_o\leq 170$) as:

$$\frac{u_w \mathsf{F}}{u_o} = \frac{2}{3} c_o^{2/5} \left(\frac{z}{\mathsf{F} d_o} \right)^{-1/3} + 3 \left(\frac{z}{\mathsf{F} d_o} \right)^{-1} \tag{A9}$$

where F is Froude number based on the nozzle size $\mathsf{F}=u_o/[gd_o(\rho_s-\rho_w)/\rho_w]$. Water velocity at the bed for all tests can be calculated by substituting the initial parameters in Eq. (A9) and assuming $u_o=0.68(gd_o)^{1/2}$ for the initial velocity of sand jets based on experimental study of Azimi et al. (2012a). Since the initial jet velocity linked with the nozzle size, Froude number becomes constant with a value of 0.53 for all tests of same release height. Values of water velocity at the bed location are listed in Table A1. The terminal velocity of individual particles u_∞ can be calculated using Haywood table (Holdich, 2002) as $u_\infty=0.102$ m/s. Based on Eq. (A9), the calculated water velocity of slurry jets at the bed location for $d_o=8$ mm is 0.083 m/s whereas these values for $d_o=10$, 13, and

15 mm are 0.105, 0.12, and 0.153 m/s, respectively. This can clearly show why no scour holes formed for slurry jests with d_o=8 mm. In addition, the release angle increases the travel distance of particles (i.e., $z/\cos\theta$) and reduces the water velocity as indicated in Table A1. The water velocity at the bed location for d_o=10 mm and θ=30° is 0.106 m/s indicating a value slightly larger than the terminal settling of individual sand particles (i.e., u_∞=0.102 m/s) whereas for the same nozzle size and θ=60° water velocity drops to 0.078 m/s indicating no sediment re-suspension and scour hole formation (see Figures A2f and A2h).

Moghadaripour et al. (2017a) proposed an empirical correlation to predict vertical velocity of particle cloud released from oblique pipes for a wide range of L/d_o and particle sizes as:

$$\frac{u_z}{u_\infty} = \varphi_1 \left(\frac{z}{d_o} \right)^{-\varphi_2} \tag{A10}$$

where u_z is the vertical velocity of oblique particle cloud, u_∞ is the terminal settling velocity of individual particles, φ_1 and φ_2 are coefficients and they are a non-linear function of L/d_o and particle size. As listed from Table A1, the values of L/d_o ranging from 8.5 to 324 for different masses of particles. However, the maximum value of L for calculation of vertical velocity in Eq. (A10) is equivalent to the vertical distance from the nozzle and the point of impact (i.e., z=0.15m). Higher L values only indicate the existence of continuous release and they should not be used in Eq. (A10). The values of u_z for present experiments are listed in Table A1. This clearly shows that at the impact location (i.e., $10 \le z/d_o \le 18.75$), particle group velocity is two to three times larger than the water velocity calculated from Eq. (A9) which is consistent with momentum driven classification determined by the characteristic length scale of l_m. Values of u_z indicate that the calculated vertical velocities are still two to three times larger than the settling velocity of individual particles (i.e., u_∞=0.102 m/s) which the excess velocity (kinetic energy) cause sediment re-suspension after the bed impact.

Appendix

The diameter of scour *w'* can be estimated by assuming a Gaussian distribution for sediment velocity profile of slurry jets at the impact location and finding the distance from the center of deposition where the sediment velocity in transverse direction u_y becomes equal to u_∞.

$$\frac{u_y}{u_z} = e^{\left[-0.693(w'/w)^2\right]} \tag{A11}$$

where w is the width of slurry jet and it can be calculated for different aspect ratios and release heights using Moghadaripour's formula as:

$$\frac{w}{d_o} = \left[\left[0.236 + 0.0029\left(\frac{L}{d_o}\right)\right] - \left(4\text{x}10^{-5}\eta^2 + 0.0017\eta\right)\right]\left(\frac{z/\cos\theta}{d_o}\right) \tag{A12}$$

where η is the normalized release height and it can be calculated using the Bernoulli's equation as $\eta=(u_o^2+2gH)^{1/2}/u_o$. The calculated radius of scour hole based on Eqs. (A11) and (A12) for all tests is listed in Table A1. Comparison of the predicted scour radiuses and images presented in Figure A2 indicates a well agreement between model prediction and deposition patterns.

Effects of release angle and height on deposition pattern and scour size of sediment mounds are shown in Figure A3. The predicted scours based on Eqs. (A11) and (A12) are also added in top view images. As can be seen, the predicted scour size for sediment depositions issued from pipes with the release angle of θ=60° is very well agreed with experimental observations. Whereas for cases with smaller angle, the assumption of $u_y \approx u_\infty$ under-estimates the scour size.

4.2 Mound dimensions and area

The characteristics length scales of sediment mound were measured to study the development of deposition due to variations of nozzle size, release mass, angle and height. According to experimental observations and dimensional considerations, the nozzle size found to be the most dominant controlling parameter on characteristics of the sediment mound. The length, width, and

area of the mound increased with increasing the nozzle diameter while the mound height slightly decreased. For example, by releasing 380 g of sand particles from two different nozzle sizes of 10 mm and 15 mm while other parameters are constant (θ=30^o, H=0.25 m), length, width, and area of deposition increased by 33%, 41%, and 200%, respectively. However, increasing the nozzle diameter led to a 25% decrease in the height of deposition. The observations showed that by increasing the nozzle diameter, sand particles enter the water ambient with higher velocity which results in considerable growth in both longitudinal and transverse dimensions of the deposition and large scour formation in the middle of deposition. Therefore, the mound area significantly increases by increasing the nozzle size. On the other hand, as particles with higher kinetic energy collide with the bed, they spread more due to higher energy level and form smaller average height.

Figure A4 shows the sensitivity of the characteristic length scales with sand mass by only changing the nozzle size from 10 mm to 15 mm while all other parameters were constant. As can be seen in Figure A4a increasing the nozzle diameter by 50% results in the average growth of mound lengths by 25% despite the changes of other parameters. The smallest change in mound lengths is around 10% (i.e., the minimum value in overbars) for smallest sand mass of 40 g and the maximum change in mound length is 40% for the largest released mass of 450 g for test A12.Release angle is considered as the second most important controlling factor on the characteristics of the sediment deposition. As the release angle increases the velocity component of the particle cloud in x direction increases which results in longer sediment deposition. In contrary, the release angle reduces the deposition width. For example, by doubling the angle of release for a test with m=380 g, d_o=0.015 m and H=0.25 m, the length increased by 13% but the width decreased by 16%. The effect of release angle on the area of the deposition did not reveal a

uniform trend. This may due to the opposite effects of the release angle on the mound length and width.

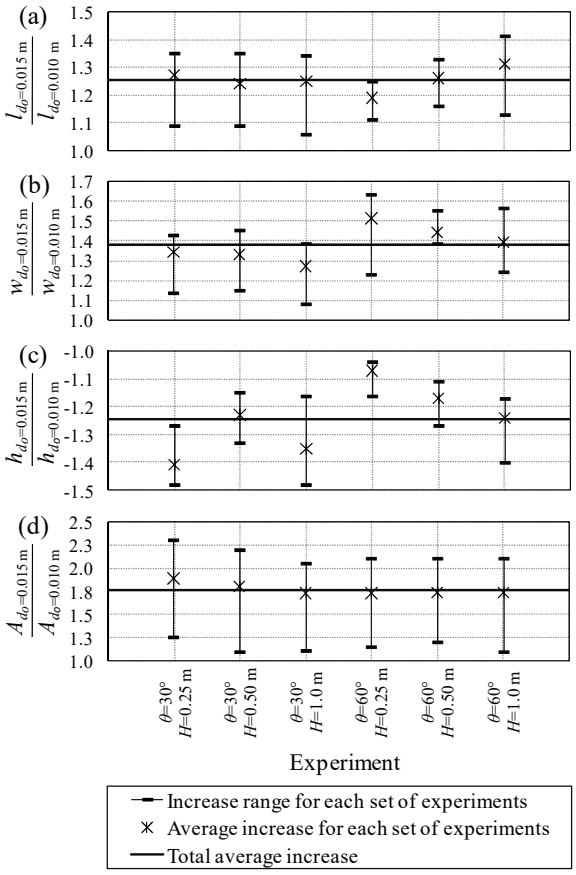

Figure A4 Effect of nozzle size on variations of the mound characteristic length scales; a) mound length; b) mound width; c) mound height; and d) mound area.

The effect of release height on sediment deposition was also considered in this study. The effect of the release height was less significant than the nozzle size and release angle. It was observed that the length and width of deposition increased by increasing the release height since particles gained more energy once they were released from higher positions. This effect was also considered in the growth of oblique particle clouds in the study of Moghadaripour et al. (2017b) and results were formulated based on the non-dimensional release height η. Therefore, it is

expected that the release height has a direct effect on the area of deposition and an adverse effect on the mound height. For example, by increasing the release height from 0.25 m to 1.00 m for test with m=380 g, d_o=0.015 m and θ=30°, the length, width and area of the sediment mound increased by 15%,14% and 32%, respectively. For the same test, the mound height decreased by 8% as the release height increased from 0.25 m to 1.00 m. Similarly, the mound scour had a direct correlation with the growth of the nozzle diameter and release height. The effects of controlling parameters on the average characteristics length scales and area of sand deposition are listed in Table A3. It can be concluded from Table A3 that the characteristics of sand deposition are highly affected by nozzle diameter compared to the other controlling parameters.

The boundary of the sand deposition was plotted for a wide range of sand mass from 40 g to 450 g to study the effect of sand mass on deposition pattern. The variations of the deposition base area with mass are shown in Figure A5. Contour plots for selected released mass of particles demonstrated formation of the mound for tests B1-B4. The deposition patterns were axisymmetric respect to the centerline of the nozzle. This behaviour was also reported for deposition pattern of coarse sediments in channel without cross flow by Bhuiyan et al. (2010). Experimental observations of Rajaratnam and Mazurek (2006) indicated that the deposition profiles would be similar after a short time from the beginning of the experiments. This idea was implied in this study to investigate the effect of mass of particles on the profiles of the mound. As can be seen in Figure A5, the mass of released particles did not have significant effect on the deposition shape. Mass of sand particles contributed more to the deposition front and sides which caused both length and width growth. As can be seen, although the growth of base area of deposition was proportional to the released mass, but the deposition shape was affected by the nozzle size and the release angle. Direct correlation was observed between mass of sand particles and mound height to a certain

extent. Once a certain mound's height was built, particles did not have enough energy to pass the mound peak and they were trapped inside the scour and filled up the center of the mound. Figure A6 shows the effect of sand mass on mound formation for Test A1 with constant release angle and nozzle size.

Table A3 Effects of each controlling parameter on variations of the characteristic length scales and area of sand mound

Dimensions of sand mound	d_o (m)	θ^o	H (m)
l (m)	+25%	+17%	+14%
w (m)	+38%	-15%	+6%
h (m)	-25%	-15%	-11%
A (m^2)	+77%	-5%	+22%

It is important to know the effect of controlling parameters on variation of the vertical mound profile and the development of the mound peak. Vertical profiles at the center of sediment mound were plotted to study the effect of nozzle size and release height. Figure A7 shows the vertical profiles of different tests with a constant release angle of 60º. As can be seen in Figure A7, the mound peak gradually moved towards downstream of deposition as more mass was released. It was noticed that both upstream and downstream faces of depositions grew at the same rate and the location of the mound peak did not change with the sand mass. However, the release height changed the location of the mound peak toward the downstream.

Appendix

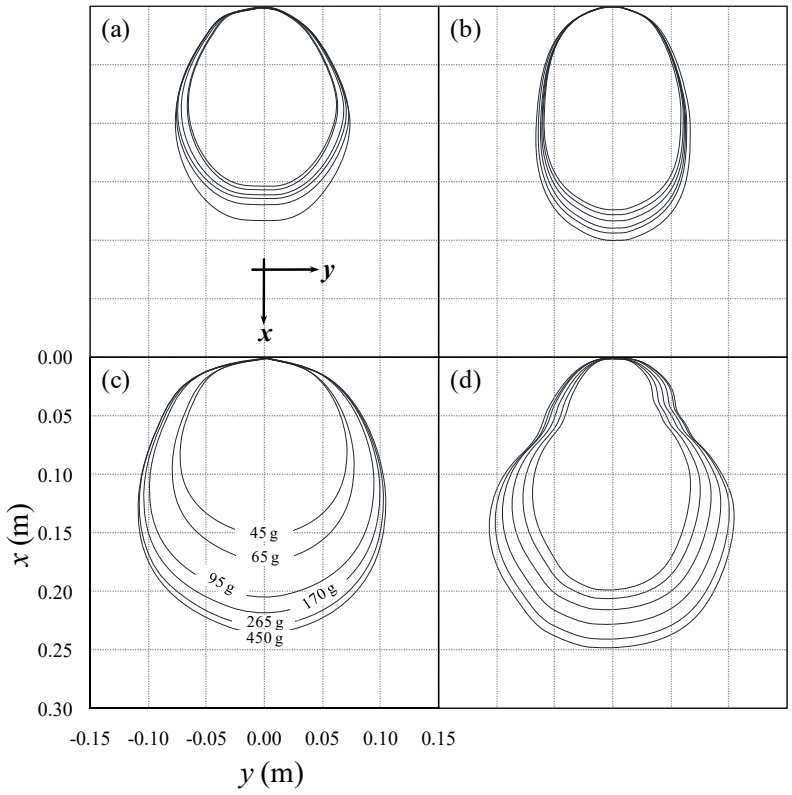

Figure A5 Effects of nozzle size and release angle during development phases of sediment deposition for constant release height of H=0.25 m; a) Test A1(B1) (d_o=0.01 m, θ=30° and H=0.25 m); b) Test A4(B2) (d_o=0.01 m, θ=60° and H=0.25 m); c) Test A7(B3) (d_o=0.015 m, θ= 30° and H=0.25 m); d) Test A10(B4) (d_o=0.015 m, θ=60° and H=0.25 m)

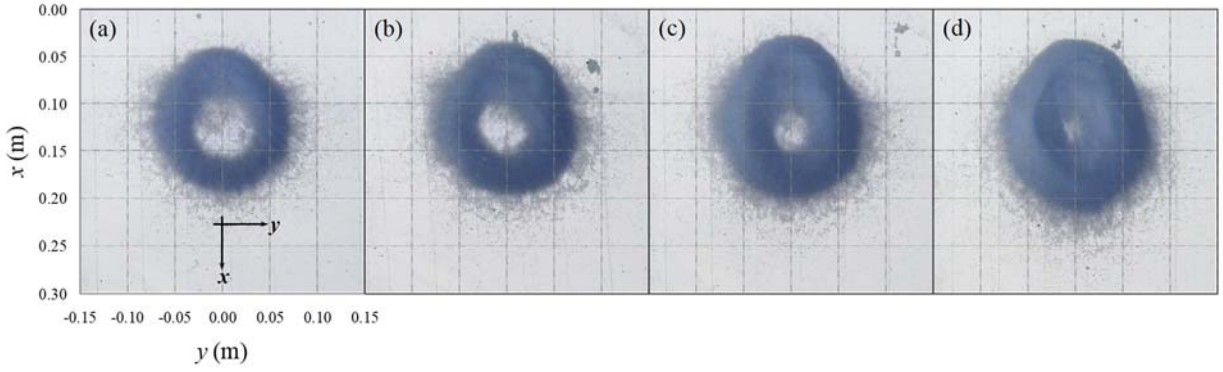

Figure A6 Effect of particle mass on bed scouring for Test A1 (d_o=0.01 m, θ= 30° and H=0.25 m); a) m=130 g; b) m=215 g; c) m=320 g; d) m=450 g

Appendix

The transverse profiles of the sediment mound can be normalized with the maximum height of the mound h_m and the mound half-width b where h is equal to $h_m/2$. The normalized longitudinal profiles of sediment mounds for tests A1-A3 and A7-A9 are plotted in Figure A8. Azimi et al. (2014) proposed a linear function to predict the deposition of subaqueous sand issued from slurry wall jets (i.e., θ=90°) as $h/h_m=-0.55(y/b)+1.05$. The deposition profiles from vertical sediment-laden jets (i.e., θ=0°) was formulated by a cosine function as $h/h_m=\cos(\pi y/3b)$ by Rajaratnam and Mazurek (2006). These two proposed formulations are added to Figure A8 for comparison. The difference between the transverse mound profiles in the present study and the proposed formulations of Azimi et al. (2014) and Rajaratnam and Mazurek (2006) indicates the effect of the release angle on the normalized mound shape.

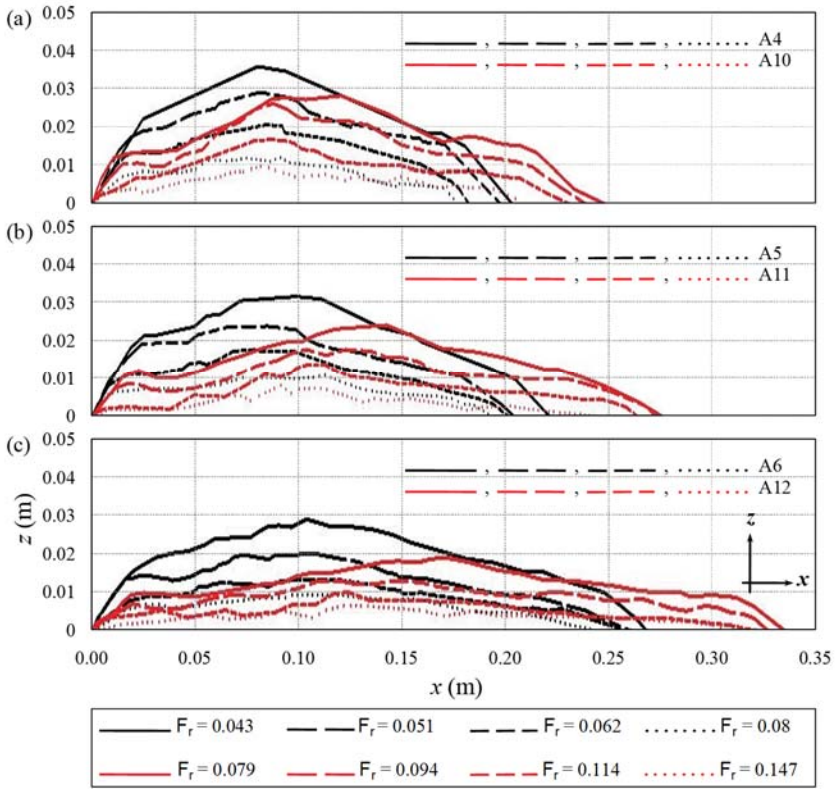

Figure A7 Effects of nozzle size and release on sand mound development for constant release angle of θ=60°; a) H=0.25 m; b) H=0.5 m; c) H=1 m

Appendix

The importance of each controlling parameters on variations of the mound length scales and area was studied. However, it is useful to develop semi-empirical formulations to predict the characteristic length scales and areas of deposition for practical engineering purposes. The proposed equations provide a clear view about the dependency mound sizes of various parameters.

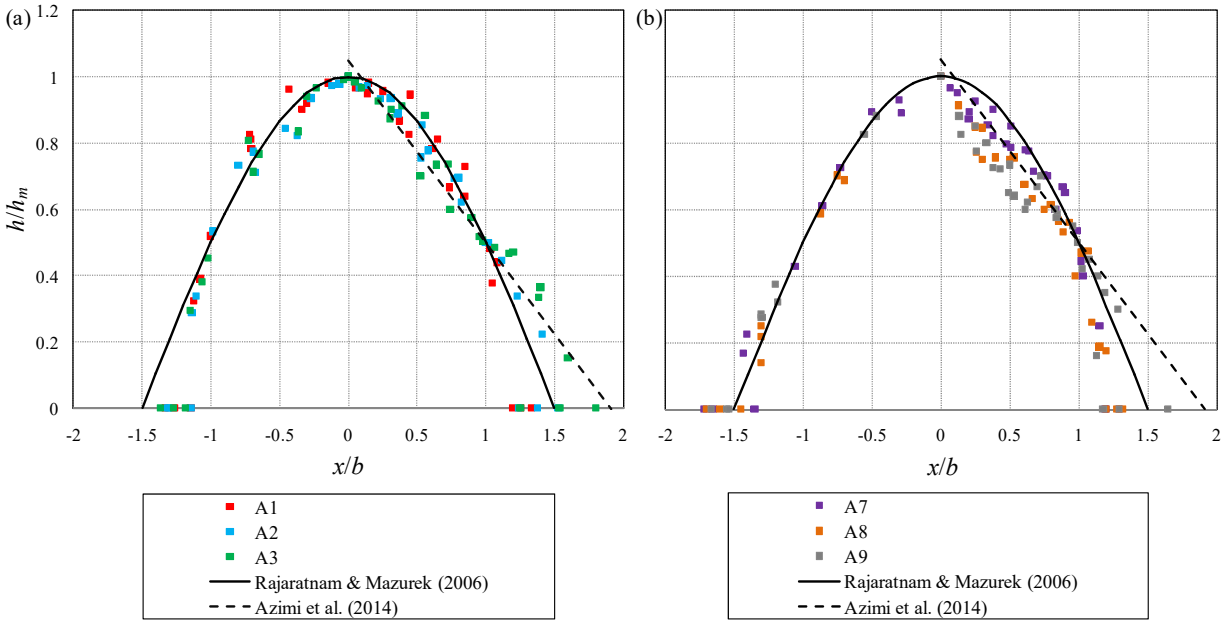

Figure A8 Sediment deposition profile of the mound for constant release angle of θ=30° and different release heights; a) Tests A1-A3 (d_o=0.01 m); b) Tests A7-A9 (d_o=0.015 m)

Figure A9 shows the variations of the mound length with sand mass for all tests. Two different regimes were observed in correlation of sand mass with mound length. In the first regime, the length of sediment mound grew linearly with particle mass for m<200 g. In the second regime, the growth of the mound sizes slightly increased with a very small slope (see Figure A9a). As described in dimensional considerations, sand mass can be converted to an equivalent pipe length L. Froude number F_r based on L can be formulated to describe the effect of sand mass on variations of the mound characteristics length scales and area. Figure A9b shows the variation of the

normalized mound length with F_r. Regression analysis was employed to provide the best fit correlation between the normalized mound length and F_r by systematically changing the power of each normalized parameter to maximize the correlation coefficient R^2. Empirical correlations were introduced to predict the mound length with F_r as:

$$\frac{l}{d_o} = 73.2 F_r^{-3/5} \left(\frac{l}{H}\right)^{-1/6} \left(\frac{z}{d_o}\right)^{-1/10} (\sin\theta)^{1/3} (R_e)^{-1/5} \quad \text{(A13)}$$

Figure A9a shows the performance of the proposed equations with measurements for tests A1 and A10. Considering measurement uncertainty, showed as an overbar for test A10 in Figure A9a, indicated that the proposed equation predicted the mound length within a reasonable accuracy.

Figure A10a shows the variations of the mound width with mass. Similar to the mound length, variations of the mound width with sand mass also indicated two separate deposition regimes with a similar threshold of m=200 g. Using systematic regression analysis provides an accurate prediction curve for mound width as:

$$\frac{w}{d_o} = 2629 F_r^{-6/5} \left(\frac{w}{H}\right)^{-1/6} \left(\frac{z}{d_o}\right)^{-4/5} (\sin\theta)^{-1/3} (R_e)^{-1/2} \quad \text{(A14)}$$

The correlation coefficients R^2 of the proposed formulations for prediction of mound length and width were 0.94 and 0.99, respectively. Eqs. (A13) and (A14) indicate that the release height has a larger impact on the mound length than that of the mound width. On average, increasing the release height from 0.25 to 1.0 m resulted in a growth of length and width by 14% and 6%, respectively. Increasing the nozzle size from 10 mm to 15 mm caused a length and width growth of 25% and 38%, respectively. The release angle has an adverse impact since it increases the mound length with a power of $^1/_3$ and reduces the mound width with a power of $-^1/_3$. Effect of water depth was also found to be more pronounced in variations of the mound width than the mound length.

Appendix

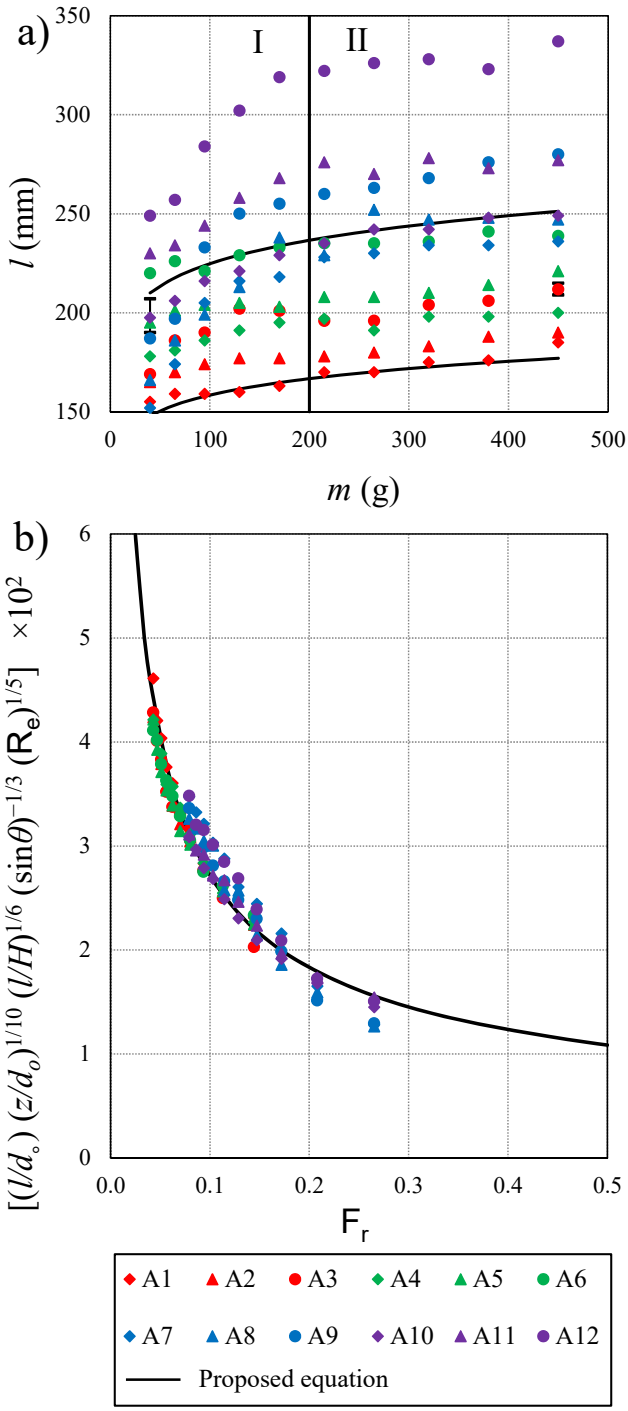

Figure A9 Variation of mound length with controlling parameters during the development phase; a) growth of sediment deposition length with mass; b) correlation of the normalized length of sediment deposition with the normalized the densimetric Froude number. Solid curves show the prediction model

Appendix

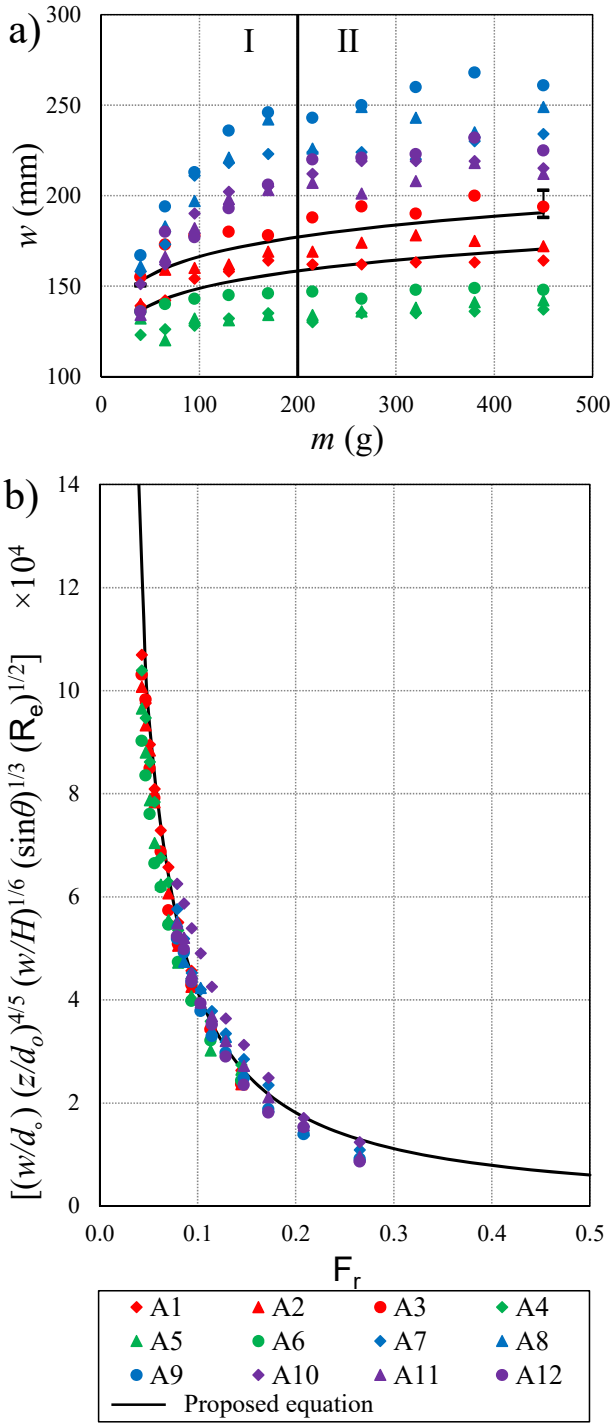

Figure A10 Variation of width of the mound with controlling parameters during the development phase; a) growth of sediment deposition width with mass; b) correlation of the normalized width of sediment deposition with the densimetric Froude number. Solid curves show the prediction model

Appendix

Figure A11a shows growth of the mound height with mass of sand particles. As can be seen, the height increases almost linearly with mass of sand particles and it is not possible to identify the deposition regimes with height data. This ascending trend found to be similar for all sets of experiments with a slight difference in the slope. Similar to the length and width, the normalized deposition height can be predicted using systematic regression analysis as:

$$\frac{h}{d_o} = 12.25 F_r^{-2} \left(\frac{h}{H}\right)^{1/6} \left(\frac{z}{d_o}\right)^{-1} (\sin\theta)^{-1/3} (R_e)^{-1/2} \quad \text{(A15)}$$

with a R^2 value of 0.98. On average, 23% reduction in the height of deposition occurred when the nozzle diameter increased from 10mmto 15 mm. The correlation of the normalized height of sediment deposition with the normalized mass is shown in Figure A11b.

Variation of the area of the mound with sand mass is shown in Figure A12a. As can be seen the growth rate of the area for experiments with θ=60° in considerably larger than that of 30°. The proposed equation to predict the mound area can be expressed as:

$$\frac{A}{d_o^{\,2}} = 10^7 x F_r^{-7/3} \left(\frac{A}{H^2}\right)^{-1/5} \left(\frac{z}{d_o}\right)^{-5/4} (\sin\theta)^{-1/6} (R_e)^{-1} \quad \text{(A16)}$$

with a correlation coefficient $R^2$of 0.98. Some irregularities were observed in development of the length, width, height and area of the mound during the tests. This data scatter may be due to experimental uncertainties. However, the overall trends were not significantly affected by those uncertainties.

Appendix

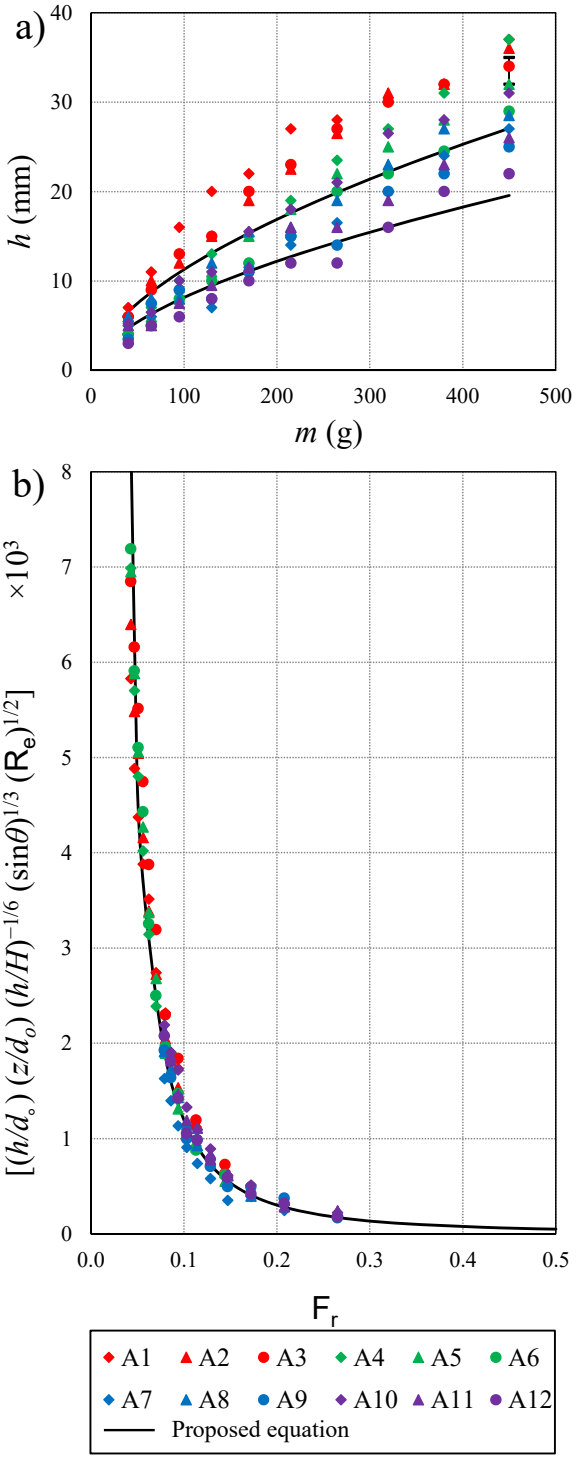

Figure A11 Variation of mound height with controlling parameters during development phase; a) growth of sediment deposition height with mass; b) correlation of the normalized height of sediment deposition with the densimetric Froude number. Solid curves show the prediction model

Appendix

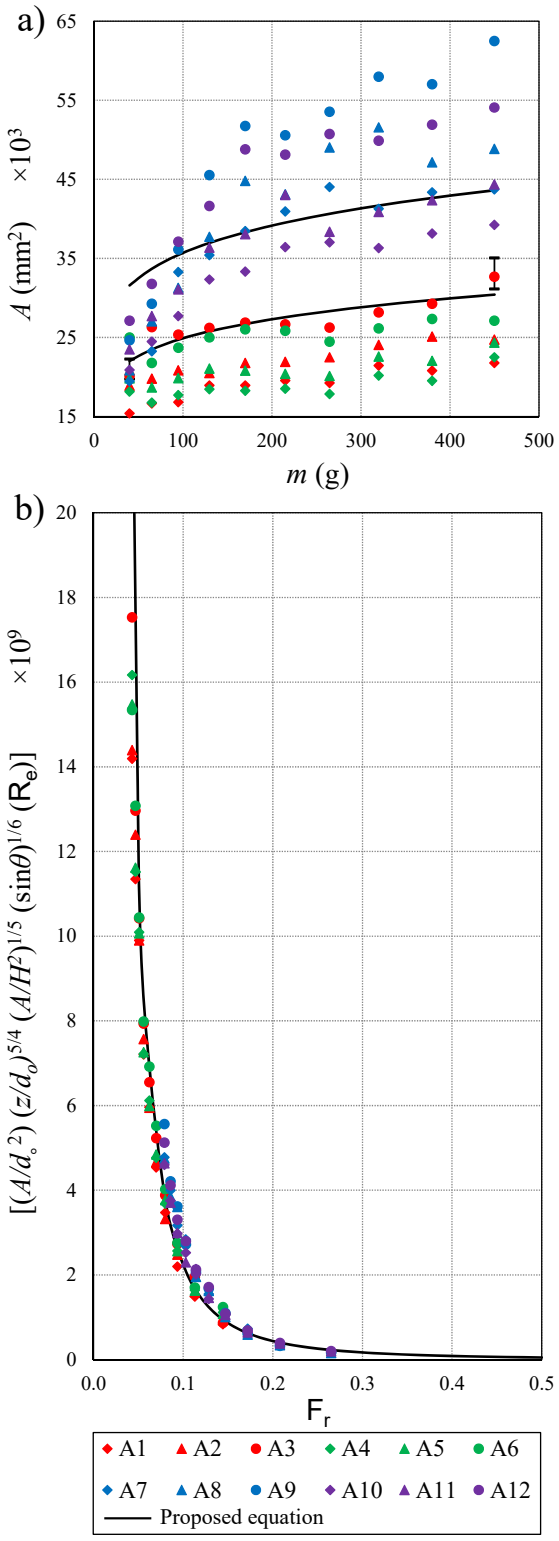

Figure A12 Variation of mound area with controlling parameters during development phase; a) growth of sediment deposition area with mass; b) correlation of the normalized area of sediment deposition with the densimetric Froude number. Solid curves show the prediction model

Appendix

4.3 Mass balance in mound formation

It is important to predict the shape of sand deposition and to identify the mound symmetry without direct underwater observations. The volume of the circle and circular-ring depositions can be calculated using the Pappus-Guldinus theorem (Beer et al., 2013) as:

$$V = 2\pi A\left(\frac{\bar{x}+\bar{y}}{2}\right) = 2\pi A\left(\frac{w+w'+l+l'}{8}\right) \tag{A17}$$

Two different cross-sectional areas of half-cosine (Rajaratnam and Mazurek, 2006) for θ=0^o and triangular (Azimi et al., 2014) for θ=90^o were proposed for sediment deposition in form of $h=f(y)$ as sketched in Figures A13b and A13c. The area of deposition can be calculated as:

$$A = \int_0^{\frac{w-w'}{2}} h\, dy \tag{A18}$$

Mass of sediment deposition can be estimated knowing the loose packed particle concentration (i.e., c_o=0.6; Julien, 2010) and volume of deposition as:

$$m = c_o \rho_s V \tag{A19}$$

Formation of circle, ellipse, circular-ring, and ellipse-ring depositions was predicted by modeling scour hole in section 4.1. The pear-shaped model can be identified by evaluating the accuracy of the predicted mass of sand particles with the actual mass of particles before release. Figure A14 shows the comparison between mass balance prediction using Pappus-Guldinus theorem and the direct sand mass measurements before releasing through circular nozzle. As can be seen, the mass balance provides a relatively accurate estimation within ±10% accuracy for Regime I (i.e., m<200 g) as it is shown with dashed lines in Figure A14. This indicates the formation of simple circle, ellipse, circular-ring, and ellipse-ring. The calculated mass balance is not accurate for larger mass due to formation of asymmetrical and pear-shaped deposition patterns.

Appendix

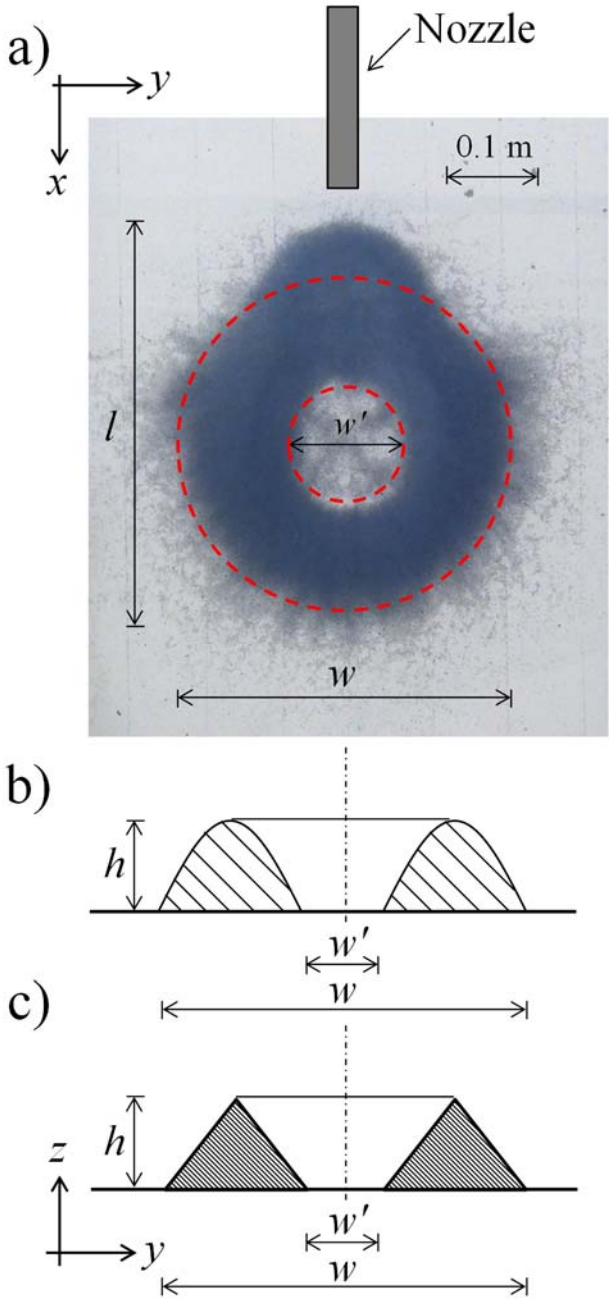

Figure A13 Mass balance based on volume integration; a) top-view image of sediment deposition for Test A10 (m=380 g, d_o=0.015 m, θ=60° and H=0.25 m); b) mound vertical cross-section based on half-cosine model; c) mound vertical cross-section based on simple triangular model

Appendix

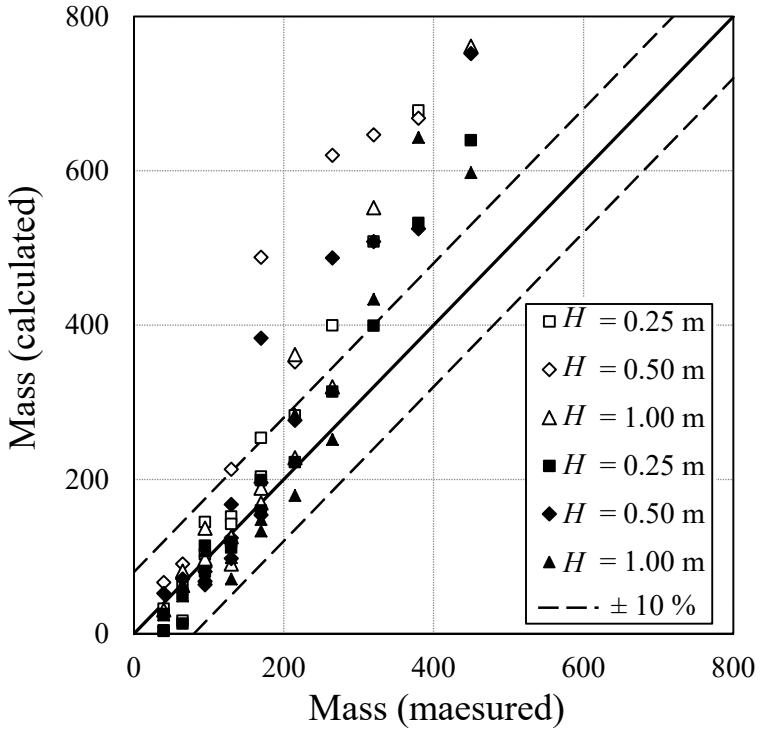

Figure A14 Comparison of both triangular (solid symbols) and half-cosine (open symbols) models on prediction of sediment deposition mass

5. Conclusions

Laboratory experiments were conducted to investigate the development of sediment mound formed by instantaneous release of sand particles. Effects of four variables of sand mass m, nozzle diameter d_o, release angle θ, and release height H on formation and growth of mound length, width, height and area were studied. Dimensional analysis and data mining models were employed to predict the shape and size of underwater mound.

Five different deposition patterns were observed named as circular, ellipse, circular-ring, ellipse-ring, and pear-shaped. The existence scour hole in the middle of deposition was predicted by comparing the magnitudes of water and sediment impact velocities at the bed location and the terminal settling velocity of individual sand particles. Using available formulations to predict sand and water velocities, it was shown why no scour hole formed for d_o=8 mm and depositions formed

from θ=60°. Predicted sediment velocity at the point of impact indicated that the vertical component of sand velocity u_y still two to three times larger than u_∞ which cusses sediment re-suspension. Size of scour *w'* for all tests was predicted by assuming that Gaussian distribution can describe particle distribution at the location of impact and sediment deposition occurs when $u_y \approx u_\infty$. It was found that the existing models can accurately predict the size of scour hole for large release angles (i.e., θ=60°) while the assumption of $u_y \approx u_\infty$ under-estimated the size of scour for θ=30°.

Effects of controlling parameters on development of mound shape were investigated. It was found that the nozzle size is the most dominant parameter on development of sediment mounds. The length, width, and area of sediment mound increased with increasing the nozzle diameter while the mound height slightly decreased. Release angle is considered as the second most important controlling factor on the characteristics of the sediment deposition. It was found that the release angle increased the mound length and reduced the mound width at the same time. Effect of release height was found to be less important that d_o and θ. It was observed that the length and width of deposition increased by increasing the release height. Experimental observations indicated a proportional growth of deposition area with sand mass; however, sand mass had no control in the mound shape. It was found that both upstream and downstream faces of depositions grew at the same rate and the location of the mound peak did not change with released sand mass. Two different regimes were observed in correlation of sand mass with mound length and width with a threshold mass of 200 g. Semi-empirical formulations were developed to predict the deposition length, width, height, and area.

In order to predict the formation of the pear-shaped sediment mound as the last classification pattern mass balance concept was employed by calculating the volume of deposition using the

Appendix

Pappus-Guldinus theorem. It was found that the mass balance provides a relatively accurate estimation within ±10% accuracy for Regime I (i.e., m<200 g) where mound shape is simple.

Acknowledgement

I would like to thank undergraduate students (Richard Twiss, Amir Shirazian, Ghazal Rohani, and Conor Sullivan) for their help to conduct part of my laboratory experiments.

Appendix

Notation

The following symbols are used in this paper:

A = mound area

b = particle cloud half width

B_o = initial buoyancy flux sand within the jet

c_o = initial sand concentration

D_{16} = sand diameters at which 16 of the sand particles present are finer

D_{50} = mean particle size

D_{84} = sand diameters at which 16 of the sand particles present are finer

F = densimetric Froude number

F_r = Froude number based on L

l_m = momentum length scale

m = sand mass

M_o = initial momentum flux of sand within the jet

R_e= Reynolds number

T = temperature

V = volume of sediment deposition

g = gravitational acceleration

g'= reduced gravity, $g'=g(\rho_s-\rho_w)/\rho_w$

L = equivalent length of sand particles in pipe

n = sand porosity

z = depth of water

u_o = initial sand velocity

Appendix

h = deposition height

h_m = deposition height at peak

w = deposition width

w' = scour width

l = deposition length

l' = scour length

H = release height

d_o = nozzle diameter

u_y= transverse velocity of particle cloud

u_z = vertical velocity of particle cloud

η = normalized release height

l_1, l_2 = thickness of deposition ring

λ_1, λ_2, λ_3, λ_4= coefficients

φ_1, φ_2 = coefficients

θ = release angle

μ = dynamic viscosity

v = kinematic viscosity

σ = uniformity coefficient of particles

u_∞ = terminal settling velocity

u_* = bed shear velocity

ρ_s = sand density

ρ_m = mixture density

ρ_w = water density

Appendix

$\bar{x}$ = center of mass in x direction

$\bar{y}$ = center of mass in y direction

Appendix

References

Azimi, A.H., Zhu, D.Z., and Rajaratnam, N. (2011). "Effect of particle size on the characteristics of sand jet in water." *ASCE, Journal of Engineering Mechanics*, 137(12), pp. 822-834.

Azimi, A.H., Zhu, D.Z., and Rajaratnam, N. (2012a). "Experimental study of sand jet front in water." *Int. J. Multiphase Flow*, 40, pp. 19-37.

Azimi, A.H., Zhu, D.Z., and Rajaratnam, N. (2012b). "Computational investigation of vertical slurry jets in water." *Int. J. Multiphase Flow*, 47, pp. 94-114.

Azimi, A.H., Zhu, D. Z., and Rajaratnam, N. (2014). "An experimental study of subaqueous sand deposition from slurry wall jets." *ASCE, Journal of Engineering Mechanics*, 140(2), pp. 296-314.

Azimi, A.H., Zhu, D.Z., Rajaratnam, N. (2015). "An experimental study of circular sand–water wall jets." *Int. J. Multiphase Flow*, 74, pp. 34-44.

Beer, F. P., Johnston, E. R., Mazurek, D. F., Cornwell, P. J., and Self, B. P. (2013). "Vector mechanics for engineers: Static and Dynamics." *McGraw Hill Education*, 1409 p.

Beuselinck, L., Govers, G., Steegen, A., and Hairsine, P. B. (1998). "Experiments on sediment deposition by overland flow." *Modeling Soil Erosion, Proc. of Sediment Transport and Closely Related Hydrological Processes*, No. 249, IAHS Publishers, U.K., pp. 91-96.

Bhuiyan, F., Rajaratnam, N., and Zhu, D. Z. (2010). "An experimental study of mounds formed by dumping coarse sediment in channel flow." *Journal of Hydraulic Research*, 48(3), pp. 283-291.

Bond, D., Johari, H. (2005). "Effect of initial geometry on the development of thermals." *Exp. Fluids*, 39, pp. 589–599.

Appendix

Breusers, H. N. C., Raudkivi, A. J. (1991). "Scouring: Hydraulic Structures Design Manual Series." Vol. 2, CRC Press, 152 p.

Buhler J. and Papanttoniou D. A. (2001). "On the motion of suspension thermals and particle swarms." *Journal of Hydraulics Research*, 39(6), pp. 643-653.

Bush, J.W.M., Thurber, B.A., and Blanchette, F. (2003). "Particle clouds in homogeneous and stratified environments." *J. Fluid. Mech.* Vol. 489, pp. 29-54.

Chan, S. N., Lee, K.W. Y., and Lee, J. H.W. (2014). "Numerical modelling of horizontal sediment-laden jets. "*Environ. Fluid Mech.*, 14(1), pp. 173-200.

Chan, S. N. and Lee, J. H.W. (2016). "A particle tracking model for sedimentation from buoyant jets." *ASCE, J. Hydraul. Eng.*, 42(5), 04016001-18.

Chin, D. A., (2012). "Water-quality engineering in natural systems." second edition, *John Wiley & Sons*, 454 p.

Cuthbertson, A. J. S., and Davies, P. A. (2008). "Deposition from particle-laden, round, turbulent, horizontal, buoyant jets in stationaryand co-flowing receiving fluids." *ASCE, J. Hydraul. Eng.*, 134(4), pp. 390-402.

Fischer, H. B., List, E. J., Koh, R. C. Y., Imberger, J, and Brooks, N. H. (1979). "Mixing inland and coastal waters." *Academic Press*.483 p.

Gu, J., Huang, J. (2008). "Experimental study on instantaneous discharge of unsorted particle cloud in cross-flow." *Journal of Hydrodynamics, Ser. B*. 20(1), pp. 10-16.

Holdich, R.G., (2002). "Fundamentals of Particle Technology." *Midland Information Technology and Publishing*, p. 173.

Julien, P. Y. (2010). "Erosion and sedimentation." 2nd Ed., *Cambridge, University Press*, Cambridge, U.K.

Appendix

Kikkert, G.A., Davidson, M.J., and Nokes, R.I. (2009). "A jet at an oblique angle to a cross-flow." *J. Hydro-Environ. Res.* 3(2), pp. 69-76.

Lane-Serff, G. F., and Moran, T. J. (2005). "Sedimentation from buoyant jets." *ASCE, J. Hydraul. Eng.*, 131(3), pp. 166-174.

Lee, K. W. Y., Li, A. C. Y., and Lee, J. H. W. (2013). "Structure of a horizontal sediment-laden momentum jet." *ASCE, J. Hydraul. Eng.*, 139(2), pp. 124-140.

Li, C.W., and Ma, F.X. (2001). "3D numerical simulation of deposition patterns due to sand disposal in flowing water." *ASCE, J. Hydraul. Eng.* 127(3), pp. 209-218.

Masuda, N., Yoshida, J., Ito, B., Furuya, T., and Sano, O. (2012). "Collision of a vortex ring on granular material: I. Interaction of the vortex ring with the granular layer." *Fluid Dyn. Res*. 44, 015501.

Miller, H.C., McNinch, J.E., Land, J.M., Battisto, G.M., and Davies, J.E. (2002). "Fate and effect of an experimental mixed-sediment mound." *Proc. 3rd Specialty Conf. Dredging and Dredged Material Disposal*, Orlando, FL, pp. 1-10.

Moghadaripour, M., Azimi, A. H., and Elyasi, S. (2017a). "Experimental Study of Oblique Particle Clouds in Water." *Int. J. Multiphase Flow*, 91, pp. 193–213.

Moghadaripour, M., Azimi, A. H., and Elyasi, S. (2017b). "Experimental Study of Particle Clouds in Stagnant Water." *ASCE, Journal of Engineering Mechanics*, 143(9), 04017082-1-17.

Mohammadidinani, N., Azimi, A. H., and Elyasi, S. (2017). "Experimental Investigation of Sand Jets Passing through Immiscible Fluids." *ASME, Journal of Fluids Engineering*, 139(5), 051303, 13 p.

Munro, R.,Bethke, N., and Dalziel, S. B. (2009). "Sediment re-suspension and erosion by vortex ring." *Physics of Fluids*, 21, 046601.

Appendix

Nakasuji K., Tamai M. and Murota A. (1990). "Dynamic behaviours of sand clouds in water." *Int. Conf. on Phys. Modelling of Transport and Dispersion. Boston*, USA, 8c: pp. 1-6.

Noh, Y., and Fernando, H.J.S. (1993). "The transition in the sedimentation pattern of a particle cloud." *Physics of Fluids*, 5(12), pp. 3049-3055.

Rahimipour, H. and Wilkinson, D. (1992). "Dynamic behavior of particle clouds." *11th Australasian Fluid Mechanics Conference*, Vols 1 and 2, University of Tasmania, Hobart, Australia, pp. 743-746.

Rajaratnam, N., and Mazurek, K.A. (2006). "An experimental study of sand deposition from sediment laden water jet." *ASCE, J. Hydraulic Res*. 44(4), pp. 560-566.

Ruggaber, G. J. (2000). "The dynamics of particle clouds related to open water sediment disposal." Ph.D. thesis, Dept. of Civil and Environmental Engineering, Massachusetts Institute of Technology, *Cambridge*, MA.

Scheffner, N.W. (1996). "Systematic analysis of long-term fate of disposed dredged material." *ASCE, J. Water Port Coastal Ocean Eng*. 122(3), pp. 127-133.

Shields, D.H., Domaschuk, L., Corkal, D.W., and McCutchon, J.R. (1984). "Controlling sand placement during the building of artificial islands." *Can. Geotech. J.* 21(2), pp. 371-375.

Tamai, M., Muraoka, K., Murota, A. (1991). "Diffusion process of turbidity in direct dumping of soil." *Environmental hydraulics*, Balkema, Rotterdam, pp. 147-152.

Wang, X., and Kikkert, G.A. (2014). "Behaviour of oblique jets released in a moving ambient." *J. Hydraul. Res.* 52 (4), pp. 490-501.

Yoshida, J. and Sano, O. (2014). "Erosion of the granular layer due to the collision of vortex ring." *Fluid Dynamics Research*, 46, 061421, 11 p.

Appendix

Zhao, B., Law, A.W.K., Adams, E.E., Shao, D., Huang, Z. (2012). "Effect of air release height on the formation of sediment thermals in water." *J. Hydraul. Res.* 50 (2), pp. 532-540.